Hierarchical Gas Model Coupling on Networks

Hierarchische Kopplung von Gasmodellen auf Netzwerken
Zur Erlangung des Grades eines Doktors der Naturwissenschaften (Dr. rer. nat.)
genehmigte Dissertation von Pascal Mindt aus Bad Soden
Tag der Einreichung: 10.08.2018, Tag der Prüfung: 07.11.2018
Darmstadt — D 17

Referent: Prof. Dr. Jens Lang
Korreferent: Prof. Dr. Michael Herty

TECHNISCHE
UNIVERSITÄT
DARMSTADT

Fachbereich Mathematik
AG Numerik und
wissenschaftliches Rechnen

Hierarchical Gas Model Coupling on Networks
Hierarchische Kopplung von Gasmodellen auf Netzwerken

Genehmigte Dissertation von Pascal Mindt aus Bad Soden

Referent: Prof. Dr. Jens Lang
Korreferent: Prof. Dr. Michael Herty

Tag der Einreichung: 10.08.2018
Tag der Prüfung: 07.11.2018

Darmstadt — D 17

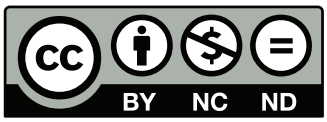

Abstract

In recent years the simulation of gas flow on networks attracts increasing interest. Since natural sources of energy, like wind and solar power, might lack of continuity, some demands in energy are compensated by gas. Therefore, accurate simulations for gas transport are essential. However, a highly detailed simulation suffers from great computational costs. Consequently, it becomes natural to use models with less physical detail in pipes with lower activity, while for pipes with greater dynamics, models with higher physical detail are used.

In the analytical part of this work, we consider a network, with one single junction and a given model hierarchy. It appears the question how these models are coupled at the junction and which kind of coupling conditions have to be posed such that a resulting solution is unique and physically correct, as far as it even exists.

In order to answer the above questions, we propose mass-, energy- and entropy- preserving coupling conditions at the junction. By introducing, a so called generalized Riemann problem at the junction, i.e., piecewise constant initial data, all models are connectible to each other through the coupling conditions. Afterwards, we show well-posedness of the generalized Riemann problem, i.e., there exists a unique physically correct solution.

The well-posedness above creates a foundation for a more general setting, the so called Cauchy problem, in which initial data needs to be integrable with small total variation only. Here, well-posedness is shown as well. Based on these results, even existence of an optimal control can be proven.

In the second part of this work, we like to give some numerical illustrations, built on our analytical results.

This work is organized as follows. In section 2, models of gas dynamics, namely the full Euler equations, the isentropic and the simplified isentropic Euler equations, as well as two compressor models are introduced. In sections 3 and 4 a brief overview of hyperbolic theory for scalar equations and systems is given, respectively. Section 5 is concerned with coupling conditions of the full Euler equations on a network as well as well-posedness of the generalized Riemann problem. Section 6 extends theory of section 5 regarding the well-posedness of all models on a network. In section 7 we prove well-posedness of our compressor models, using techniques of previous sections. Section 8 is concerned with well-posedness of Cauchy problems. In our last section, we give an overview of numerical methods, followed by some numerical illustrations.

Zusammenfassung

In den vergangen Jahren erfuhr die Simulation von Gasfluss in Netzwerken gesteigertes Interesse. Auf Grund des schwankenden Energieflusses durch natürliche Ressourcen, wie Wind und Solarenergie, werden einige Nachfragen durch Gas kompensiert.

Folglich ist eine detaillierte Simulation des Gastransportes essentiell. Kehrseite ist jedoch der, damit verbundene, hohe Rechnungsaufwand. Um dies zu vermeiden, nutzt man Modelle mit niedrigem physikalischem Detail, bei wenig Gasdynamik im Rohr und Modelle mit hohem Detailgrad bei steigender Dynamik.

Im analytischen Teil dieser Arbeit betrachten wir ein Netzwerk, versehen mit einer Modellhierarchie und einem einzigen Verzweigungspunkt. Es stellt sich nun die Frage, wie die vorhandenen Modelle an der Verzweigung zu koppeln sind und wie die Kopplungsbedingungen gestellt werden müssen, sodass eine resultierende Lösung physikalisch korrekt ist, sofern diese überhaupt existiert.

Um diese Fragen zu beantworten, fordern wir Bedingungen an der Verzweigung zur Masse-, Energie- und Entropieerhaltung. Durch Einführung eines sogenannten verallgemeinerten Riemann-Problems am Verzweigungspunkt, i.e. stückweise konstante Anfangsdaten, lassen sich alle Modelle durch die Kopplungsbedingungen miteinander verbinden. Anschließend zeigen wir Wohlgestelltheit des verallgemeinerten Riemann-Problems, i.e. es existiert eine physikalisch korrekte Lösung.

Die Wohlgestelltheit des obigen Problems dient als Grundlage für ein allgemeineres Problem, dem sogenannten Cauchy-Problem. Hier müssen Anfangsdaten lediglich integrierbar und von beschränkter totaler Variation sein. Die Wohlgestelltheit des allgemeineren Problems wird ebenfalls gezeigt. Basierend auf den obigen Resultaten, weisen wir ferner die Existenz einer optimalen Steuerung nach.

Im zweiten Teil dieser Arbeit werden einige numerische Beispiele illustriert, welche auf den analytischen Ergebnissen fußen.

Die Arbeit ist wie folgt organisiert. In Abschnitt 2 werden Modelle zur Beschreibung der Gasdynamik, die sogenannten Euler-Gleichungen, isentropen Euler-Gleichungen und vereinfachten isentropen Euler-Gleichungen, sowie zwei Kompressormodelle, vorgestellt. Abschnitte 3 und 4 beinhalten eine kurze Übersicht zur Theorie hyperbolischer Differentialgleichungen. In Abschnitt 5 werden die Kopplungsbedingungen der Euler-Gleichungen auf Netzwerken eingeführt, sowie Wohlgestelltheit des verallgemeinerten Riemann-Problems gezeigt. Abschnitt 6 erweitert dann die vorhergehende Theorie auf alle Modelle am Verzweigungspunkt. In Abschnitt 7 zeigen wir Wohlgestelltheit der Kompressormodelle im Kontext verallgemeinerter Riemann-Probleme. In Abschnitt 8 ist die Wohlgestelltheit der Cauchy-Probleme zu finden. Im letzten Abschnitt geben wir eine Übersicht zu den verwendeten numerischen Methoden sowie die Illustration einiger numerischer Beispiele.

Acknowledgements

First of all, I would like to thank my supervisor Prof. Dr. Jens Lang for his great advice and support during the development of this thesis. I may say, he is one of the most professional persons I have ever met, while never lacking of kindness. I also would like to thank my co-supervisor Prof. Dr. Michael Herty.

Furthermore, I like to thank my colleagues in the numerical research group and especially Dr. Pia Domschke for many fruitful discussions and a very pleasant working atmosphere.

Special thanks go to my best friend Sven Dahms for his proofreading of my thesis and his great companionship as well as our regular cinema evenings.

However, my deepest gratitude belongs to my mother Petra and my brother Felix for all of their support and love through difficult times. Without you this thesis would never have been possible. Thank you, so much!

This work was supported by the German Research Foundation within the collaborative research center TRR154 Mathematical Modeling, Simulation and Optimization Using the Example of Gas Networks

Contents

1 Introduction

Since renewable energy sources like wind and solar power lack from continuity, some energy demand is compensated with gas to energy stations. Consequently, a highly detailed simulation of gas transport in networks becomes important, in order to respond to rapidly changing energy demand.

Publications, which are concerned with the numerical simulation of gas transport on networks, are for example Domschke, Kolb and Lang in their work [2, 20, 21], Schmidt, Steinbach and Willert [40] as well as Steinbach [44], just to name a few.

However, in Schmidt, Steinbach and Willert [40] it is mentioned, that simulations of gas networks suffer from great computational costs. To overcome this issue, Domschke, Kolb and Lang [20] posed a model hierarchy, such that gas models with high physical detail are used in pipes, which consist of complicated gas dynamics, whereas models with less physical detail are used in pipes with low gas dynamics.

Furthermore, the physically correct solvability of gas models, like the full Euler equations, on networks remained unclear for many years. This is due to the fact, that coupling conditions are not unique and modeling needs to be involved.

Since gas is transported only, the requirement of mass conservation at a junction is obvious. Nonetheless, further coupling conditions, which are necessary to state a well-posed problem, had been unsettled through out the literature.

Banda, Herty and Klar studied in [3] coupling conditions of isothermal homogeneous Euler equations at junctions, by using mass conservation and equality of pressure, connecting finitely many ingoing and outgoing pipes. Previously, Colombo and Garavello [12] utilized conservation of mass and equality of dynamic pressure at junctions for the isothermal and isentropic homogeneous Euler equations on networks. Colombo and Mauri made in [18] a first attempt to couple the full homogeneous Euler equations at a junction by providing mass conservation, equality of dynamic pressure and energy conservation. However, these coupling conditions allow a junction with finitely many ingoing pipes and *one* outgoing pipe only. Furthermore, well-posedness of the isentropic Euler equations, if coupled with a compressor model, have been studied in the work [16] of Colombo, Guerra, Herty and Schleper. Also, an investigation of isothermal homogeneous Euler equations with different pipe cross sections, coupled by mass conservation and equality of dynamic pressure can be found in the work [17] of Colombo, Herty and Sachers.

After all, Reigstad showed in her publication [38], that any usage of pressure or dynamic pressure equality results in a production of energy at a junction and therefore in an unphysical solution. Furthermore, a desired physically correct solution for the isentropic Euler equations is discovered by the utilization of enthalpy equality, which has also been demonstrated numerically by Reigstad and Morin in [36]. All before mentioned references rely on a deep investigation of so called Riemann problems at junctions. Here, the regarded set of hyperbolic partial differential equations are posed with piecewise constant initial data on the half space $\mathbb{R}_+$, while the junction itself is located in $x = 0$. Referring to the literature above, this problem is also called generalized homogeneous Riemann problem at the junction.

Now, a piecewise constant and self-similar solution occurs. For the pipe only case, this solution structure was already known, see for example the very detailed work of Smoller [43] for general hyper-

bolic equations, or Toro [45] for a complete construction of a solution to the full homogeneous Euler equations with piecewise constant initial data.

However, these solution structures inherent continuously differentiable parametrization curves, the so called *Lax-curves*, which allow a physically correct connection of states in a pipe with the junction. By an utilization of Lax-curves, a certain degree of freedom coincides. In regard of the full Euler equations, any ingoing pipe at a junction, if connected through Lax-curves, adds *one* degree of freedom, while outgoing pipes have *two* degrees of freedom. The sum of all degrees of freedom dictates the number of coupling conditions at a junction.

Once coupling conditions are posed, all involved states at a junction are described by the before mentioned Lax-curves, defining a composition of mappings. Now, well-posedness of the resulting mapping can be obtained by an application of the implicit function theorem.

In order to show well-posedness of homogeneous Cauchy problems, initial data is approximated by piecewise constant functions, inflicting local Riemann problems. Latter are successively solved in space and time. However, it needs to been proven, that the appearing algorithm does not break down after finite time, which has been done by Bressan [5] for the inner of a pipe, and by Colombo and Garavello [12] as well as Colombo and Mauri [18], for junctions. Accordingly, a sequence of solutions to the Riemann problem is produced. Then, a suitable functional guarantees in combination with Helly's theorem [5], the existence of the limit of the sequence, and well-posedness of the Cauchy problem is proven.

An extension to inhomogeneous Cauchy problems follows by a splitting argument, in which the solution of an homogeneous Cauchy problem is used as initial condition for a set of first order ordinary differential equations. Here, the right hand side consists of the inhomogeneous part of the Cauchy problem. For example, this can be found in the work [16] of Colombo, Guerra, Herty and Schleper.

1.1 Contribution

In our work, we contribute a set of novel coupling conditions, which allow a coupling of the full Euler equations with finitely many ingoing and outgoing pipes, following the work of Lang and Mindt in [32]. If homogeneity is assumed, these conditions allow mass and energy conservation at a junction. Afterwards, we consider the full homogeneous Euler equations and prove well-posedness of the resulting homogeneous Riemann problem at the junction, using before mentioned techniques, i.e., the composition of our coupling conditions with Lax-curves and an application of the implicit function theorem.

In a second step, our coupling conditions are adapted, such that the full Euler equations can also be coupled with the isentropic or simplified isentropic Euler equations at a junction. These models form a model hierarchy according to their listing above. Here, we follow the approach of Domschke, Kolb and Lang in [20] to reduce computational costs in gas network simulations.

Again, mass and energy are preserved, if homogeneity is assumed, and well-posedness of the underlying Riemann problem is shown. Additionally, we prove well-posedness of the compressor models appearing in Ehrhardt, Steinbach [23] and Menon [34], if coupled with the full, isentropic or simplified isentropic Euler equations.

In the second part of our work, all before mentioned homogeneous Riemann problems are adapted to homogeneous Cauchy problems.

Regarding solvability of the homogeneous Cauchy problems at junctions, we proceed analogously to the literature, i.e., any initial data is approximated by piecewise constant data first, which results in local Riemann problems in all pipes and at the junction itself. The solution of latter, has already been constructed in our first part. In case of local Riemann problems in pipes and their solutions, we refer to SMOLLER [43], TORO [45] and BRESSAN [5]. By examining the situation at the junction, equipped with our posed coupling conditions, we show, that the produced sequence of solutions to the Riemann problem admits a limit, which states well-posedness of the homogeneous Cauchy problem.

The extension to inhomogeneous Cauchy problems on networks is straight forward and is therefore briefly reviewed, referring to COLOMBO, GUERRA, HERTY and SCHLEPER [16].

1.2 Outline

This work is organized as follows. In section 2, models of gas dynamics, namely the full Euler equations, the isentropic and the simplified isentropic Euler equations, which form a model hierarchy, as well as two compressor models of EHRHARDT, STEINBACH [23] and MENON [34] are introduced. In sections 3 and 4 a brief overview of hyperbolic theory for scalar equations and systems is given, respectively. Here, the concept of characteristics is discussed as well as the construction of Lax-curves in dependence of the underlying gas model. Section 5 is concerned with our novel set of coupling conditions for the full Euler equations on a network. Furthermore, we introduce the generalized homogeneous Riemann problem at the junction and show its well-posedness by a suitable composition of our coupling conditions with the before mentioned Lax-curves and an application of the implicit function theorem to the resulting mapping. Section 6 extends the coupling conditions of section 5, such that all introduced gas models can be coupled at a junction, while conserving mass and energy. Afterwards, the appearing generalized Riemann problem is proven to be well-posed by proceeding analogously to section 5. In section 7 we prove well-posedness of our compressor models. Again, using the techniques of previous sections. Section 8 is concerned with well-posedness of homogeneous Cauchy problems. Here, the front-tracking algorithm of BRESSAN [5] is introduced as well as its adaption to networks, consisting of a single junction. By a definition of a suitable functional, which incorporates the total variation as well as an interaction functional, one can proof the non-increase of total variation. Together with uniformly boundedness of all approximating Riemann solutions, the existence of the limit of the sequence follows by an application of Helly's theorem [5]. Furthermore, we show, that the solution has a L^1-stable dependence on the initial data. This is mainly done by already existing work of BRESSAN [5] for pipes. At the junction, we proof stability by adapting the theory of COLOMBO, HERTY and SACHERS [17] for our purposes. Afterwards, a brief overview to well-posedness of inhomogeneous Cauchy problems at junctions is given. In our last section, we provide some information regarding the implementation of gas networks, followed by numerical illustrations.

2 Modeling Introduction

In this section, we introduce models for describing gas dynamics as well as definitions regarding network topology, on which gas flow is considered.

The gas dynamics, independent from any surroundings, are described by the full Euler equations in one space dimension, i.e.,

$$\begin{pmatrix} \rho \\ q \\ E \end{pmatrix}_t + \begin{pmatrix} q \\ p + \rho u^2 \\ u(E+p) \end{pmatrix}_x = 0, \tag{$\mathscr{E}_1$}$$

where ρ, u, E and p stand for density, velocity, energy and pressure, respectively. Since we want to investigate gas networks, the real spatial axis represents one pipe and all variables are meant to be mean values of pipe cross-sections, see figure 1. The first, second and third equation in ($\mathscr{E}_1$) describe

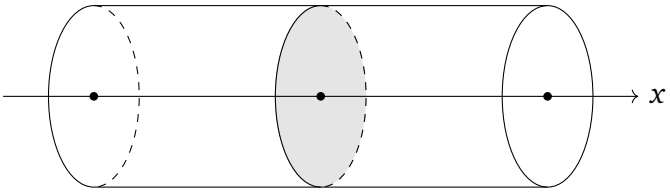

Figure 1: Mean values of $\rho, \rho u, E$ over a cross-section (gray) in a schematic pipe, are projected onto the real axes.

conservation of mass, impulse and energy, respectively. For a full derivation of ($\mathscr{E}_1$), we refer to the work of Feireisl in [25, Sect. 1.1.1]. By an introduction of the so called *equation of state* for ideal gas

$$E = \frac{p}{\gamma - 1} + \frac{\rho u^2}{2} \tag{2.1}$$

with adiabatic exponent $\gamma > 1$, the above system ($\mathscr{E}_1$) becomes closed, i.e., the number of variables matches the number of equations. At this point, we like to mention that ideal gas is considered throughout this work only, since the regarded theory becomes quite involved already.

However, at suitable sections some remarks on a possible extension to real gases are made. For later use, we introduce mass flux $q = \rho u$, the specific entropy $s = c_v \ln(p/\rho^\gamma) + s_0$ with $s_0 \geq 0$ and heat capacity $c_v > 0$, the total enthalpy $h = (E+p)/\rho$, the speed of sound $c = \sqrt{dp/d\rho|_s}$ and the temperature $\mathsf{T} = p/(R\rho)$ with gas constant R. The relation $\mathsf{T} = p/(R\rho)$ results from the assumption, that gas molecules are monoatomic with a spatial size of zero. Furthermore, it is assumed that these molecules move along the canonical basis vectors, in form of translation, only. For a more detailed thermodynamical derivation, see for example [45, Sect. 1.2.4].

Given the expression for entropy s above, we receive in regard of model ($\mathscr{E}_1$) for the speed of sound

$$c = \sqrt{\partial p/\partial \rho|_s} = \sqrt{\gamma e^{(s-s_0)/c_v} \rho^\gamma / \rho} = \sqrt{\gamma p/\rho}.$$

If a solution to $(\mathscr{E}_1)$ exists and is regular, i.e., (ρ, q, E) are differentiable and fulfill $(\mathscr{E}_1)$, an additional equations can be discovered, namely the so called *entropy equation*, which is given by

$$(\rho s)_t + (\rho u s)_x = 0. \tag{2.2}$$

For its derivation, see LeVeque [33, Sect. 14.5]. In section 5, where coupling conditions for $(\mathscr{E}_1)$ are examined, a replacement of the impulse equation in $(\mathscr{E}_1)$ with (2.2) becomes handy.

Since a gas network does not consist of one pipe only, some network topology will be introduced. Gas networks are defined through a pair $\mathscr{G} = (\mathscr{A}, \mathscr{V})$ with arc set $\mathscr{A}$ and a set of vertices $\mathscr{V}$. Due to our application in gas dynamics, arcs are also referred to pipes and vertices to nodes. Latter can also be boundary nodes, junctions or compressors, see figure 2 for an example network. According to Schmidt,

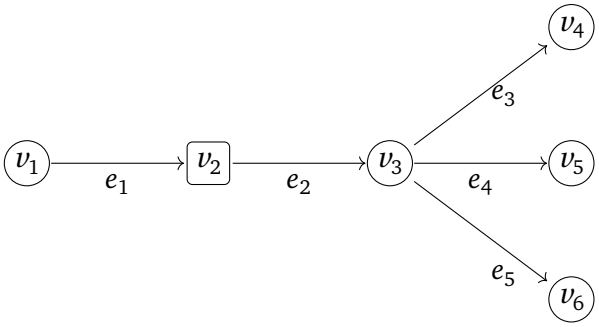

Figure 2: Schematic presentation of a network. Here v_1, v_4, v_5, v_6 are boundary nodes, v_2 is a compressor and v_3 is a junction.

Steinbach and Willert [41], simulations of real life gas networks demand high computational costs. To overcome this issue, Domschke, Kolb and Lang already proposed a model hierarchy in their work [20], in which models of low computational costs are taken, if gas consists of low dynamics, like stationary states or the consideration of short pipes. But as soon as greater gas dynamics arise, a model of higher physical detail is used.

Motivated by this approach, we introduce a model hierarchy as well. On top of our hierarchy, the full Euler equations $(\mathscr{E}_1)$ are placed. These are able to describe shock phenomena and increasing entropy.

If the solution is regular and entropy stays constant, i.e., $s \equiv s_0$, the *isentropic Euler equations*

$$\begin{pmatrix} \rho \\ q \end{pmatrix}_t + \begin{pmatrix} q \\ p + \rho u^2 \end{pmatrix}_x = 0, \tag{$\mathscr{E}_2$}$$

are considered with equation of state given by $p = \rho^\gamma$. Hence, speed of sound and enthalpy take the form $c = \sqrt{\gamma \rho^{\gamma-1}}$ and $h = \gamma/(\gamma-1)\rho^{\gamma-1} + u^2/2$, respectively.

For the last model in our hierarchy, we assume a sufficiently low velocity, i.e., $|u| \ll c$, additionally to condition $s \equiv s_0$, and conclude a simplification through

$$p(\rho) + \rho u^2 = \rho c^2 \left(\frac{p}{\rho c^2} + \frac{u^2}{c^2} \right) \approx \rho c^2 \left(\frac{p}{\rho c^2} + 0 \right) = p. \tag{2.3}$$

Replacing $p(\rho)+\rho u^2$ by $p(\rho)$ in the impulse equation of model $(\mathscr{E}_2)$, defines the *simplified isentropic Euler equations*

$$\begin{pmatrix}\rho\\ q\end{pmatrix}_t+\begin{pmatrix}q\\ p\end{pmatrix}_x=0, \tag{$\mathscr{E}_3$}$$

Accordingly, $(\mathscr{E}_3)$ is received from $(\mathscr{E}_2)$ by neglecting kinetic energy ρu^2. Furthermore, equation of state, speed of sound and enthalpy are given by $p=\rho^\gamma$, $c=\sqrt{\gamma\rho^{\gamma-1}}$ and $h=\gamma/(\gamma-1)\rho^{\gamma-1}$, respectively. The model hierarchy, as well as assumptions of every model therein, is summarized in table 1.

Model & Assumptions	Quantities
full Euler equations $(\mathscr{E}_1)$	$p = (\gamma-1)(E-\rho u^2/2)$ $h = (E+p)/\rho$ $c = \sqrt{\gamma p/\rho}$
U regular, $s\equiv s_0$ $\rightsquigarrow$ isentropic Euler equations $(\mathscr{E}_2)$	$p = \rho^\gamma$ $h = \gamma/(\gamma-1)\rho^{\gamma-1}+\rho u^2/2$ $c = \sqrt{\gamma\rho^{\gamma-1}}$
U regular, $s\equiv s_0$ and $\lvert u\rvert \ll c$ $\rightsquigarrow$ simplified isentropic Euler equations $(\mathscr{E}_3)$	$p = \rho^\gamma$ $h = \gamma/(\gamma-1)\rho^{\gamma-1}$ $c = \sqrt{\gamma\rho^{\gamma-1}}$

Table 1: Overview of our model hierarchy.

Since our model hierarchy has been built, we present some theory now, by starting with the conservation property of models $(\mathscr{E}_1)$-$(\mathscr{E}_3)$.

Definition 2.1 (Conservation)**.** *A system of partial differential equations*

$$U_t+F(U)_x=0,$$

with $U:\mathbb{R}\times\mathbb{R}_+\supseteq\Omega_x\times\Omega_t\to D\subseteq\mathbb{R}^n$ *and* $F\in C^1(D;\mathbb{R}^n)$, $n\in\mathbb{N}$ *is called conservative.*

In our work Ω_x takes the form $\Omega_x=\mathbb{R}$ if a pipe is considered and $\Omega_x=\mathbb{R}_+$, if the pipe is connected to a junction. For Ω_t, we chose either $\Omega_t=\mathbb{R}_+$ or $\Omega_t=[0,T]$, $T>0$. All cases will always be clear from the underlying setting. Definition 2.1 is motivated as follows. Consider a domain $\Omega_x\subseteq\mathbb{R}$. Then, integration by parts of $U_t+F(U)_x=0$ over Ω_x results in

$$0=\frac{d}{dt}\int_{\Omega_x}U\,dx+F(U)|_{\delta\Omega_x}.$$

Consequently, a change of the *volume* $\int_{\Omega_x} U\,dx$ is due to the flux $F(U)|_{\delta\Omega_x}$ over the boundary $\delta\Omega_x$ only. Some of our main results are based on this conservative form, see sections 5 and 6.

However, in real world applications, U is not always conserved. So it comes that impulse is reduced due to friction in a pipe; or energy, which is not conservative due to heat exchange with the surroundings.

In order to model this behavior, a *source* term is introduced on the right hand side, replacing the zero of each model. In regard of $(\mathscr{E}_1)$, this source term reads as follows

$$G(\rho,\rho u,E)=\begin{pmatrix}0\\ -\frac{\lambda}{d}\,\rho u|u|\\ -k_w(\mathsf{T}-\mathsf{T}_w)\end{pmatrix} \tag{2.4}$$

while for models $(\mathscr{E}_2)$ and $(\mathscr{E}_3)$ the third component is neglected, i.e.,

$$G(\rho,\rho u,E)=\begin{pmatrix}0\\ -\frac{\lambda}{d}\,\rho u|u|\end{pmatrix} \tag{2.5}$$

In (2.4) and (2.5), $d>0$ is the pipe diameter, $\lambda>0$ the pipe friction coefficient and $k_w>0$ is the heat exchange rate of T with the wall temperature T_w. All coefficients are assumed to be constant. An overview of more involved friction models λ, which also depend on U, can be found in Schmidt, Steinbach and Willert [41].

Besides conservation, models $(\mathscr{E}_1)$-$(\mathscr{E}_3)$ are classified as *hyperbolic*, which is defined next.

Definition 2.2 (Hyperbolicity)**.** *A system of partial differential equations*

$$U_t+F(U)_x=G(U),$$

with $U:\mathbb{R}\times\mathbb{R}_+\supseteq\Omega_x\times\Omega_t\to D\subseteq\mathbb{R}^n$, $F\in C^1(D;\mathbb{R}^n)$ *and* $G\in L^1(D;\mathbb{R}^n)$ *is called hyperbolic, if the Jacobian* JF *has linearly independent eigenvectors with real eigenvalues only.*

Let denote $F^{(j)}$, $j=1,2,3$ the flux functions of models $(\mathscr{E}_1)$-$(\mathscr{E}_3)$, respectively. Then, one deduces the Jacobian matrices

$$JF^{(1)}(U)=\begin{pmatrix}0 & 1 & 0\\ \frac{\gamma-3}{2}u^2 & (\gamma-3)u & \gamma-1\\ \frac{\gamma-2}{2}u^3-\frac{c^2u}{\gamma-1} & \frac{3-2\gamma}{2}u^2 & \gamma u\end{pmatrix},$$

$$JF^{(2)}(U)=\begin{pmatrix}0 & 1\\ c^2-u^2 & 2u\end{pmatrix},\quad JF^{(3)}(U)=\begin{pmatrix}0 & 1\\ c^2 & 0\end{pmatrix},$$

which admit the real eigenvalues

$$\lambda_1^{\mathscr{E}_1}(U) = u - c, \quad \lambda_2^{\mathscr{E}_1}(U) = u, \quad \lambda_3^{\mathscr{E}_1}(U) = u + c$$
$$\lambda_1^{\mathscr{E}_2}(U) = u - c, \quad \lambda_2^{\mathscr{E}_2}(U) = u + c,$$
$$\lambda_1^{\mathscr{E}_3}(U) = -c, \quad \lambda_2^{\mathscr{E}_3}(U) = c.$$

with corresponding eigenvectors

$$r_1^{\mathscr{E}_1} = \begin{pmatrix} 1 \\ u-c \\ h-uc \end{pmatrix}, \quad r_2^{\mathscr{E}_1} = \begin{pmatrix} 1 \\ u \\ \frac{u^2}{2} \end{pmatrix}, \quad r_3^{\mathscr{E}_1} = \begin{pmatrix} 1 \\ u+c \\ h+uc \end{pmatrix}$$
$$r_1^{\mathscr{E}_2} = \begin{pmatrix} -\frac{u+c}{c^2-u^2} \\ 1 \end{pmatrix}, \quad r_2^{\mathscr{E}_2} = \begin{pmatrix} -\frac{u-c}{c^2-u^2} \\ 1 \end{pmatrix}$$
$$r_1^{\mathscr{E}_3} = \begin{pmatrix} -\frac{1}{c} \\ 1 \end{pmatrix}, \quad r_2^{\mathscr{E}_3} = \begin{pmatrix} \frac{1}{c} \\ 1 \end{pmatrix}$$

Since these eigenvectors are linearly independent, all models are hyperbolic. Eigenvalues play a key role in the theory of hyperbolic problems, since they are involved in the *transport of information*. The meaning of this terminology is explained in section 3 for scalar conservation laws.

Next, all before mentioned network components are extended by two compressor models. Both models are located between an ingoing and outgoing pipe, according to figure 3.

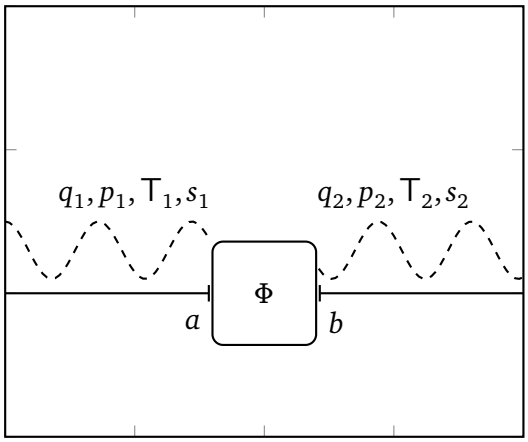

Figure 3: Schematic presentation of the compressor network with one ingoing and outgoing pipe. The compressor □ is located in the middle.

Our first compressor model is an *adiabatic isentropic compression*, referring to the work of Cerbe [8, Gl. 5.13 & Gl. 5.14], and is described through

$$\Phi = \begin{pmatrix} q_1(a-,t) - q_2(b+,t) \\ \frac{\gamma}{\gamma-1} R \mathsf{T}_1(a-,t) \left(\left(\frac{p_2(b+,t)}{p_1(a-,t)} \right)^{\frac{\gamma-1}{\gamma}} - 1 \right) \\ s_1(a-,t) - s_2(b+,t) \end{pmatrix} \overset{!}{=} \begin{pmatrix} 0 \\ H(t) \\ 0 \end{pmatrix}. \tag{2.6}$$

The term *adiabatic* means, that there is no energy transfer between compressor and its surroundings. Due to the first and last equation in (2.6), mass and entropy are preserved. Second equation models the pressure difference between in- and outgoing pipes, in which $H \geq 0$ stands for invested enthalpy into the compressor. Accordingly, if $H = 0$, the pressure difference is zero and gas passes the compressor without compression.

However, in optimal control problems, $H(t)$ is often replaced by the theoretical compressor power $\tilde{H}(t) = C_p q_2(b+,t) H(t), C_p \equiv const$, see for example Erhardt and Steinbach [23] as well as Menon [34]. In this case, we have

$$\tilde{\Phi} = \begin{pmatrix} q_1(a-,t) - q_2(b+,t) \\ \frac{\gamma}{\gamma-1} R C_p q_2(b+,t) \mathsf{T}_1(a-,t) \left(\left(\frac{p_2(b+,t)}{p_1(a-,t)} \right)^{\frac{\gamma-1}{\gamma}} - 1 \right) \\ s_1(a-,t) - s_2(b+,t) \end{pmatrix} \overset{!}{=} \begin{pmatrix} 0 \\ \tilde{H}(t) \\ 0 \end{pmatrix}. \tag{2.7}$$

For simplicity later on, we set $a = b = 0$ and perform a coordinate transformation, such that both pipes are pointing away from our compressor models.

In the next section, theory about hyperbolic equations is discussed by starting with scalar equations.

3 Scalar Hyperbolic Conservation Laws in One Space Dimension

Before studying systems of hyperbolic conservation laws in more detail, a brief overview to scalar equations is given. Here, we like to introduce the concept of characteristics first, which reappears for systems of hyperbolic partial differential equations on $\mathbb{R}$, in section 4, as well as for networks in sections 5, 6 and 8. Let us consider the following problem in one space dimension

$$\begin{cases} u_t + f(u)_x &= 0, \\ u(x,0) &= u_0(x), \end{cases} \tag{3.1}$$

with $u\colon \mathbb{R}\times\mathbb{R}_+ \supseteq \Omega_x \times \Omega_t \to D \subseteq \mathbb{R}$ and $f \in C^1(D;\mathbb{R})$. In regard of problem (3.1), a line $x(t)$ in the x-t-plane is called *characteristic*, if solution u of (3.1) is constant along $x(t)$, i.e., $\frac{d}{dt}u(x(t),t) = 0$. Furthermore, the derivative $\dot{x}(t)$ is named *characteristic speed*.

As an illustration, take $f(u) = au,\ a > 0$. This problem is named *linear transportation problem* and admits the solutions

$$u(x,t) = u_0(x - at). \tag{3.2}$$

On the lines $x(t) = x_0 + at$, u is constant, since $u(x(t),t) = u_0(x_0)$, see also figure 4a and 4b. In other words, the initial value $u_0(x_0)$ is just transported along $x(t)$ with slope $a > 0$.

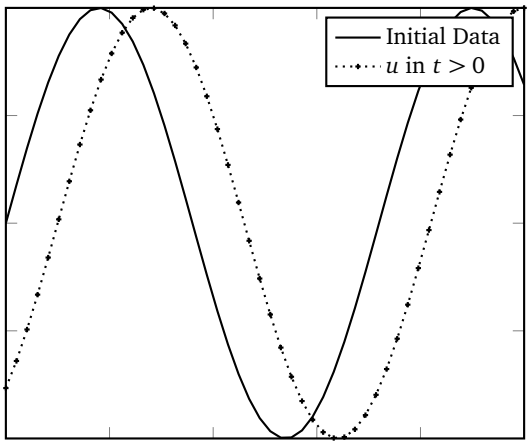

(a) Solution of the linear transport problem in $t > 0$.

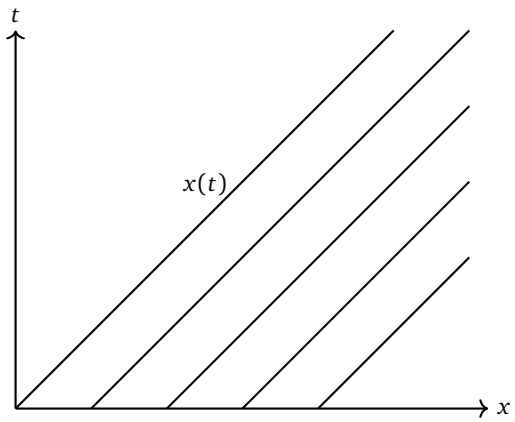

(b) Characteristics of the linear transport problem.

Figure 4: Schematic presentation of the solution and characteristics of linear transportation problem.

In general, a characteristic can be derived by considering u as regular solution to problem (3.1). Then, differentiation of $u(x(t),t)$ in t gives

$$0 = \frac{d}{dt}u(x(t),t) = u_t + \dot{x}u_x. \tag{3.3}$$

By comparing (3.3) with (3.2), we conclude $\dot{x}(t) = f'(u_0(x_0))$, which results in

$$x(t) = x_0 + f'(u_0(x_0))t. \tag{3.4}$$

A nonlinear example is provided by posing $f(u) = u^2/2$. This problem is also called *Burgers' equation*, see for example [43, Sect 15 §], [33, Sect. 11.3] for more detail. Given initial condition through

$$u_0(x) = \begin{cases} 1, & x < -1 \\ -x, & -1 \le x \le 1 \\ -1, & 1 < x \end{cases} \tag{3.5}$$

the solution to Burgers' equation reads

$$u(x,t) = \begin{cases} 1, & x < -1 + t \\ -x/(1-t), & -1 \le x/(1-t) \le 1 \\ -1, & x > t - 1 \end{cases} \tag{3.6}$$

see also figure 5a. In figure 5b, the characteristics of u are presented, which intersect at time $t = 1$

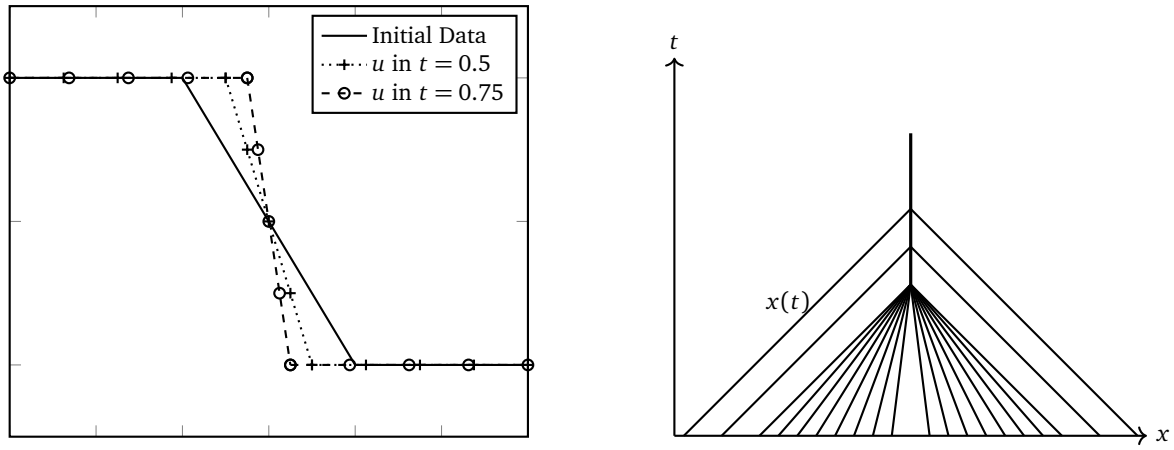

(a) Solution of the Burgers' equation. Here, a shock is formed after finite time.

(b) Characteristics of the shock solution. Here, the characteristics intersect after finite time.

Figure 5: Schematic presentation of the solutions and its characteristics to the Burgers' equation with initial data (3.5).

and form a discontinuity there. Latter example stands representative for the difficulties in the field of hyperbolic partial differential equations, namely a development of discontinuities after finite time, even with arbitrarily regular initial data u_0, see for example [5, Sect. 1]. Consequently, derivatives of solutions might become distributional in the x-t-plane or weak in the L^1 sense. Motivated by above observations, we introduce the next definition.

Definition 3.1. *Consider a system of hyperbolic partial differential equations*

$$U_t + F(U)_x = G(U),$$

with $U : \mathbb{R} \times \mathbb{R}_+ \supseteq \Omega_x \times \Omega_t \to D \subseteq \mathbb{R}^n$, $F \in C^1(D;\mathbb{R}^n)$ *and* $G \in L^1(D;\mathbb{R}^n)$ *as well as initial data* $U_0 \in L^1(\Omega_x;\mathbb{R}^n)$. *Then* U *is a weak solution, if it fulfills the integral equation*

$$\int_{\mathbb{R}_+}\int_{\mathbb{R}} (U\phi_t + F(U)\phi_x)\,dx\,dt + \int_{\mathbb{R}_+} U_0(x)\phi\,dx = -\int_{\mathbb{R}}\int_{\mathbb{R}_+} G(U)\phi\,dt\,dx \tag{3.7}$$

for all test functions $\phi \in C_0^1(\mathbb{R}\times\mathbb{R}_+;\mathbb{R}^n)$. *Here,* $\mathscr{C}_0^1(\mathbb{R}\times\mathbb{R}_+;\mathbb{R}^n)$ *is the space of all* C^1 *regular functions, which have a compact support in space and vanish for* $t > 0$ *large enough. Furthermore, the multiplication in* (3.7) *is meant to be component-wise.*

Now, let us reconsider the concept of characteristics and in particular solution (3.6) again. Obviously, u is discontinuous for $t \geq 1$ and a derivation like (3.4) is not possible, since $u \in C^1$ has been assumed in order to derive characteristics.

However, the shock characteristic in (3.6), which occurs at time $t = 1$, can be discovered by an application of the next proposition.

Proposition 3.2. *Consider a system of hyperbolic partial differential equations*

$$U_t + F(U)_x = 0$$

with $U : \mathbb{R} \times \mathbb{R}_+ \supseteq \Omega_x \times \Omega_t \to D \subseteq \mathbb{R}^n$, $F \in C^1(D;\mathbb{R}^n)$ *and eigenvalues* $\lambda_1 < \ldots < \lambda_n$. *For any discontinuity with left and right states* U_L *and* U_R, *there exists* $\sigma \in \mathbb{R}$ *such that*

$$\sigma(U_L - U_R) = F(U_L) - F(U_R). \tag{3.8}$$

The proof of proposition 3.2 follows by an application of the divergence theorem and can be found in standard literature like [43, Sect. 15§B], [45, Sect. 2.4] or [33, Sect. 11.9]. In these references, condition (3.8) is also referred to as *Rankine-Hugoniot* condition. According to proposition 3.2, a shock characteristic is given by $x(t) = x_0 + \sigma t$.

Another issue in the field of hyperbolic equations is, that weak solutions need *not* to be unique. For illustration, consider Burgers' equation $u_t + (u^2/2)_x = 0$ again, equipped with initial data

$$u_0(x) = \begin{cases} -1, & x < 0, \\ 1, & x > 1. \end{cases} \tag{3.9}$$

Now, two possible solutions u_1 and u_2 are given through

$$u_1(x,t) = u_0(x,t) \tag{3.10a}$$

$$u_2(x,t) = \begin{cases} -1, & x < -t, \\ x/t, & -1 \le x/t \le 1, \\ 1, & x > t. \end{cases} \tag{3.10b}$$

Both solutions, as well as their characteristics, are plotted in subfigures 6a, 6b and 6c, 6d. The *physically*

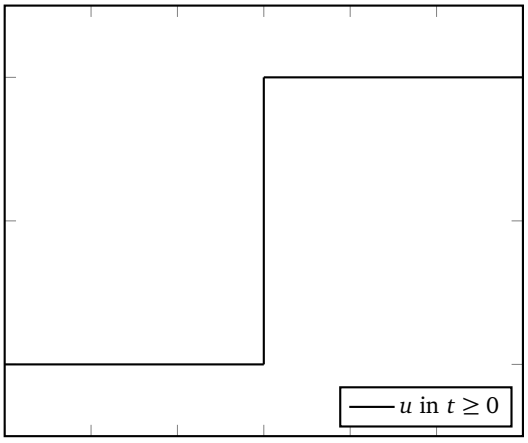

(a) Unstable shock as solution to Burgers' equation with initial data (3.9).

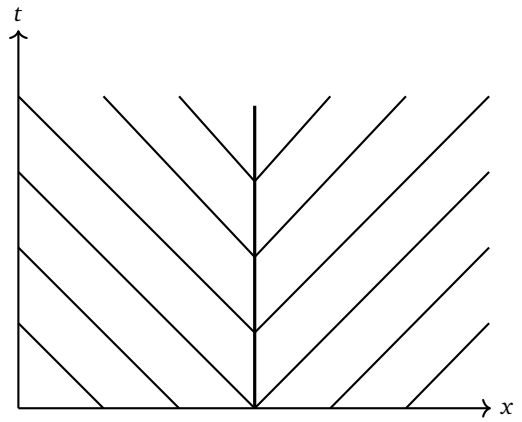

(b) Characteristics of the unstable shock.

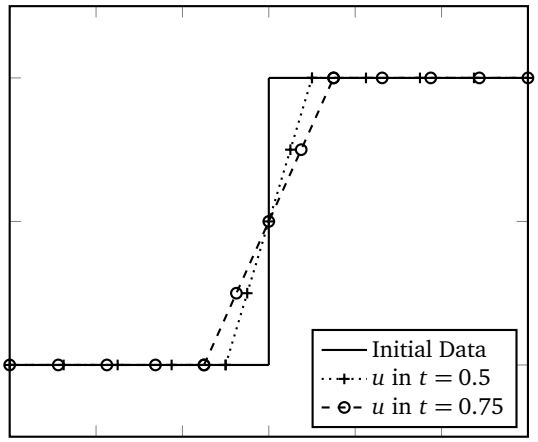

(c) Rarefaction wave as solution to the Burgers' equation with initial data (3.9).

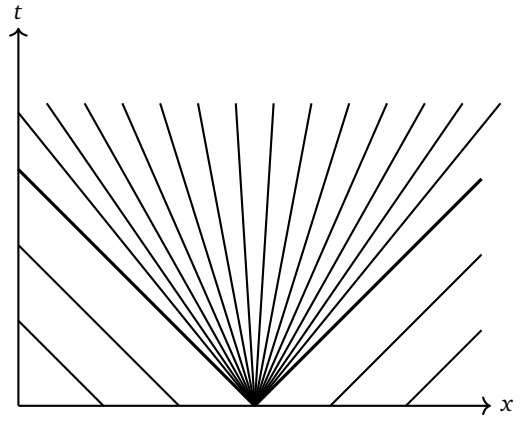

(d) Characteristics of the rarefaction wave.

Figure 6: In subfigures 6a and 6c two different weak solutions for Burgers' equation with initial data (3.9) are presented.

correct solution is now identified by the so called *entropy condition* for scalar hyperbolic problems in our next definition, see also [43, Sect. 15 §B].

Definition 3.3. *Consider a hyperbolic partial differential equation*

$$u_t + f(u)_x = 0$$

with $u\colon \mathbb{R}\times\mathbb{R}_+ \supseteq \Omega_x\times\Omega_t \to D\subseteq\mathbb{R}$, $f\in C^1(D;\mathbb{R})$ *convex and initial data*

$$u_0(x)=\begin{cases} u_l, & x<0\\ u_r, & x>0\end{cases}$$

An intermediate state ξ *between* u_l *and* u_r *is called entropic if*

$$f'(u_l)>f'(\xi)=\left(f(u_l)-f(u_r)\right)/(u_l-u_r)>f'(u_r). \tag{3.11}$$

Concerning (3.11), only the second solution u_2 appears to be feasible, while $u_1(x,t)=u_0(x)$ violates (3.11) and is therefore classified as *non-physical*.

In [43, Sect. 15 §B] and [33, Sect. 11.13] a more general definition for entropic correct solutions is given, which also applies for non-linear systems, and is presented next.

Definition 3.4. *Consider the system of hyperbolic partial differential equations*

$$U_t+F(U)_x=G(U)$$

with $U\colon \mathbb{R}\times\mathbb{R}_+ \supseteq \Omega_x\times\Omega_t \to D\subseteq\mathbb{R}^n$, $F\in C^1(D;\mathbb{R}^n)$, $G\in L^1(D;\mathbb{R}^n)$, *initial data* $U_0\in L^1(\Omega_x)$ *and functions* ν,ψ, *with* ν *convex, which satisfy*

$$\nu'(U)=\psi'(U)F'(U). \tag{3.12}$$

Then a weak solution U *is entropic, if it fulfills*

$$\int_{\mathbb{R}_+}\int_{\mathbb{R}} \phi_t\,\nu(U)+\phi_x\psi(U)\,dx\,dt+\int_{\mathbb{R}}\phi(x,0)\,\nu(U_0(x))\,dx\geq-\int_{\mathbb{R}_+}\int_{\mathbb{R}}\nu'(U)G(U)\phi\;dxdt \tag{3.13}$$

for all $\phi\in\mathscr{C}_0^1(\mathbb{R}\times\mathbb{R}_+;\mathbb{R})$ *with* $\phi\geq 0$.

Functions (ν,ψ) are called *entropy-entropy flux pair* and can be derived from (3.12). Nonetheless, a solution to (3.12) does not necessarily exist, since this expression is underdetermined. For models $(\mathscr{E}_1)$-$(\mathscr{E}_3)$ entropy-entropy flux pairs are derived in [9, Remark 2.1] and [24, Sect. 6].

However, the more applicable condition (3.11) can be extended to systems as well, see next proposition, and becomes useful in order to single out non-physical solutions in our results later on.

Proposition 3.5. *Consider a system of hyperbolic partial differential equations*

$$U_t+F(U)_x=0$$

with $F \in C^1(D;\mathbb{R}^n)$ and solution $U : \mathbb{R} \times \mathbb{R}_+ \supseteq \Omega_x \times \Omega_t \to D \subseteq \mathbb{R}^n$, consisting of a shock with speed σ, separating a left state U_L and right state U_R. Then, there exists $k \in \{1, \dots, n\}$ such that

$$\begin{aligned} \lambda_k(U_R) &< \sigma < \lambda_{k+1}(U_R), \\ \lambda_{k-1}(U_L) &< \sigma < \lambda_k(U_L). \end{aligned} \tag{3.14}$$

As a reference to this proposition see for example [43, Sect. 15 §E]. Additionally, in appearance of a shock, condition (3.13) and (3.14) are equivalent, see [43, Sect. 20 §B].

In our next section, we examine systems of hyperbolic conservation laws on $\mathbb{R}$ in more detail and start with the linear case.

4 Systems of Hyperbolic Partial Differential Equations in One Space Dimension

This section is mainly concerned with nonlinear systems of homogeneous hyperbolic partial differential equations. However, in subsection 4.1, we give a brief overview to *linear* systems, which are still analytically solvable. By posing constant initial data consisting of a single discontinuity, so called *Riemann problems*, the solution admits a special step structure, which reappears for *nonlinear* systems.

In subsection 4.2, we examine nonlinear systems of homogeneous hyperbolic partial differential equations and start with a system, in which the initial data might not be piecewise constant. This problem is also referred to as *Cauchy* problem.

However, the before mentioned Riemann problems are a building block in order to solve Cauchy problems, and are therefore examined in more detail, by following the work of SMOLLER [43, Sect. 17 §A & §B]. Afterwards the resulting theory is applied to our gas models $(\mathscr{E}_1)$-$(\mathscr{E}_3)$.

4.1 Linear Systems

In this section, we give a brief overview to linear systems of hyperbolic partial differential equations, i.e.,

$$\begin{cases} U_t + AU_x &= 0, \\ U(x,0) &= U_0(x) \end{cases} \tag{4.1}$$

where $A \in \mathbb{R}^{n\times n}$ has n distinct real eigenvalues $\lambda_1 < \ldots < \lambda_n$ with corresponding linear independent eigenvectors $R = (r_1, \ldots, r_n)$. Due to the hyperbolicity, equation (4.1) can be rewritten to $(RU)_t + (RAR^{-1})(RU)_x = 0$. By setting $V = R^{-1}U$, one gets a decoupled system

$$\begin{cases} V_t + \Lambda V_x &= 0, \\ V(x,0) &= R^{-1}U_0(x), \end{cases} \tag{4.2}$$

where $\Lambda = \operatorname{diag}(\lambda_1, \ldots, \lambda_n)$. Now, every single component in (4.2) is a linear transport equation, i.e., $\partial_t V_i + \lambda_i \partial_x V_i = 0$, and solved through $V_i(x,t) = V_i(x - \lambda_i t, 0)$. The solution of our original problem (4.1) is then given by $U(x,t) = RV(x,t)$.

Now, consider piecewise constant initial data U_0 with a single discontinuity located in $x = 0$, i.e.,

$$U_0(x) = \begin{cases} U_L, & x < 0, \\ U_R, & x > 0. \end{cases} \tag{4.3}$$

Since, eigenvectors $R = (r_1, \ldots, r_n)$ form a basis in $\mathbb{R}^n$, the initial data (U_L, U_R) can be expressed as

$$U_L = \sum_{i=1}^{n} \alpha_i r_i = R\boldsymbol{\alpha}, \quad U_R = \sum_{i=1}^{n} \beta_i r_i = R\boldsymbol{\beta}.$$

with $\boldsymbol{\alpha} = \begin{pmatrix} \alpha_1 & \cdots & \alpha_n \end{pmatrix}^T$ and $\boldsymbol{\beta} = \begin{pmatrix} \beta_1 & \cdots & \beta_n \end{pmatrix}^T$. Therefore, problem (4.1) is solved through

$$U(x,t) = \sum_{i=1}^{n} \big(\beta_i H(x-\lambda_i t) + \alpha_i (1 - H(x-\lambda_i t))\big) r_i, \tag{4.4}$$

in which H stands for the Heaviside function

$$H(x) = \begin{cases} 0, & x < 0, \\ 1, & x \geq 1. \end{cases}$$

According to (4.4), the solution U is piecewise constant and self-similar, i.e., $U(x,t) = U(cx,ct)$, $c > 0$. As an illustrative example, consider (4.1) with coefficient matrix A given through

$$A = \begin{pmatrix} 1 & 2 \\ 2 & -2 \end{pmatrix}.$$

Then, the solution takes the form

$$U(x,t) = \frac{1}{5} \begin{pmatrix} -2 & 4 \\ 2 & 1 \end{pmatrix} \begin{pmatrix} (-\frac{U_{0,1}}{2} + 2U_{0,2})(x-\lambda_1 t) \\ (U_{0,1} + U_{0,2})(x-\lambda_2 t) \end{pmatrix} \tag{4.5}$$

where $U_0 = \begin{pmatrix} U_{0,1} & U_{0,2} \end{pmatrix}^T$. Equipped with piecewise constant initial data

$$U_0(x,t) = \begin{cases} \begin{pmatrix} \frac{1}{2} & -1 \end{pmatrix}^T, & x < 0 \\ \begin{pmatrix} -2 & 1 \end{pmatrix}^T, & x > 0 \end{cases}$$

expression (4.5) is illustrated in the x-t-plane in figure 7.

In (4.4), the intermediate states take the form

$$w_k = \sum_{i=1}^{k} \big(\beta_i H(x-\lambda_i t) + \alpha_i (1 - H(x-\lambda_i t))\big) r_i \tag{4.6}$$

and are separated by shock characteristics $x_i(t) = 0 + \lambda_i t$. Additionally, all occurring discontinuities satisfy the Rankine-Hugoniot condition (3.8), since

$$\begin{aligned} A(w_k - w_{k-1}) &= A\big(\big(\beta_k H(x-\lambda_k t) + \alpha_k (1 - H(x-\lambda_k t))\big) r_k\big) \\ &= \big(\beta_k H(x-\lambda_k t) + \alpha_k (1 - H(x-\lambda_k t))\big) \lambda_k r_k \\ &= \lambda_k (w_k - w_{k-1}). \end{aligned}$$

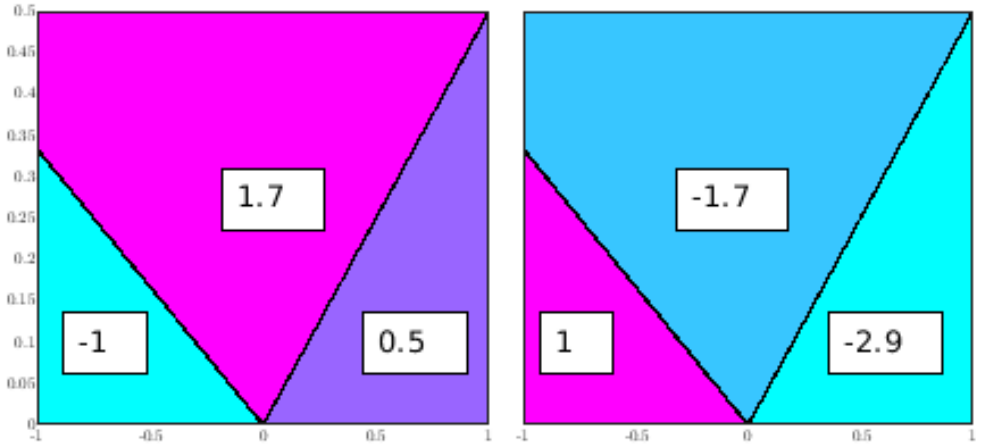

Figure 7: First and second component of U are depicted left and right respectively for $(x,t) \in [-1,1] \times [0,0.5]$. Both components are piecewise constant, in which the single plateaus are divided by characteristics $x(t) = \lambda_i t,\ i = 1,2$.

Concerning the nonlinear case, one recognizes self-similarity as well as piecewise constant intermediate states. But even more important, we will *construct* solutions to Riemann problems similar to (4.6). Furthermore, this becomes a handy tool, if nonlinear systems of hyperbolic partial differential equations at a junction are considered, compare sections 5-7.

4.2 Nonlinear Systems

In this subsection, we examine nonlinear homogeneous systems of hyperbolic partial differential equations

$$\begin{cases} U_t + F(U)_x &= 0, \\ U(x,0) &= U_0(x), \end{cases} \tag{4.7}$$

with $U : \mathbb{R} \times \mathbb{R}_+ \supseteq \Omega_x \times \Omega_t \to D \subseteq \mathbb{R}^n$, $F \in C^1(D;\mathbb{R}^n)$ and n distinct eigenvalues $\lambda_1 < ... < \lambda_n$. Since initial data $U_0 \in L^1(\Omega_x; D)$ does not need to be piecewise constant here, (4.7) is called *Cauchy* problem. These kind of problems are quit difficult to solve. Up to the current date, there are only two known algorithms, that show solvability, namely Glimm's *method of random choice* [26] and the *front tracking scheme* by Bressan [5]. For latter, we give a brief overview, since it is used for our main results in section 8. Key point in solving (4.7) is a piecewise approximation $\bar{U}_0 \in L^1(\Omega_x; D)$ of the initial data U_0, such that

$$TV\{\bar{U}_0\} \leq TV\{U_0\}, \tag{4.8}$$

with *total variation* TV defined through

$$TV\{U\} = \sup_{\{\xi_i\}_i \subset \Omega_x} \sum_i |U(\xi_{i+1}) - U(\xi_i)|.$$

Here, $\{\xi_i\}_i \subset \Omega_x$ is countable set, for which the sum of jumps in U, i.e., $\sum_i |U(\xi_{i+1}) - U(\xi_i)|$ takes its supreme value. Furthermore, we denote the set of all functions $U\colon \mathbb{R} \times \mathbb{R}^+ \to D$ with *bounded* total variation by $BV(\mathbb{R}^+; D) = \{TV(U(t)) < \infty\}$. In subsections 8.1, 8.3 and 8.4, property (4.8) becomes necessary.

Afterwards, problem (4.7) is equipped with $\bar{U}_0$, instead of U_0, and solved for all occurring *local* Riemann problems. In regard of *linear* systems on $\mathbb{R}$, solutions of Riemann problems have been constructed in the previous section. Under assumption $TV\{U_0\} < \delta$ for $\delta > 0$ suitable small as well as $\|U_0 - \bar{U}_0\|_{L^1} < \epsilon$, a series of Riemann solutions can be constructed for $\epsilon \to 0$, whose limit solves the Cauchy problem.

In section 5, we extend Riemann problems on $\mathbb{R}$ to Riemann problems at junctions.

A possible technique to achieve property (4.8) is the so called *finite volume approach*. Here, the real axis is divided into intervals first, i.e., $\mathbb{R} = \bigcup_{i\in\mathbb{Z}} I_i$ with $I_i = [x_{i-\frac{1}{2}}, x_{i+\frac{1}{2}}]$ and interval lengths $\Delta x_i = x_{i+\frac{1}{2}} - x_{i-\frac{1}{2}}$. Then, the initial data U_0 is approximated by its *cell volumes*, i.e.,

$$\bar{U}_{0,i} = \frac{1}{\Delta x} \int_{I_i} U_0(x)\, dx. \tag{4.9}$$

with $\bar{U}_{i,0} \to U_0,\ \Delta x_i \to 0$. For purpose of simplicity, we chose equidistant lengths $\Delta x_i = \Delta x,\ \forall i \in \mathbb{Z}$. Compare also figure 8 for an illustration of $\bar{U}$. Now, property (4.8) holds

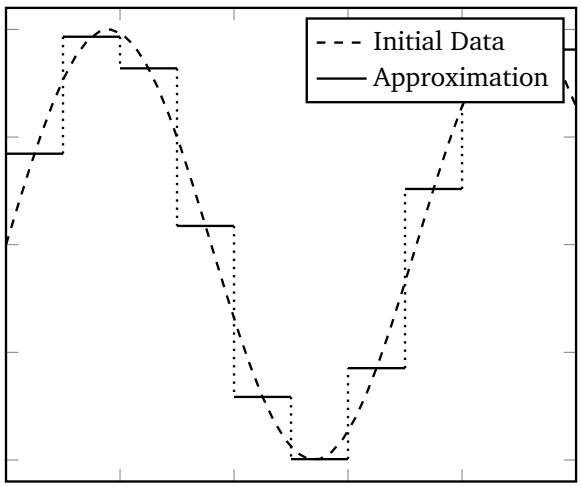

Figure 8: Approximation of initial data by the finite volume approach.

$$\begin{aligned} TV\{\bar{U}_{0,i}\} = \sum_{i\in\mathbb{Z}} |\bar{U}_{0,i+1} - \bar{U}_{0,i}| &\le \sum_{i\in\mathbb{Z}} \frac{1}{\Delta x} \int_{I_i} |U_0(x+\Delta x) - U_0(x)|\, dx \\ &\le \sup_{\{\xi_i\}_i} \sum_{i\in\mathbb{Z}} \frac{1}{\Delta x} \int_{I_i} |U_0(\xi_i+\Delta x) - U_0(\xi_i)|\, dx \\ &\le \sup_{\{\xi_i\}_i} \sum_{i\in\mathbb{Z}} |U_0(\xi_{i+1}) - U_0(\xi_i)| \\ &= TV(U_0), \end{aligned}$$

where $\{\xi_i\}_i \subset \Omega_x = \mathbb{R}$.

Since, the necessity of Riemann problems to Cauchy problems has been made clear, former problems are investigated in more detail next.

4.2.1 Riemann Problem for Nonlinear Partial Differential Systems in One Space Dimension

In this subsection, some theory will be given, regarding Riemann problems in the nonlinear system case, i.e., equation (4.7) equipped with initial data

$$U_0(x) = \begin{cases} U_L, & x < 0, \\ U_R, & x > 0. \end{cases} \tag{4.10}$$

Afterwards, all presented techniques are applied to models $(\mathscr{E}_1)$-$(\mathscr{E}_3)$ in context of (4.10).

The basic idea in solving (4.7) equipped with (4.10), is to find all states U which are entropy admissible connected to U_L and U_R by a parametrization, i.e.,

$$\begin{aligned} U_1(\sigma_1) &= U(\sigma_1, U_L), \\ U_2(\sigma_2) &= U(\sigma_2, U_R) \end{aligned}$$

such that U_1 and U_2 fulfill condition (3.14). Afterwards, the intersection of both parameterizations, i.e., $U = U_1(\sigma_1) = U_2(\sigma_2)$ solves the Riemann problem.

In section 3, we already discovered the Rankine-Hugoniot condition (3.8), namely

$$F(U_L) - F(U_R) = \sigma(U_L - U_R),$$

which has to be satisfied at discontinuities. By letting $U = U_R$ *variable*, (3.8) has $n+1$ variables and n equations. Consequently, a parametrization might result from this expression.

Theorem 4.1. *For U sufficiently close to U_L, there exists n distinct one-parameter curves $U = U_k(\sigma), k = 1, ..., n$, which fulfill the Rankine-Hugoniot condition* (3.8).

Proof. An application of the implicit function theorem states the proof, see [43, section 17 §B]. □

One proceeds analogously to $U = U_L$, connected to the state U_R. As we have already seen in the scalar case, a solution, which consists of a shock only, might violate the entropy condition (3.14). There, a rarefaction wave was the correct entropy solution, see subfigures 6a and 6c. Consequently, it arises the question, if a rarefaction wave is parameterizable as well.

We want to remind, that the Jacobian JF in (4.7), is assumed to possess n distinct eigenvalues $\lambda_1 < ... < \lambda_n$. Let the corresponding eigenvectors be denoted by $r_1, ..., r_n$. Now, we suppose $U(x,t) = V(x/t) = V(\xi)$ with $\xi = x/t$ to be an one-parameter solution of (4.7). This approach is motivated by the rarefaction wave (3.10) in section 3. For $t > 0$ we observe

$$0 = U_t + F(U)_x = \frac{1}{t}\left(-\xi + JF(V)\right)V'. \tag{4.11}$$

Equation (4.11) holds true, if V is an integral curve of eigenvector r_k, i.e.,

$$V'(\xi) = c(\xi) r_k(V(\xi)),\ c(\xi) \in \mathbb{R} \setminus \{0\}. \tag{4.12}$$

Then ξ corresponds to the k-th eigenvalue, i.e.,

$$\xi = \lambda_k(V(\xi)). \tag{4.13}$$

Differentiation of (4.13) by ξ results in

$$0 = 1 - \nabla\lambda_k(V(\xi))V'(\xi) = 1 - c(\xi)\nabla\lambda_k(V(\xi)) \cdot r_k(V(\xi)) \tag{4.14}$$

Consequently, the self-similar function $V(\xi)$ is indeed a solution to (4.7), if it fulfills (4.12) as well as (4.14). This motivates the following definition.

Definition 4.2. *The k-th eigenvalue λ_k is called genuinely nonlinear if $\nabla\lambda_k \cdot r_k \neq 0$. Otherwise, λ_k is linearly degenerated.*

Accordingly, if λ_k is genuinely nonlinear, the solution of problem

$$\begin{cases} V'(\xi) &= r_k(V(\xi)), \\ V(\lambda_k(U_L)) &= U_L, \\ \xi &> \lambda_k(U_L) \end{cases} \tag{4.15}$$

gives an one-parameter solution $U(x,t) = V(x/t)$, $\xi = x/t$, to problem (4.7) in appearance of a rarefaction wave. Obviously, both conditions, (4.12) and (4.14), are included into (4.15).

Unfortunately, the solution of (4.15) itself does not give a parametrization yet, such that all feasible states are connectible to U_L or U_R. Here, the following definition becomes useful.

Definition 4.3. *A C^1 function w is a k-Riemann invariant, if it solves*

$$r_k(U) \cdot \nabla w(U) = 0 \tag{4.16}$$

for all U in a neighborhood of U_L or U_R.

We want to remark, that these Riemann invariants do not necessarily exist. Now, let w be a k-Riemann invariant, then for all integral curves V of r_k it holds

$$\frac{d}{d\xi} w(V(\xi)) = \nabla w(\xi) \cdot V'(\xi) = \nabla w(V(\xi)) \cdot r_k(V(\xi)) = 0.$$

Therefore, w is constant on $V(\xi) = U(x,t)$, and forms our desired parametrization since $w(U_L) = w(U)$. Motivated by this observation, we pose our next definition.

Definition 4.4 (Solution in the k-th field)**.** *Consider a system of hyperbolic partial differential equations*

$$U_t + F(U)_x = 0$$

with $U : \mathbb{R}\times\mathbb{R}_+ \supseteq \Omega_x \times \Omega_t \to D \subseteq \mathbb{R}^n$, $F \in C^1(D;\mathbb{R}^n)$ *and eigenvalues* $\lambda_1 < \ldots < \lambda_n$ *genuinely nonlinear. Let* $U \in C^1$ *be a solution in domain* $D \subset \mathbb{R}^n$*, and suppose that all k-Riemann invariants are constant in D. Then* $U(\sigma)$ *is called k-rarefaction wave. Additionally,* $U(\sigma)$ *is a k-shock wave, if it fulfills the Rankine-Hugoniot condition* (3.8)*, i.e.,*

$$\sigma(U(\sigma-) - U(\sigma+)) = F(U(\sigma-)) - F(U(\sigma+))$$

and there exists a λ_k*, such that*

$$\begin{aligned} \lambda_k(U(\sigma+)) &< \sigma < \lambda_{k+1}(U(\sigma+)) \\ \lambda_{k-1}(U(\sigma-)) &< \sigma < \lambda_k(U(\sigma+)) \end{aligned}$$

according to (3.14).

Proposition 4.5. *As far as* $r_k(U)\cdot\nabla w(U) = 0$ *is solvable, there are* $(n-1)$ *k-Riemann invariants, whose gradients are linear independent.*

Proof. [43, Section 17 §B, Prop. 17.2]. □

And in regard of the rarefaction waves' geometry, it holds the next theorem.

Theorem 4.6. *Let* U *be a k-rarefaction wave in domain* $D \subseteq \mathbb{R}^n$*. Then the characteristics, i.e.,* $x(t)$ *such that* $\frac{d}{dt}U(t,x(t)) \equiv c$*, are straight lines. Furthermore, the characteristic speed* $\dot{x}$ *is given through*

$$\lambda_k(U_L) \le \dot{x}(t) = \lambda_k(V(\xi)) \le \lambda_k(U_R).$$

Proof. [43, Section 17 §B, Theorem 17.5] and [5, Sect. 5.1]. □

Accordingly, rarefaction waves for systems have the same structure as in the scalar case, see figure 6c.

If the characteristic is linear degenerated, rarefaction and shock coincide and the resulting solution is a transported discontinuity, which is also called *contact discontinuity* or *contact wave*, see figure 9. The complete solution to a Riemann problem can be summarized in the next theorem.

Theorem 4.7. *Consider a system of hyperbolic partial differential equations*

$$U_t + F(U)_x = 0$$

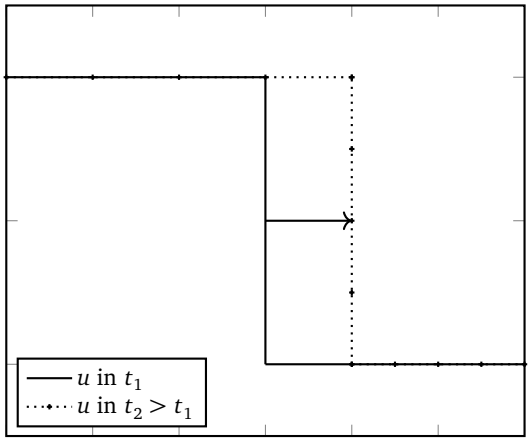

Figure 9: Contact discontinuity.

with $U\colon \mathbb{R}\times\mathbb{R}_+ \supseteq \Omega_x\times\Omega_t \to D\subseteq\mathbb{R}^n$, $F\in C^1(D;\mathbb{R}^n)$ *and eigenvalues* $\lambda_1 < \ldots < \lambda_n$, *which are either genuinely nonlinear or linearly degenerated. Assume initial condition*

$$U(0,x) = \begin{cases} U_L, & x<0,\\ U_R, & x>0. \end{cases}$$

If λ_k *is genuinely nonlinear, then solution* U_k *in the k-field is given by*

$$U_k(\sigma) = \begin{cases} U_k^S(\sigma), & \sigma\le 0,\\ U_k^R(\sigma), & \sigma\ge 0, \end{cases}$$

where U_k^S *and* U_k^R *are k-th shock and rarefaction wave, respectively. Furthermore,* $U_k(\sigma)$ *is continuously differentiable in* σ. *If* λ_k *is linear degenerated, then the k-th field solution is a contact discontinuity* $U_k(\sigma)$ *with speed* $\sigma = \lambda_k(U_L) = \lambda(U_R)$.

Proof. Theorems 17.9, 17.14 and 17.15 in [43, Sect. 17 §B]. □

In the next subsection, we give a brief derivation of all above curves for models $(\mathscr{E}_2)$ and $(\mathscr{E}_3)$ following [45, Sect. 4] and [43, Sect. 17 §B]. For model $(\mathscr{E}_1)$, these derivatives are more involved, see [45, Sect. 3.1], and will be skipped here.

4.2.2 Application to Gas Models

We like to begin with the simplified isentropic model ($\mathscr{E}_3$) and take therefore a closer look to a more general model, a variant of the so called p-system with Riemann data, i.e.,

$$\begin{cases} u_t + v_x &= 0, \\ v_t + p(u)_x &= 0, \\ y(x,0) &= \begin{cases} y_L, & x < 0 \\ y_R, & x > 0 \end{cases} \end{cases} \tag{4.17}$$

in which $y = (u, v)^T$, $p' > 0$ and $p'' > 0$. Consequently, model ($\mathscr{E}_3$) is a special case of (4.17). The p-system in the literature is slightly different, see for example [43, Sect. 17 §A], [5, Sect. 5.4], [33, Sect. 2.14]. Therefore, we derive contact wave, shock and rarefaction curves of (4.17), as far as existent, analogously to [43, Sect. 17 §A].

In (4.17), the flux function F is identified by $F(y) = (v, p(u))^T$. Its Jacobian reads

$$JF(y) = \begin{pmatrix} 0 & 1 \\ p'(u) & 0 \end{pmatrix},$$

which has two distinct eigenvalues $\lambda_1 = -\sqrt{p'}$, $\lambda_2 = \sqrt{p'}$ with corresponding eigenvectors $r_1 = (-1/\sqrt{p'}, 1)^T$ and $r_2 = (1/\sqrt{p'}, 1)^T$, respectively. According to definition 4.2, both eigenvalues are genuinely nonlinear, since

$$\nabla\lambda_k \cdot r_k = \left(\mp\tfrac{1}{2}\tfrac{p''}{\sqrt{p'}} \quad 0\right)^T \cdot \left(\mp\tfrac{1}{\sqrt{p'}} \quad 1\right)^T = \frac{1}{2}\frac{p''}{p'} > 0,\ k = 1, 2.$$

Therefore, the solution consists of shock and rarefaction waves only, which are constructed next.

In regard of the left state y_L, the Rankine-Hugoniot condition (3.8) reads

$$\begin{aligned} \sigma(u - u_L) &= (v - v_L) \\ \sigma(v - v_L) &= (p(u) - p(u_L)) \end{aligned} \tag{4.18}$$

and can be transformed to

$$v = v_L \pm \sqrt{(u - u_L)(p(u) - p(u_L))}. \tag{4.19}$$

Referring to model ($\mathscr{E}_3$), this becomes

$$q = q_L \pm \sqrt{(\rho - \rho_L)(p(\rho) - p(\rho_L))}. \tag{4.20}$$

Later, it will be shown whether plus or minus sign has to be taken in (4.19), respectively (4.20).

Now, we come to the rarefaction wave. The 1-Riemann invariant w can be received by solving $r_1 \cdot \nabla w = 0$, see (4.16), and reads

$$-\frac{w_u}{\sqrt{p'}} + w_v = 0. \tag{4.21}$$

From (4.21), one concludes $w_u = \sqrt{p'}$, $w_v = 1$. Integration results in $w = \int_{u_L}^{u} \sqrt{p'(s)} ds + C_1(v)$ as well as $w = v - v_L + C_2(u)$. By comparing both expressions and the fact, that $w(u,v) \equiv c \in \mathbb{R}$, it follows

$$v(u) = v_L(u) - \int_{u_L}^{u} \sqrt{p'(s)}\, ds + c. \tag{4.22}$$

However, a one-parameter continuously differentiable solution, according to theorem 4.7, can be achieved only, if $c = 0$. This becomes clear in proposition 4.8 later on.

From proposition 4.5, we conclude, that (4.22) is the only 1-Riemann invariant. Under consideration of model $(\mathscr{E}_3)$, the rarefaction wave becomes

$$q(\rho) = q_L - \frac{2\sqrt{\gamma}}{\gamma+1}\left(\rho^{\frac{\gamma-1}{2}} - \rho_L^{\frac{\gamma-1}{2}}\right). \tag{4.23}$$

Analogously, the 2-Riemann invariant reads

$$q(\rho) = q_R + \frac{2\sqrt{\gamma}}{\gamma+1}\left(\rho^{\frac{\gamma-1}{2}} - \rho_R^{\frac{\gamma-1}{2}}\right). \tag{4.24}$$

Now, we have to determine the sign in (4.19), and distinguish between shock and rarefaction parametrization in dependence of ρ. Let $\sigma \in \mathbb{R}$ denote the shock speed from the Rankine-Hugoniot condition (3.8). Then, by entropy condition (3.14) , it follows for the left parametrization

$$\sigma < \lambda_1(y_L), \quad \lambda_1(y) < \sigma < \lambda_2(y).$$

Consequently, it must hold

$$\lambda_1(y) < \sigma < \lambda_1(y_L) \Rightarrow -\sqrt{p'(v)} < -\sqrt{p'(v_L)},$$

and since $p'' > 0$, it follows $v > v_L$. Accordingly, in the first equation of (4.18) combined with $v > v_L$, we conclude $u > u_L$ and the plus sign in (4.19) has to be taken.

If $v \leq v_L$, the rarefaction parametrization (4.23) has to be considered. All derivatives are done analogously in regard of the right parametrization connecting y_R.

Overall, the complete parametrization of model $(\mathscr{E}_3)$ is given through

$$q(\rho) = q_L - \theta^{\mathscr{E}_3}(\rho, U_L) = q_R + \theta^{\mathscr{E}_3}(\rho, U_R), \tag{4.25}$$

with

$$\theta^{\mathscr{E}_3}(\rho,\bar{U}) = \begin{cases} \frac{2\sqrt{\gamma}}{\gamma+1}\left(\rho^{\frac{\gamma+1}{2}} - \bar{\rho}^{\frac{\gamma+1}{2}}\right) & \text{if } \rho \le \bar{\rho} \text{ (rarefaction)}, \\ \sqrt{(\rho-\bar{\rho})(\rho^\gamma - \bar{\rho}^\gamma)} & \text{if } \rho > \bar{\rho} \text{ (shock)}. \end{cases} \tag{4.26}$$

Now, all entropic states are described by functions

$$U = \mathscr{L}_1^{\mathscr{E}_3}(\sigma, U_L) = \begin{pmatrix} \sigma \\ q_L - \theta^{\mathscr{E}_3}(\sigma, U_L) \end{pmatrix}, \qquad U = \mathscr{L}_2^{\mathscr{E}_3}(\sigma, U_R) = \begin{pmatrix} \sigma \\ q_R + \theta^{\mathscr{E}_3}(\sigma, U_R) \end{pmatrix}, \tag{4.27}$$

which will be called *Lax curves* from now on, see [12, 18, 32]. In (4.27), density ρ has been replaced by a more general variable $\sigma \in \mathbb{R}$. The intersection of both curves form the unique entropic solution of a Riemann problem, see also figure 10 for an illustration.

Proposition 4.8. *Lax curves* (4.25) *of the simplified isentropic model* ($\mathscr{E}_3$) *are continuously differentiable in* $\sigma \in \mathbb{R}$.

Proof. It suffices to show, that $\theta^{\mathscr{E}_3}(\sigma,\bar{U})$ is continuous differentiable and since shock and rarefaction parametrization are both compositions of C^1-functions, we only need to prove

$$\lim_{\sigma\to\bar{\rho}-} \partial_\sigma\left[\theta^{\mathscr{E}_3}(\sigma,\bar{U})\right] = \lim_{\sigma\to\bar{\rho}+} \partial_\sigma\left[\theta^{\mathscr{E}_3}(\sigma,\bar{U})\right].$$

In regard of the rarefaction wave, one receives $\partial_\sigma\theta^{\mathscr{E}_3}(\sigma,\bar{U}) = \sqrt{\gamma}\sigma^{\frac{\gamma-1}{2}}$ and therefore $\lim_{\sigma\to\bar{\rho}+}\sqrt{\gamma\bar{\rho}^{\gamma-1}}$. For the shock parametrization it holds

$$\begin{aligned} \partial_\sigma\theta^{\mathscr{E}_3}(\sigma,\bar{U}) &= \frac{(\sigma^\gamma - \bar{\rho}^\gamma) + (\sigma-\bar{\rho})\sigma^{\gamma-1}\gamma}{2\sqrt{(\sigma-\bar{\rho})(\sigma^\gamma-\bar{\rho}^\gamma)}} \\ &= \frac{1}{2}\sqrt{\frac{\sigma^\gamma-\bar{\rho}^\gamma}{\sigma-\bar{\rho}}} + \frac{1}{2}\gamma\sigma^{\gamma-1}\frac{1}{\sqrt{\frac{\sigma^\gamma-\bar{\rho}^\gamma}{\sigma-\bar{\rho}}}} \\ &\xrightarrow[\sigma\to\bar{\rho}-]{} \frac{1}{2}\sqrt{\gamma\bar{\rho}^{\gamma-1}} + \frac{1}{2}\gamma\bar{\rho}^{\gamma-1}\frac{1}{\sqrt{\gamma\bar{\rho}^{\gamma-1}}} \\ &= \sqrt{\gamma\bar{\rho}^{\gamma-1}}, \end{aligned}$$

which shows continuity of both derivatives in $\sigma = \bar{\rho}$. □

The 1- and 2-Lax curve of model ($\mathscr{E}_2$) can be found in [12, 11, 38], and are provided by

$$U = \mathscr{L}_1^{\mathscr{E}_2}(\sigma, U_L) = \begin{pmatrix} \sigma \\ u_L\sigma - \theta^{\mathscr{E}_2}(\sigma, U_L) \end{pmatrix}, \qquad U = \mathscr{L}_2^{\mathscr{E}_2}(\sigma, U_R) = \begin{pmatrix} \sigma \\ u_R\sigma + \theta^{\mathscr{E}_2}(\sigma, U_R) \end{pmatrix}, \tag{4.28}$$

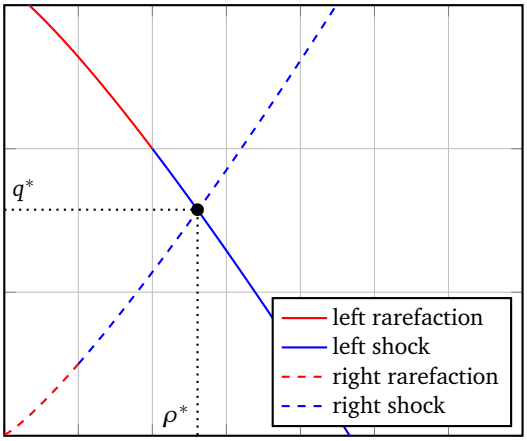

Figure 10: Lax curves of model $(\mathscr{E}_3)$ and their intersection (q^*, ρ^*) for velocities $u_L = 2, u_R = 1$ and densities $\rho_L = 2, \rho_R = 1$.

with

$$\theta^{\mathscr{E}_2}(\sigma, \bar{U}) = \begin{cases} \frac{2\sqrt{\gamma}}{\gamma-1}\sigma\left(\sigma^{\frac{\gamma-1}{2}} - \bar{\rho}^{\frac{\gamma-1}{2}}\right) & \text{if } \sigma \le \bar{\rho} \text{ (rarefaction)}, \\ \sqrt{\sigma/\bar{\rho}(\sigma-\bar{\rho})(\sigma^\gamma - \bar{\rho}^\gamma)} & \text{if } \sigma > \bar{\rho} \text{ (shock)}. \end{cases} \tag{4.29}$$

A schematic presentation of the self-similar solutions to $(\mathscr{E}_2)$ and $(\mathscr{E}_3)$ with Riemann data, are given in figure 11. An intersection of both Lax curves form the unique intermediate entropic solution $U_*^{\mathscr{E}_k}$, $k =$

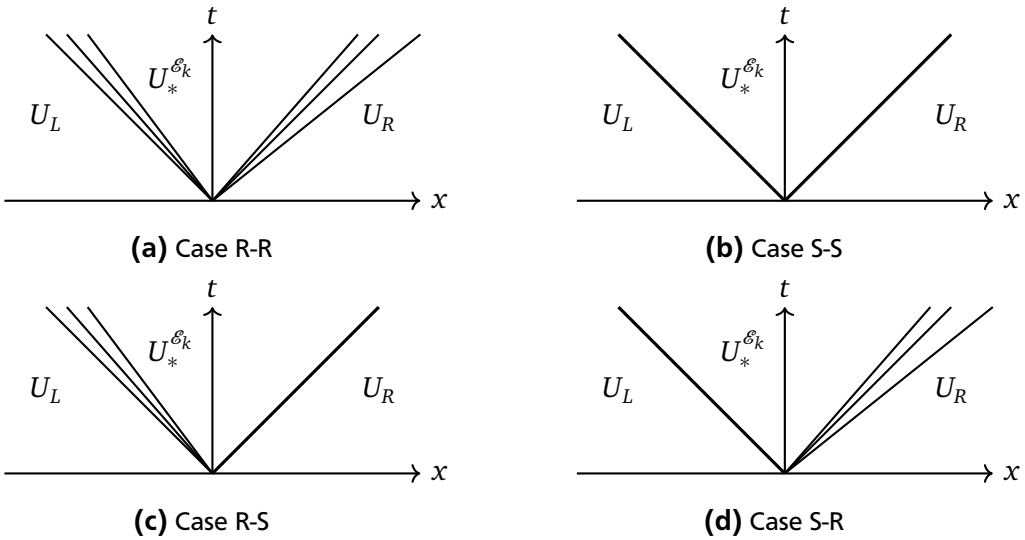

(a) Case R-R **(b)** Case S-S

(c) Case R-S **(d)** Case S-R

Figure 11: Possible wave patterns in the solution of Riemann problems for the isotropic and simplified isotropic Euler equations: shock (S) and rarefaction (R).

2, 3 of the Riemann problem, see also figure 12.

Since we have not found any derivation of (4.28) in the literature above or references therein, this will be done here.

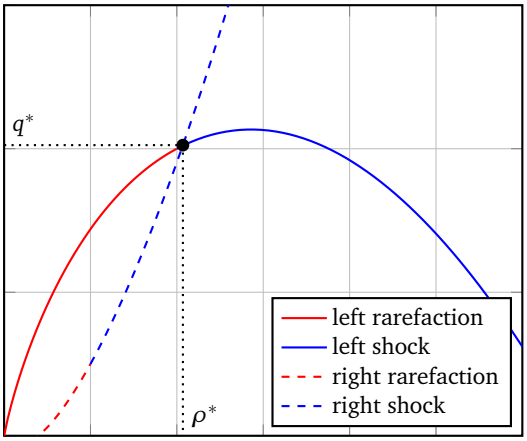

Figure 12: Lax curves of model $(\mathscr{E}_2)$ and their intersection (q^*, ρ^*) for velocities $u_L = 2, u_R = 1$ and densities $\rho_L = 2, \rho_R = 1$.

Eigenvalues of model $(\mathscr{E}_2)$ are given by $\lambda_1^{\mathscr{E}_2} = u - c$, $\lambda_2^{\mathscr{E}_2} = u + c$ with corresponding eigenvectors $r_1^{\mathscr{E}_2} = (-u/(c^2-u^2) - c/(c^2-u^2), 1)^T$ and $r_2^{\mathscr{E}_2} = (-u/(c^2-u^2) + c/(c^2-u^2), 1)^T$, see section 2. Referring to definition 4.2, both eigenvalues are genuinely nonlinear, since

$$\nabla \lambda_k^{\mathscr{E}_2} \cdot v_k^{\mathscr{E}_2} = \frac{cu}{\rho(c^2-u^2)} > 0, \; k = 1, 2.$$

Accordingly, a solution consists of shock and rarefaction waves only, which are constructed next.

First, the Rankine-Hugoniot condition (3.8) for the left state is formulated

$$\begin{aligned} \sigma(\rho - \rho_l) &= q - q_L \\ \sigma(q - q_L) &= (q^2/\rho + p(\rho) - q_L^2/\rho_L^2 - p(\rho_L)). \end{aligned} \tag{4.30}$$

From (4.30), we conclude

$$\begin{aligned} (q-q_L)^2 &= (\rho-\rho_L)\left(\frac{q^2}{\rho} - \frac{q_L^2}{\rho_L}\right) + (\rho-\rho_L)(p(\rho)-p(\rho_L)), \\ \Leftrightarrow (q-q_L)^2 - (\rho-\rho_L)\left(\frac{q^2}{\rho} - \frac{q_L^2}{\rho_L}\right) &= (\rho-\rho_L)(p(\rho)-p(\rho_L)), \\ \Leftrightarrow \frac{\rho_L}{\rho}\left(q - q_L\frac{\rho}{\rho_L}\right)^2 &= (\rho-\rho_L)(p(\rho)-p(\rho_L)), \end{aligned}$$

which is equivalent to

$$q(\rho) = u_L\rho \pm \sqrt{\rho/\rho_L(\rho-\rho_L)(p(\rho)-p(\rho_L))}. \tag{4.31}$$

The correct sign is again given by an utilization of (3.14) and will be determined later on in more detail.

Now, the rarefaction wave is derived. In order to receive the Riemann invariants w_1 and w_2, the following expressions have to be solved

$$\nabla w_k \cdot v_k^{\mathscr{E}_2} = 0,\ k = 1,2, \tag{4.32}$$

according to (4.16). Here, this will be done for w_1 only, since all derivations are analog for w_2. Equation (4.32) reads in more detail

$$w_\rho / \lambda_1^{\mathscr{E}_2} + w_q = 0. \tag{4.33}$$

Our first suggestion is $w_\rho = \lambda_1$ and $w_q = -1$. But since, this is not integratable, a multiplication of (4.33) with $1/\rho > 0$ becomes necessary and leads to $w_\rho = \lambda_1/\rho$, $w_q = 1/\rho$. Subsequently, the potential w is given through integration

$$c \equiv w = \int_{\rho_l}^{\rho} \lambda_1(s,q)\, ds + C(q) = q\left(\frac{1}{\rho} - \frac{1}{\rho_L}\right) - \frac{2\sqrt{\gamma}}{\gamma - 1}\left(\rho^{\frac{\gamma-1}{2}} - \rho_L^{\frac{\gamma-1}{2}}\right) + C(q).$$

The function $C(t)$ is determined by $w_q \overset{!}{=} 1/\rho$, and reads $C(q) = -q/\rho_L$. Again, a one-parameter continuously differentiable solution, based on theorem 4.7, can be achieved only, if $c = 0$. This becomes clear in proposition 4.9. Altogether, potential w reads

$$w = -\frac{q}{\rho} + \frac{q_L}{\rho_L} - \frac{2\sqrt{\gamma}}{\gamma - 1}\left(\rho^{\frac{\gamma-1}{2}} - \rho_L^{\frac{\gamma-1}{2}}\right) = 0$$

and can be rearranged to

$$q(\rho) = \frac{q_L}{\rho_L}\rho - \frac{2\sqrt{\gamma}}{\gamma - 1}\rho\left(\rho^{\frac{\gamma-1}{2}} - \rho_L^{\frac{\gamma-1}{2}}\right).$$

For the right state U_R, we get analogously

$$q(\rho) = \frac{q_R}{\rho_R}\rho + \frac{2\sqrt{\gamma}}{\gamma - 1}\rho\left(\rho^{\frac{\gamma-1}{2}} - \rho_R^{\frac{\gamma-1}{2}}\right).$$

In appearance of a shock wave, connecting the left state U_L, it must hold

$$\sigma < \lambda_1^{\mathscr{E}_2}(U_L), \quad \lambda_1^{\mathscr{E}_2}(U) < \sigma < \lambda_2^{\mathscr{E}_2}(U).$$

referring to (3.14). Consequently, we receive $\lambda_1^{\mathscr{E}_2}(U) < \lambda_1^{\mathscr{E}_2}(U_L)$, i.e., $u(\rho) - c(\rho) < u(\rho_L) - c(\rho_L)$. Since, $u(\rho) = q(\rho)/\rho$ and $c(\rho) = \sqrt{\gamma\rho^{\gamma-1}}$, one concludes, by an utilization of (4.31), that

$$\pm\sqrt{\frac{1}{\rho\rho_L}(\rho - \rho_L)(\rho^\gamma - \rho_L)^\gamma} + \sqrt{\gamma\rho^{\gamma-1}} > \sqrt{\gamma\rho_L^{\gamma-1}},$$

which is fulfilled by taking the plus sign and $\rho > \rho_L$ only. Furthermore, in presence of a rarefaction wave, connecting left state U_L, we conclude $\rho \leq \rho_L$. This shows (4.28).

Proposition 4.9. *Lax curves* (4.28) *of isentropic model* ($\mathscr{E}_2$) *are continuously differentiable in* $\sigma \in \mathbb{R}$.

Proof. It suffices to show, that $\theta^{\mathscr{E}_2}(\sigma, \bar{U})$ is continuous differentiable. And since shock and rarefaction parametrization are both compositions of C^1 functions, we only need to prove

$$\lim_{\sigma \to \bar{\rho}-} \partial_\sigma \left[\theta^{\mathscr{E}_2}(\sigma, \bar{U})\right] = \lim_{\sigma \to \bar{\rho}+} \partial_\sigma \left[\theta^{\mathscr{E}_3}(\sigma, \bar{U})\right].$$

In regard of the rarefaction, one receives $\partial_\sigma \theta^{\mathscr{E}_2}(\sigma, \bar{U}) = \sqrt{\gamma}\sigma^{\frac{\gamma-1}{2}}$ and therefore $\lim_{\sigma\to\bar{\rho}+} \sqrt{\gamma\bar{\rho}^{\gamma-1}}$. For the shock parametrization we have

$$\begin{aligned}\partial_\sigma \theta^{\mathscr{E}_2}(\sigma, \bar{U}) &= \frac{2\sigma - \bar{\rho}}{2\sqrt{\sigma\bar{\rho}}}\sqrt{\frac{\sigma^\gamma - \bar{\rho}^\gamma}{\sigma - \bar{\rho}}} + \frac{\gamma\sigma^\gamma}{2\sqrt{\sigma\bar{\rho}}}\frac{1}{\sqrt{\frac{\sigma^\gamma - \bar{\rho}^\gamma}{\sigma - \bar{\rho}}}} \\ &\xrightarrow{\sigma\to\bar{\rho}+} \frac{1}{2}\sqrt{\gamma\bar{\rho}^{\gamma-1}} + \frac{\gamma\bar{\rho}^{\gamma-1}}{2}\frac{1}{\sqrt{\gamma\bar{\rho}^{\gamma-1}}} = \sqrt{\gamma}\bar{\rho}^{\frac{\gamma-1}{2}}.\end{aligned}$$

□

Considering the full Euler equations ($\mathscr{E}_1$), the set of waves is extended by a contact discontinuity, which is located as middle wave, see figure 13. Thus, a solution is separated into four states $(U_L, U_{L*}, U_{R*}, U_R)$.

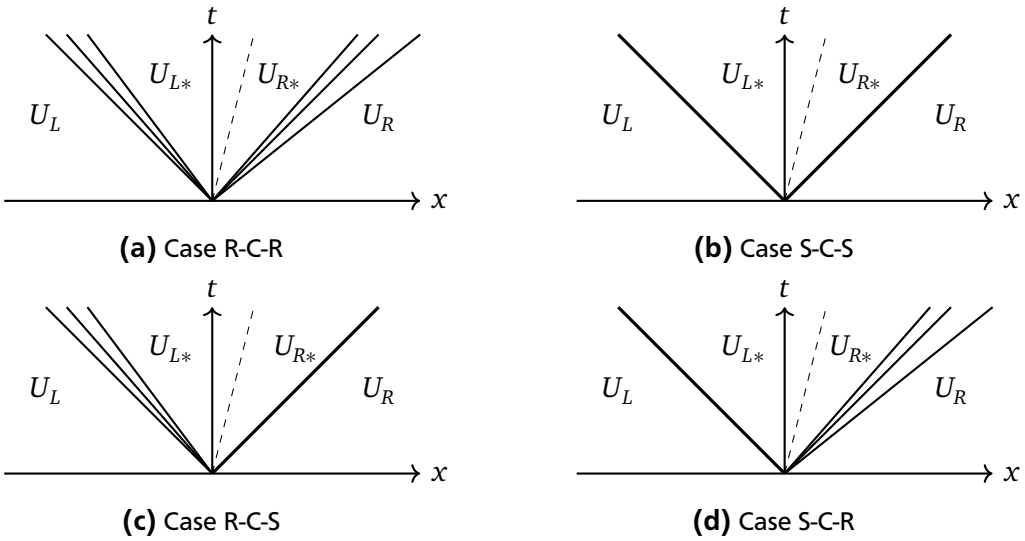

(a) Case R-C-R **(b)** Case S-C-S

(c) Case R-C-S **(d)** Case S-C-R

Figure 13: Possible wave patterns in the solution of Riemann problems for the full Euler equations: shock (S), contact (C) and rarefaction (R).

Velocity and pressure are constant across the contact discontinuity, i.e.,

$$p_* = p_{L*} = p_{R*} \quad \text{and} \quad u_* = u_{L*} = u_{R*} \tag{4.34}$$

and accordingly 2-Riemann invariants, see [45, Sect. 3.1]. Similar to models ($\mathscr{E}_2$) and ($\mathscr{E}_3$), the four sought variables $(p_*, u_*, \rho_{L*}, \rho_{R*})$ are again implicitly defined by means of parametrization, see [45, Sect. 4] or [33, Sect. 14.11] for more details. It follows

$$u_* = u_L - \psi(p_*, U_L) = u_R + \psi(p_*, U_R), \tag{4.35}$$

$$\rho_{L*} = \phi(p_*, U_L), \quad \rho_{R*} = \phi(p_*, U_R), \tag{4.36}$$

where for $k = L, R$

$$\psi(p_*, U_k) = \begin{cases} \frac{2c_k}{\gamma-1}\left(\left(\frac{p_*}{p_k}\right)^{\frac{\gamma-1}{2\gamma}} - 1\right) & \text{if } p_* \le p_k \text{ (rarefaction)} \\ (p_* - p_k)\left(\frac{1-\mu^2}{\rho_k(p_*+\mu^2 p_k)}\right)^{\frac{1}{2}} & \text{if } p_* > p_k \text{ (shock)} \end{cases} \tag{4.37a}$$

$$\phi(p_*, U_k) = \begin{cases} \rho_k\left(\frac{p_*}{p_k}\right)^{\frac{1}{\gamma}} & \text{if } p_* \le p_k \text{ (rarefaction)} \\ \rho_k \frac{p_*+\mu^2 p_k}{\mu^2 p_* + p_k} & \text{if } p_* > p_k \text{ (shock)} \end{cases} \tag{4.37b}$$

with $\mu^2 = (\gamma-1)/(\gamma+1)$ and $c_k^2 = \gamma p_k/\rho_k$. Then, the Lax curves read

$$\mathscr{L}_1^{\mathscr{E}_1}(\sigma, U_L) = \begin{pmatrix} \phi(\sigma, U_L) \\ \phi(\sigma, U_L)(u_L - \psi(\sigma, U_L)) \\ \frac{\sigma}{\gamma-1} + \frac{1}{2}\phi(\sigma, U_L)(u_L - \psi(\sigma, U_L))^2 \end{pmatrix}, \tag{4.38a}$$

$$\mathscr{L}_2^{\mathscr{E}_1}(\tau, \bar{U}) = \bar{U} + \tau\left(1, \bar{u}, \frac{1}{2}\bar{u}^2\right)^T, \tag{4.38b}$$

$$\mathscr{L}_3^{\mathscr{E}_1}(\sigma, U_R) = \begin{pmatrix} \phi(\sigma, U_R) \\ \phi(\sigma, U_R)(u_R + \psi(\sigma, U_R)) \\ \frac{\sigma}{\gamma-1} + \frac{1}{2}\phi(\sigma, U_R)(u_R + \psi(\sigma, U_R))^2 \end{pmatrix}. \tag{4.38c}$$

Remark 4.10. *If an equation of state for real gases is considered, it becomes unclear, whether all required Riemann invariants exists. However, one can also use approximated Riemann solvers, that solely rely on Rankine-Hugoniot condition* (3.8)*, see for example [33, Sect. 15.3], [45, Sect. 11] and [27]. In the latter literature, approximate Riemann solvers for the full Euler equations* ($\mathscr{E}_1$) *equipped with real gases are constructed. But without further treatment, these approximated Riemann solvers can produce unphysical solutions, see [45, Sect. 9.6 & 10.9].*

In our next section, we introduce the Cauchy and Riemann problem at the junction and pose our novel set of coupling conditions, which ensure mass and energy conservation as well as the ability to couple the full Euler equations at a junction. Furthermore, well-posedness of the Riemann problem is proven by an utilization of the Lax-curves of this section.

5 The Euler Equations at the Junction

In this section, out coupling conditions for the full Euler equations ($\mathscr{E}_1$) on networks with a single junction are introduced. Here, we follow the work of Lang and Mindt in [32]. If the source term is neglected, i.e., homogeneity is assumed, these coupling conditions ensure mass and energy conservation on the network. Furthermore, we introduce the generalized homogeneous Riemann problem at the junction and state its well-posedness. For this purpose, we utilize the same techniques as in Colombo and Mauri [18], Reigstadt [38], Colombo, Guerra, Herty and Schleper [16], as well as Lang and Mindt in [32], i.e., all involved states in our couplings conditions are described through Lax curves. Afterwards, the occurring mapping is proven to be well-posed by an application of the implicit function theorem.

Then, in subsections 8.3 and 8.4, these results are extended to ($\mathscr{E}_1$) with Cauchy data and non-trivial source term $G \not\equiv 0$, respectively.

Similar to the literature [11, 12, 16, 18, 28, 32, 38], we restrict our analysis to networks with finitely many pipes and the region of subsonic flow, i.e., $|u| < c$. Latter is described by domains

$$D_- = \{U = (\rho, \rho u, E) \in \mathring{\mathbb{R}}^+ \times \mathbb{R} \times \mathring{\mathbb{R}}^+ \colon \lambda_1(U) < \lambda_2(U) < 0 < \lambda_3(U)\}, \tag{5.1}$$

$$D_+ = \{U = (\rho, \rho u, E) \in \mathring{\mathbb{R}}^+ \times \mathbb{R} \times \mathring{\mathbb{R}}^+ \colon \lambda_1(U) < 0 < \lambda_2(U) < \lambda_3(U)\}. \tag{5.2}$$

Accordingly, D^- and D^+ characterize ingoing and outgoing pipes, with corresponding index sets $\mathbb{I}_i^{\mathscr{E}_1} = \{i \colon U^{(i)} \in D_-\}$ and $\mathbb{I}_o^{\mathscr{E}_1} = \{i \colon U^{(i)} \in D_+\}$, respectively and $N := |\mathbb{I}_i^{\mathscr{E}_1}| + |\mathbb{I}_o^{\mathscr{E}_1}|$, see figure 14. The overall domain is defined by

$$D = \bigtimes_{i \in \mathbb{I}_i^{\mathscr{E}_1}} D_-^{\mathscr{E}_1} \times \bigtimes_{i \in \mathbb{I}_o^{\mathscr{E}_1}} D_+^{\mathscr{E}_1}.$$

We like to mention, that a coordinate transformation has been performed in the above definitions. So it comes, that velocities of *ingoing* pipes are *negative*, while underlying pipes are pointing away from the junction. This is justified in a simpler identification of in- and outgoing pipes, since the signs of velocities

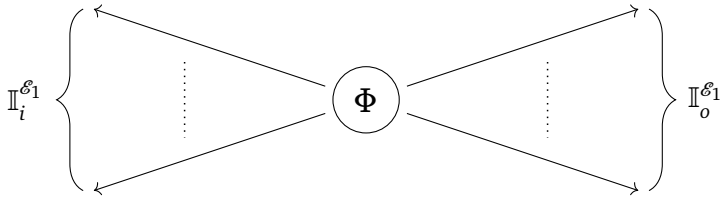

Figure 14: Schematic presentation of an network with $|\mathbb{I}_i^{\mathscr{E}_1}|$ ingoing pipes, $|\mathbb{I}_o^{\mathscr{E}_1}|$ outgoing pipes, and coupled by a single junction Φ, located in the middle.

have to be checked only. However, in our numerical part of this work, the above transformation is not applied. Instead a network is initialized by an incidence matrix. Now, we state the complete problem first, see also [32].

Definition 5.1. *The generalized inhomogeneous Cauchy problem at the junction with N pipes is defined through the set of equations*

$$\begin{cases} \partial_t U^{(i)} + \partial_x F(U^{(i)}) &= G(U^{(i)}), \quad (x,t) \in \mathbb{R}^+ \times \mathbb{R}^+, \\ \Phi\left(U^{(1)}(0^+,t), ..., U^{(N)}(0^+,t)\right) &= \Pi(t), \qquad t \in \mathbb{R}^+, \\ U^{(i)}(x,0) &= U_0^{(i)}, \qquad x \in \mathbb{R}^+ \end{cases} \tag{5.3}$$

for $i \in \mathbb{I}_i^{\mathscr{E}_1} \cup \mathbb{I}_o^{\mathscr{E}_1}$ *and* $\Pi(t) \in \mathbb{R}^d,\ t \geq 0$.

In (5.3), F is the flux function defined in $(\mathscr{E}_1)$. Our coupling conditions are encoded in Φ. For the case of two connected pipes, i.e., $N = 2$, Φ can be formulated as compressor, while $\Pi = (0\ H\ 0)^T$ or $\Pi = (0\ \tilde{H}\ 0)^T$ serve as compressor control, see subsection 8.5 for more detail.

Definition 5.2. *A function* $U \in C([0,T]; \bar{U} + L^1(\mathbb{R}^+; D))$ *is a weak solution to problem* (5.3)*, if* $U(t) \in BV(\mathbb{R}^+; D),\ \forall t \in [0,T],\ T > 0$*, satisfies the initial condition* $U(x,0) = U_0(x)$*, as well as the coupling condition at the junction, i.e.,* $\Phi(U(0^+,t)) = \Pi(t)$*, for a.e.* $t > 0$*. Furthermore, for all test functions* $\varphi \in C_c^\infty(\mathbb{R}^+ \times (0,T); \mathbb{R})$ *it holds*

$$\int_0^T \int_{\mathbb{R}^+} \left(U^{(i)} \partial_t \varphi + F(U^{(i)}) \partial_x \varphi + G(U^{(i)}) \varphi\right) dx dt = \int_0^T F(U^{(i)})(0^+,t) \varphi(0^+,t)\, dt$$

for all $i = 1, ..., N$*. The weak solution is entropic if for all non-negative* $\varphi \in C_c^\infty(\mathring{\mathbb{R}}^+ \times (0,T); \mathbb{R}^+)$ *and for all* $i = 1, ..., N$ *it holds*

$$\int_0^T \int_{\mathbb{R}^+} \left(\nu(U^{(i)}) \partial_t \varphi + \psi(U^{(i)}) \partial_x \varphi + \partial_v G(U^{(i)}) \varphi\right) dx dt \geq 0,$$

with entropy-entropy flux pair (ν, ψ) *of the full Euler equations* $(\mathscr{E}_1)$.

In definition 6.2, $\bar{U}$ is a stationary state, which will be introduced in our further proceeding.

Before posing our coupling conditions, we study some structure of the corresponding Riemann problem 5.1 in the beginning. This structure becomes crucial for the *number of equations* in our coupling conditions.

With neglection of the source term, i.e., $G \equiv 0$ and an application of the finite volume approach, in subsection 4.2, one receives piecewise constant initial states on each pipe, forming a *generalized homogeneous Riemann problem* at the junction for model $(\mathscr{E}_1)$.

Definition 5.3. *The homogeneous generalized Riemann problem at a junction with N pipes is defined through the set of equations*

$$\begin{cases} \partial_t U^{(i)} + \partial_x F(U^{(i)}) &= 0, & (x,t) \in \mathbb{R}^+ \times \mathbb{R}^+, \\ \Phi\left(U^{(1)}(0^+,t), \dots, U^{(N)}(0^+,t)\right) &= \bar{\Pi}, & t \in \mathbb{R}^+, \\ U^{(i)}(x,0) &= \bar{U}_0^{(i)}, & x \in \mathbb{R}^+ \end{cases} \tag{5.4}$$

for $i \in \mathbb{I}_i^{\mathscr{E}_1} \cup \mathbb{I}_o^{\mathscr{E}_1}$, where $\bar{U}_0^{(1)}, \dots, \bar{U}_0^{(N)}$ are constant thermodynamic states in D, F the flux function of model $(\mathscr{E}_1)$ and $\bar{\Pi} \in \mathbb{R}^d$ is a constant.

At this point it is useful to consider the solution structure of standard Riemann problems again, see subsections 4.1 or 4.2. Since the junction lies at $x = 0$, the self-similar solution is splitted, along the axes $(0,t)$, $t \geq 0$, compare figure 15.

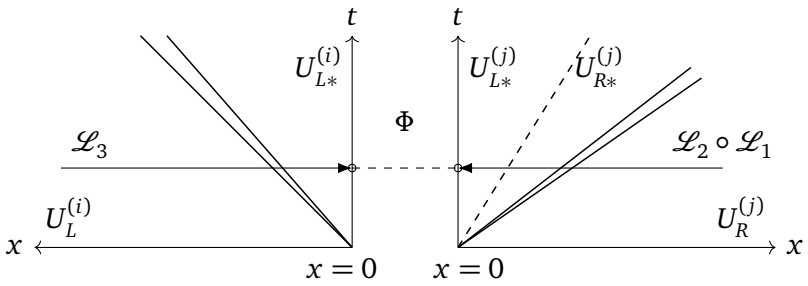

Figure 15: Schematic presentation of the coupling at a junction with Lax curves of model $(\mathscr{E}_1)$

The appearing problem is also called *half Riemann* problem, see [29, 32, 37, 39]. For ingoing pipes, all states $U^{(i)}(0^+,t)$ are connected with constant states $\bar{U}_0^{(i)}$, $i \in \mathbb{I}_i^{\mathscr{E}_1}$ via Lax curve $\mathscr{L}_2^{\mathscr{E}_1}$ in (4.38), while states $U^{(i)}(0^+,t)$ of outgoing pipes are coupled with constant states $\bar{U}_0^{(i)}$, $i \in \mathbb{I}_o^{\mathscr{E}_1}$ by Lax curves $\mathscr{L}_2^{\mathscr{E}_1} \circ \mathscr{L}_3^{\mathscr{E}_1}$ given through (4.38). We conclude, that any coupling condition must have $|\mathbb{I}_i^{\mathscr{E}_1}| + 2|\mathbb{I}_o^{\mathscr{E}_1}|$ equations to match the degree of freedom, inflicted by the Lax curves in (4.38).

5.1 Coupling Conditions at the Junction

Let us assume, there exists a smooth solution U on a compact support to (5.3). From the homogeneous right hand side, i.e., $G \equiv 0$, it follows, that hyperbolic equations become conservative, see definition 2.1. Now, we like to recover this property for hyperbolic conservation laws posed on networks as well, from which the physical correct coupling condition can be concluded.

Summation over all pipes and spatial integration of (5.3) gives in the *first* equation

$$0 = \sum_{i=1}^{N} \partial_t \int_{\mathbb{R}^+} \rho^{(i)} \, dx - \sum_{i=1}^{N} q^{(i)}(0^+,t).$$

Consequently, $\int \rho\, dx$ is preserved, if $\sum_{i=1}^N q^{(i)} = 0$, which describes conservation of mass at the junction. In regard of the *third* equation, an utilization of enthalpy $h = (E+p)/\rho$ and the same technique as above, results in

$$0 = \sum_{i=1}^N \partial_t \int_{\mathbb{R}^+} E^{(i)}\, dx - \sum_{i=1}^N q^{(i)}(0^+,t) h^{(i)}(0^+,t).$$

By demanding enthalpy to be continuous at the junction, i.e., $h_* = h^{(i)},\ \forall i = 1,...,N$, conservation of energy follows immediately, see [38]. Difficulties arises in the *second* equation, where an usage of $\sum_{i=1}^N q^{(i)}(0^+,t) = 0$ is not possible. In section 2, the entropy equations (2.2) has been introduced, which is suitable for smooth solutions of the Euler equations $(\mathscr{E}_1)$.

Therefore, second equation is replaced by (2.2). Now, integration by parts and summation over all pipes results in

$$0 = \sum_{i=1}^N \int_{\mathbb{R}_+} \partial_t s - \sum_{i=1}^N q^{(i)}(0^+,t) s^{(i)}(0^+,t). \tag{5.5}$$

By stating the coupling condition

$$\frac{1}{\sum_{i\in\mathbb{I}_i^{\mathscr{E}_1}} q_i(0^+,t)} \sum_{i\in\mathbb{I}_i^{\mathscr{E}_1}} (q_i s_i)(0^+,t) \;=\; s_*(t), \tag{5.6}$$

$$s_j(t) \;=\; s_*(t),\ j \in \mathbb{I}_o^{\mathscr{E}_1} \tag{5.7}$$

we fulfill equation (5.5) and match the degree of freedom $N_0 + 2N_1$ as well. Equation (5.6) can be interpreted as convex combination of information of every pipe entering the junction. Afterwards, this information is passed to the outgoing pipes continuously, i.e., expression (5.7). Summarizing all before mentioned conditions, the algebraic equation Φ in definition 5.3 has to fulfill

$$\sum_{j=1}^N q_j(0^+,t) = 0,\ t>0 \qquad \text{(conservation of mass)} \tag{5.8a}$$

$$h_j(0^+,t) = h_*(t),\ t>0 \qquad \text{(equality of enthalpy)}, \tag{5.8b}$$

$$s_j(0^+,t) = s_*(t),\ t>0,\ j\in\mathbb{I}_o^{\mathscr{E}_1} \qquad \text{(entropy mixture)}, \tag{5.8c}$$

with $h_*(t)$ as parameter. The function $s_*(t)$ in (5.8c) is defined by (5.6). In recent years, various coupling conditions have been posed next to ours above. We find

$$\sum_{i=1}^N (u_i(E_i+p_i))(0+,t) = 0,\ t>0 \qquad \text{(conservation of energy)} \tag{5.9a}$$

$$p_i(0+,t) = p_*(t),\ t>0 \qquad \text{(equality of pressure)} \tag{5.9b}$$

$$(\rho_i u_i^2 + p_i)(0+,t) = P_*(t),\ t>0 \qquad \text{(equality of dynamic pressure)} \tag{5.9c}$$

In [18], conditions (5.8a), (5.9c) and (5.9a) have been introduced. Due to these coupling conditions, networks equipped with model $(\mathscr{E}_1)$ and $|\mathbb{I}_i^{\mathscr{E}_1}| \in \mathbb{N}$, $\mathbb{I}_o^{\mathscr{E}_1} = \{1\}$ were able to be solved only. [28] uses (5.8a) and (5.9b) for $(\mathscr{E}_2)$ equipped with $p(\rho) = c^2\rho$, where the speed of sound c is assumed to be constant. For the considered network here, one has $|\mathbb{I}_i|, |\mathbb{I}_o| \in \mathbb{N}$.

However, in [38], conditions (5.8a), (5.8b) have been used for $|\mathbb{I}_i|, |\mathbb{I}_o| \in \mathbb{N}$ and model $(\mathscr{E}_2)$, which results in conservation of mass and energy at the junction, and consequently rejects any usage of (5.9b) as well as (5.9c). Furthermore, [38] proved that (5.9c) and (5.9b) results in an increase of energy at the junction, which has been numerically illustrated in [36] as well.

In our next section, we show well-posedness of (5.4) equipped with conditions (5.8).

5.2 Well-posedness of the Euler Equations with Riemann Data at the Junction

Similar to [11, 12, 16, 18, 28, 32], well-posedness of $(\mathscr{E}_1)$ with coupling conditions (5.8) is shown by solving the generalized homogeneous Riemann problem at the junction (5.4). Due to this approach, states $U^{(i)}(0^+, t)$, $t \geq 0$, $i \in \mathbb{I}_i \cup \mathbb{I}_o$ at the junction are connected by left and right Lax curves $\mathscr{L}_1^{\mathscr{E}_1}$ and $\mathscr{L}_2^{\mathscr{E}_1} \circ \mathscr{L}_3^{\mathscr{E}_1}$ in (4.38), like already mentioned previously. An application of the implicit function theorem shows, that the resulting mapping is invertible in a neighborhood of the Riemann data.

However, based on the coordinate transformation of the network and property

$$\mathscr{L}_1(\sigma, \bar{U}) = -\mathscr{L}_3^{\mathscr{E}_1}\left(\sigma, \bar{U}\big|_{-\bar{q}}\right),$$

we replace Lax curve $\mathscr{L}_1^{\mathscr{E}_1}$ by $\mathscr{L}_3^{\mathscr{E}_1}$ on ingoing pipes.

Since subsonic flow in the network is considered only, all states $U^{(i)}(0^+, t)$, $t \geq 0$, $i \in \mathbb{I}_i \cup \mathbb{I}_o$, lie in the inner wedges of the solutions to half Riemann problems at the junction, see again figure 15. In subsection 4.2 we showed, that solutions to Riemann problems on $\mathbb{R}$ are piecewise constant. This remains true for half Riemann problems. In this context, all states $U^{(i)}(0^+, t)$, $t \geq 0$, $i \in \mathbb{I}_i^{\mathscr{E}_1} \cup \mathbb{I}_o^{\mathscr{E}_1}$ are denoted by $U_{L*}^{(i)}$, $i \in \mathbb{I}_i^{\mathscr{E}_1} \cup \mathbb{I}_o^{\mathscr{E}_1}$ and are determined due to Lax curves, i.e.,

$$U_{L*}^{(i)} = \mathscr{L}_3(\sigma_i, \bar{U}_0^{(i)}),\ i \in \mathbb{I}_i^{\mathscr{E}_1}, \tag{5.10}$$

$$U_{L*}^{(i)} = \mathscr{L}_2\left(\tau_i, \mathscr{L}_3(\sigma_i, \bar{U}_0^{(i)})\right),\ i \in \mathbb{I}_o^{\mathscr{E}_1}. \tag{5.11}$$

Given the construction in (5.10) and (5.11), our coupling function Φ in 5.3 becomes

$$\Phi\left(\left(U_{L*}^{(i)}\right)_{i\in\mathbb{I}_i^{\mathscr{E}_1}}, \left(U_{L*}^{(i)}\right)_{i\in\mathbb{I}_o^{\mathscr{E}_1}}\right) = \bar{\Pi} \in \mathbb{R}^d. \tag{5.12}$$

Before examining the Jacobian of (5.12), we assume without loss of generality $\mathbb{I}_o^{\mathscr{E}_1} = \{1, ..., N_0\}$, $\mathbb{I}_i^{\mathscr{E}_1} = \{N_0 + 1, ..., N\}$ and introduce the notation

$$\begin{aligned} f_i(\sigma_i, \tau_i) &= f_i(\mathscr{L}_2(\tau_i, \mathscr{L}_3(\sigma_i, \bar{U}_0^{(i)}))), && i = 1, ..., N_0 \\ f_i(\sigma_i) &= f_i(\mathscr{L}_3(\sigma, \bar{U}_0^{(i)})), && i = N_0 + 1, ..., N \end{aligned} \tag{5.13}$$

with $f = q, h, s$. For convenience of the reader, equation (5.12) can now be formulated in more detail

$$\bar{\Pi} \overset{!}{=} \Phi(\sigma, \tau) = \begin{pmatrix} \sum_{i=1,\dots,N_0} q_i(\sigma_i, \tau_i) + \sum_{i=N_0+1,\dots,N} q_i(\sigma_i) \\ h_{N_0+1}(\sigma_{N_0+1}) - h_1(\sigma_1, \tau_1) \\ \vdots \\ h_{N_0+1}(\sigma_{N_0+1}) - h_{N_0}(\sigma_{N_0}, \tau_{N_0}) \\ h_{N_0+1}(\sigma_{N_0+1}) - h_{N_0+2}(\sigma_{N_0+2}) \\ \vdots \\ h_{N_0+1}(\sigma_{N_0+1}) - h_N(\sigma_N) \\ s_1(\sigma_1, \tau_1) - s_*(\sigma_{N_0+1}, \dots, \sigma_N) \\ \vdots \\ s_{N_0}(\sigma_{N_0}, \tau_{N_0}) - s_*(\sigma_{N_0+1}, \dots, \sigma_N) \end{pmatrix} \tag{5.14}$$

with

$$s_*(\sigma_{N_0+1}, .., \sigma_N) = \frac{1}{\sum_{i=N_0+1,\dots,N} q_i(\sigma_i)} \sum_{i=N_0+1,\dots,N} (q_i s_i)(\sigma_i). \tag{5.15}$$

Equipped with these expressions, we state the following theorem, regarding well-posedness of equation (5.14), see also [32, Thm. 2.1].

Theorem 5.4. *Let $N > N_0 > 0$ and Φ defined through* (5.8a)- (5.8c). *Assume constant initial data $\bar{U}^{(i)} \in D^+,\ i = 1, \dots, N_0$ and $\bar{U}^{(i)} \in D^-,\ i = N_0 + 1, \dots, N$, with $\Phi(\bar{U}) = \bar{\Pi}$ are given. Then there exist positive constants δ and K such that for all initial states $\tilde{U} \in (\mathring{\mathbb{R}}^+ \times \mathbb{R} \times \mathring{\mathbb{R}}^+)^N$ with $\sum_{i=1}^N \|\tilde{U}^{(i)} - \bar{U}^{(i)}\| < \delta$, the generalized homogeneous Riemann problem* (5.4) *admits a unique solution $U(x,t) = \mathscr{R}^\Phi(\tilde{U})$ satisfying $\Phi(U(0^+, t)) = \bar{\Pi}$ and*

$$\|\mathscr{R}^\Phi(\tilde{U}) - \mathscr{R}^\Phi(\bar{U})\|_{L^\infty(\Omega)} \leq K \sum_{i=1}^N \|\tilde{U}^{(i)} - \bar{U}^{(i)}\|. \tag{5.16}$$

Proof. The proof can be found in [32], but will be repeated here in order of completeness. As already mentioned, the proof relies on an application of the implicit function theorem. The Jacobian of (5.14) is evaluated in the stationary state $(\sigma, 0) = (\bar{p}, 0) \in \mathbb{R}^N \times \mathbb{R}^{N_0}$ in which $\Phi(\sigma, 0) = \bar{\Pi}$ holds. Due to continuous differentiability of the coupling conditions Φ and Lax curves $\mathscr{L}^{\mathscr{E}_1}$ in $(\bar{p}, 0)$, there exists a neighborhood in which $\Phi(\sigma, \tau)$ is uniquely solvable.

First, we provide some useful derivatives. For ingoing pipes in (5.14) one has

$$q_i'(\bar{p}_i) = \frac{\lambda_3(\bar{u}_i)}{\bar{c}_i^2}, \quad h'(\bar{p}_i) = \frac{\lambda_3(\bar{u}_i)}{\bar{c}_i \bar{\rho}_i}. \tag{5.17}$$

Differentiation of the entropy condition on ingoing pipes will be done in more detail, since the outcome is mandatory for the well-posedness later on. Now, a composition of entropy mix s^* with Lax curves $\mathscr{L}^{\mathscr{E}_1}$ for $U^{(i)}$, $i \in \mathbb{I}_i^{\mathscr{E}_1}$ results in

$$s^*(\boldsymbol{\sigma}) = \frac{\sum_{i\in\mathbb{I}_i^{\mathscr{E}_1}} q(\sigma_i)s(\sigma_i)}{\sum_{i\in\mathbb{I}_i^{\mathscr{E}_1} q(\sigma_i)}} = \frac{\langle \mathbf{q}(\boldsymbol{\sigma}), \mathbf{s}(\boldsymbol{\sigma})\rangle}{\langle \mathbf{q}(\boldsymbol{\sigma}), \mathbf{1}\rangle} \tag{5.18}$$

with $\boldsymbol{\sigma} = (\sigma_i)_{i\in\mathbb{I}_i^{\mathscr{E}_1}}$, $\boldsymbol{q}(\boldsymbol{\sigma}) = (q_i(\sigma_i))_{i\in\mathbb{I}_i^{\mathscr{E}_1}}$ and $\boldsymbol{s}(\boldsymbol{\sigma}) = (s_i(\sigma_i))_{i\in\mathbb{I}_i^{\mathscr{E}_1}}$. A straight forward differentiation of (5.18) gives us

$$\partial_{\sigma_i} s^*(\boldsymbol{\sigma}) = \frac{\partial_{\sigma_i}[q(\sigma_i)]s(\sigma_i) + q(\sigma_i)\partial_{\sigma_i}[s(\sigma_i)]}{\langle \mathbf{q}(\boldsymbol{\sigma}), \mathbf{1}\rangle} - \frac{\langle \mathbf{q}(\boldsymbol{\sigma}), \mathbf{s}(\boldsymbol{\sigma})\rangle \partial_{\sigma_i}[q(\sigma_i)]}{\langle \mathbf{q}(\boldsymbol{\sigma}), \mathbf{1}\rangle^2}. \tag{5.19}$$

But due to the fact that any derivative of s vanishes in the stationary state, i.e., $\partial_{\sigma_i} s(\sigma)\big|_{\bar{U}} = \partial_{\sigma_i} s(\bar{p}_i) = 0$, $i \in \mathbb{I}_i^{\mathscr{E}_1}$, expression (5.19) can be reduced to

$$\partial_{\sigma_i} s^*(\bar{\boldsymbol{p}}) = \frac{1}{\langle \mathbf{q}(\bar{\boldsymbol{p}}), \mathbf{1}\rangle^2} \langle \mathbf{q}(\bar{\boldsymbol{p}}), \bar{s}_i \mathbf{1} - \mathbf{s}(\bar{\boldsymbol{p}})\rangle \partial_{\sigma_i}[q(\sigma_i)]\big|_{\bar{U}} \tag{5.20}$$

with $\boldsymbol{\sigma}\big|_{\bar{U}} = \bar{\boldsymbol{p}}$. By assumption $q_i(\bar{p}_i) < 0$, $\forall i \in \mathbb{I}_i^{\mathscr{E}_1}$, and therefore $\mathbf{q}(\bar{\mathbf{p}}) < 0$. From (5.17), one concludes $\partial_{\sigma_i} q(\sigma_i)\big|_{\bar{U}} > 0$. Now, we make the following observation, if $i \in \mathbb{I}_i^{\mathscr{E}_1}$ is chosen such that $\bar{s}_i = \min_{k\in\mathbb{I}_i^{\mathscr{E}_1}} \bar{s}_k$, then $\partial_{\sigma_i} s^*(\bar{\boldsymbol{p}}) \geq 0$, on which we fall back later. For outgoing pipes in (5.14), it holds

$$\partial_{\sigma_i} q_i(\bar{p}_i, 0) = \frac{\lambda_3(\bar{u}_i)}{\bar{c}_i^2},\ \partial_{\sigma_i} h_i(\bar{p}_i, 0) = \frac{\lambda_3(\bar{u}_i)}{\bar{c}_i \bar{\rho}_i},\ \partial_{\sigma_i} s_i(\bar{p}_i, 0) = 0, \tag{5.21}$$

$$\partial_{\tau_i} q_i(\bar{p}_i, 0) = \lambda_2(\bar{u}_i),\ \partial_{\tau_i}(\bar{p}_i, 0) = -\frac{\bar{c}_i^2}{(\gamma-1)\bar{\rho}_i},\ \partial_{\tau_i} s_i(\bar{p}_i, 0) = -\frac{\gamma c_v}{\bar{\rho}_i} \tag{5.22}$$

for $i = 1, ..., N_0$. This yields the following matrix for the Jacobian $D_{(\sigma,\tau)}\Phi(\bar{p}, 0)$:

$$\left(\begin{array}{ccc|ccc|ccc}
q_{\sigma_1} & \cdots & q_{\sigma_{N_0}} & q_{\sigma_{N_0+1}} & q_{\sigma_{N_0+2}} & \cdots & q_{\sigma_N} & q_{\tau_1} & \cdots & q_{\tau_{N_0}} \\
\hline
-h_{\sigma_1} & & & h_{\sigma_{N_0+1}} & & & & -h_{\tau_1} & & \\
 & \ddots & & \vdots & & & & & \ddots & \\
 & & -h_{\sigma_{N_0}} & h_{\sigma_{N_0+1}} & & & & & & -h_{\tau_{N_0}} \\
\hline
 & & & h_{\sigma_{N_0+1}} & -h_{\sigma_{N_0+2}} & & & & & \\
 & & & \vdots & & \ddots & & & & \\
 & & & h_{\sigma_{N_0+1}} & & & -h_{\sigma_N} & & & \\
\hline
 & & & -s^*_{\sigma_{N_0+1}} & -s^*_{\sigma_{N_0+2}} & \cdots & -s^*_{\sigma_N} & s_{\tau_1} & & \\
 & & & \vdots & & & \vdots & & \ddots & \\
 & & & -s^*_{\sigma_{N_0+1}} & -s^*_{\sigma_{N_0+2}} & \cdots & -s^*_{\sigma_N} & & & s_{\tau_{N_0}}
\end{array}\right) \tag{5.23}$$

Here, we have used the short notations $f_{\mu_i} := \partial_{\mu_i} f$, for $f = h, s, q$ and $\mu = \sigma, \tau$. In regard of the signs of the derivatives, we observe

$$q_{\sigma_i} > 0,\ q_{\tau_i},\ h_{\sigma_i} < 0,\ s_{\tau_i} < 0, \quad \text{for } i = 1, ..., N_0. \tag{5.24}$$

Without loss of generality, a numbering of incoming pipes is chosen in such a way, that $\bar{s}_{N_0+1} = \min_{i \in \mathbb{I}_i} \bar{s}_i$ and consequently $\partial_{\sigma_{N_0+1}} s^*(\bar{p}) \geq 0$, which follows by expression (5.20). From the special structure in (5.23) one concludes, that the Jacobian has full rank if and only if all 3×3-matrices

$$D_i = \begin{pmatrix} q_{\sigma_i} & q_{\sigma_{N_0+1}} & q_{\tau_i} \\ -h_{\sigma_i} & h_{\sigma_{N_0+1}} & -h_{\tau_i} \\ 0 & -s^*_{N_0+1} & s_{\tau_i} \end{pmatrix},\ i = 1, ..., N_0 \tag{5.25}$$

have full rank. Taking into account the signs of all derivatives, it follows

$$\det(D_i) = q_{\sigma_i}(h_{\sigma_{N_0+1}} s_{\tau_i} - h_{\tau_i} s^*_{\sigma_{N_0+1}}) + h_{\sigma_i}(q_{\sigma_{N_0+1}} s_{\tau_i} + q_{\tau_i} s^*_{\sigma_{N_0+1}}) < 0. \tag{5.26}$$

Therefore, $\det(D_{(\sigma,\tau)}\Phi(\sigma_0, \tau_0)) \neq 0$ and by the implicit function theorem, there exist $\delta > 0$, a neighborhood $\mathcal{U}(v_0)$ of $v_0 = (\sigma_0, \tau_0)$, and a function $\varphi : B(\bar{U}, \delta) \to \mathcal{U}(v_0)$ such that $\varphi(\bar{U}) = v_0$ and $\Phi(v; U) = 0$ if and only if $v = \varphi(U)$ for all $U \in B(\bar{U}, \delta)$. Solution $U(x,t) = \mathscr{R}^{\Phi}(\tilde{U})$ can be identified by restriction to $x \in \mathbb{R}^+$ of the solution to standard Riemann problem 5.3 with

$$U^{(i)}_* = \mathscr{L}_3(\varphi(\tilde{U}), \tilde{U}),\ i \in \mathbb{I}_i^{\mathscr{E}_1}, \tag{5.27}$$

$$U^{(i)}_* = \mathscr{L}_2(\phi(\tilde{U})_{i+N}, \mathscr{L}_3(\varphi(\tilde{U})_i, \tilde{U})),\ i \in \mathbb{I}_o^{\mathscr{E}_1}. \tag{5.28}$$

The Lipschitz estimate (5.16) follows by C^1-regularity of the coupling function Φ and becomes crucial for the Cauchy problem (5.3) in section 8.

□

Remark 5.5. *The proof of well-posedness remains even at flow stagnation, i.e., $q_i = 0$. Then, the determinant becomes*

$$\det(D_i) = q_{\sigma_i}(h_{\sigma_{N_0+1}} s_{\tau_i} - h_{\tau_i} s^*_{\sigma_{N_0+1}}) < 0.$$

In case of a change in flow direction, this observation becomes essential and is examined in more detail in our numerical part of this work, see subsection 9.3.

If two pipes are coupled, the solution of the generalized Riemann problem 5.3 coincides with the solution of the standard Riemann problem of $(\mathscr{E}_1)$. We have

Lemma 5.6. *Let $N = 2$ and $U(x,t)$ be the solution to the standard Riemann problem for* (5.4) *with initial data*

$$U(x,0) = (\rho, q, E)(x,0) = \begin{cases} (\bar{\rho}_1, \bar{q}_1, \bar{E}_1), & \text{for } x > 0, \\ (\bar{\rho}_2, \bar{q}_2, \bar{E}_2), & \text{for } x < 0, \end{cases} \tag{5.29}$$

and $(\bar{\rho}_i, \bar{q}_i, \bar{E}_i)$, $i = 1,2$ constant. Then the functions

$$\begin{array}{rcccll} U^{(1)}(x,t) & = & (\rho_1, q_1, E_1)(x,t) & = & (\rho, q, E)(x,t) & \text{if } x > 0, \\ U^{(2)}(x,t) & = & (\rho_2, q_2, E_2)(x,t) & = & (\rho, -q, E)(x,t) & \text{if } x < 0, \end{array} \tag{5.30}$$

are a solution in the sense of 5.3, that satisfies the coupling conditions (5.8)*. And vice versa, if $U^{(i)}(x,t)$, $i = 1,2$, are such solutions, then $U(x,t)$ is the solution of the standard Riemann problem with initial data* (5.29)*.*

Proof. Observe, that the assertion holds true if the following equivalence is satisfied: $\Phi(U^{(1)}_{L*}, U^{(2)}_{L*}) = 0$ if and only if $(\rho^{(1)}_{L*}, q^{(1)}_{L*}, E^{(1)}_{L*}) = (\rho^{(2)}_{L*}, q^{(2)}_{L*}, E^{(2)}_{L*})$. The coupling conditions simplify to $q^{(1)}_{L*} = -q^{(2)}_{L*}$, $h^{(1)}_{L*} = h^{(2)}_{L*}$, and $s^{(1)}_{L*} = s^{(2)}_{L*}$. Since the solution is smooth along $x = 0$, density and energy are uniquely determined by the values of h and s. This gives the desired equality. □

In the next section, we consider *all* gas models $(\mathscr{E}_1)$-$(\mathscr{E}_3)$ at the junction and show well-posedness by proceeding similar to this section.

6 Model Coupling at the Junction

In this section, we extend the work of Lang and Mindt [32] by allowing different gas models, namely $(\mathscr{E}_1)$-$(\mathscr{E}_3)$ at the junction. Again, mass and energy conservation are posed at the junction and encoded into our coupling conditions. Afterwards, the resulting generalized homogeneous Riemann problem is proven to be well-posed by an utilization of Lax curves, followed by an application of the implicit function theorem. However, these results show, that our model hierarchy of section 2 has a solution, if Riemann data is considered. Furthermore, this approach is the foundation for a more general problem, the generalized Cauchy problem, which is examined in section 8.

Analogously to section 5, we restrict ourself to the subsonic region, i.e., $|u| < c$ for all models. Since $\lambda_1^{\mathscr{E}_k}(U) < 0$ and $\lambda_2^{\mathscr{E}_k}(U) > 0$ for $k = 2,3$, a distinction between ingoing and outgoing pipes, as in the case of $\mathscr{E}_1$, is not necessary. Nevertheless, a separation between ingoing and outgoing pipes of models $(\mathscr{E}_2)$ and $(\mathscr{E}_3)$ becomes crucial if coupled with model $(\mathscr{E}_1)$ and results in an additional information s_0 at incoming pipes, which will be explained in more detail down below.

Similarly to model $(\mathscr{E}_1)$, we define domains of subsonic ingoing and outgoing flow

$$D_-^{\mathscr{E}_k} = \{U = (\rho, \rho u) \in \mathring{\mathbb{R}}^+ \times \mathbb{R} \colon \lambda_1^{\mathscr{E}_k}(U) < u < 0 < \lambda_2^{\mathscr{E}_k}(U)\}, \tag{6.1}$$

$$D_+^{\mathscr{E}_k} = \{U = (\rho, \rho u) \in \mathring{\mathbb{R}}^+ \times \mathbb{R} \colon \lambda_1^{\mathscr{E}_k}(U) < 0 < u < \lambda_2^{\mathscr{E}_k}(U)\}, \tag{6.2}$$

as well as the index sets of ingoing and outgoing pipes, i.e., $\mathbb{I}_i^{\mathscr{E}_k} = \{i \colon U^{(i)} \in D_-^{\mathscr{E}_k}\}$, $\mathbb{I}_o^{\mathscr{E}_k} = \{i \colon U^{(i)} \in D_+^{\mathscr{E}_k}\}$ for $k = 2,3$, respectively. See also figure 16 for some intuition. Again, only finitely many pipes are

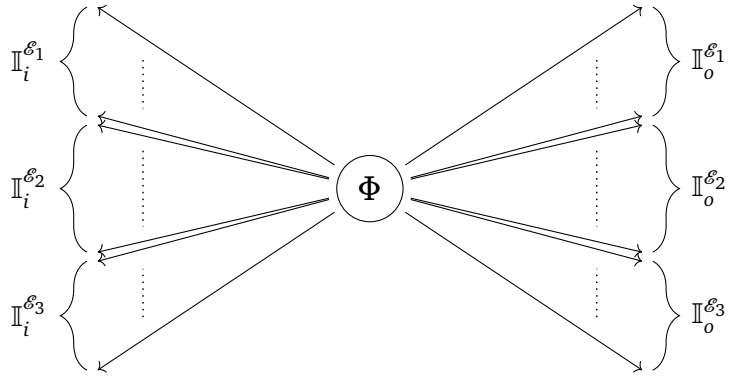

Figure 16: Schematic presentation of an network with $|\mathbb{I}_i^{\mathscr{E}_1}| + |\mathbb{I}_i^{\mathscr{E}_2}| + |\mathbb{I}_i^{\mathscr{E}_3}|$ ingoing pipes, $|\mathbb{I}_o^{\mathscr{E}_1}| + |\mathbb{I}_o^{\mathscr{E}_2}| + |\mathbb{I}_o^{\mathscr{E}_3}|$ outgoing pipes, coupled by a single junction Φ, located in the middle.

considered, that is, $\mathbb{I}_i^{\mathscr{E}_1} \cup \mathbb{I}_o^{\mathscr{E}_1} \cup \mathbb{I}_i^{\mathscr{E}_2} \cup \mathbb{I}_o^{\mathscr{E}_2} \cup \mathbb{I}_i^{\mathscr{E}_3} \cup \mathbb{I}_o^{\mathscr{E}_3} = \{1, ..., N\}$. Let $\mathbb{I}_i = \mathbb{I}_i^{\mathscr{E}_1} \cup \mathbb{I}_i^{\mathscr{E}_2} \cup \mathbb{I}_i^{\mathscr{E}_3}$ and $\mathbb{I}_o = \mathbb{I}_o^{\mathscr{E}_1} \cup \mathbb{I}_o^{\mathscr{E}_2} \cup \mathbb{I}_o^{\mathscr{E}_3}$ as well as $\mathbb{I}_i, \mathbb{I}_o \neq \emptyset$. Latter states, that there is at least one ingoing and one outgoing pipe. Additionally, we denote the set cartesian $D_\pm = D_\pm^{\mathscr{E}_1} \times D_\pm^{\mathscr{E}_2} \times D_\pm^{\mathscr{E}_3}$.

For simplicity in our main result of this section, the index sets are sorted as follows

$$\begin{aligned} \mathbb{I}_o^{\mathscr{E}_1} &= \{1, .., N_1\}, & \mathbb{I}_i^{\mathscr{E}_1} &= \{N_1 + 1, .., N_2\}, \\ \mathbb{I}_i^{\mathscr{E}_2} &= \{N_2 + 1, .., N_3\}, & \mathbb{I}_i^{\mathscr{E}_3} &= \{N_3 + 1, .., N_4\}, \\ \mathbb{I}_o^{\mathscr{E}_2} &= \{N_4 + 1, .., N_5\}, & \mathbb{I}_o^{\mathscr{E}_3} &= \{N_5 + 1, .., N\}. \end{aligned} \tag{6.3}$$

The overall domain is defined through

$$D = \bigtimes_{i \in \mathbb{I}_i} D_- \times \bigtimes_{i \in \mathbb{I}_o} D_+. \tag{6.4}$$

Definition 6.1. *In regard of model hierarchy $(\mathscr{E}_1)$-$(\mathscr{E}_3)$, the generalized inhomogeneous Cauchy problem at the junction with N pipes is defined through the set of equations*

$$\begin{cases} \partial_t U^{(i)} + \partial_x F^{\mathscr{E}_{k_i}}(U^{(i)}) &= G^{\mathscr{E}_{k_i}}(U^{(i)}), & (x,t) \in \mathbb{R}^+ \times \mathbb{R}^+, \\ \Phi\left(U^{(1)}(0^+,t), \dots, U^{(N)}(0^+,t)\right) &= \Pi(t), & t \in \mathbb{R}^+, \\ U^{(i)}(x,0) &= U_0^{(i)}, & x \in \mathbb{R}^+ \end{cases} \tag{6.5}$$

for $i \in \mathbb{I}_i \cup \mathbb{I}_o$, $k_i \in 1, 2, 3$ and $\Pi(t) \in \mathbb{R}^d$, $t \geq 0$.

Definition 6.2. *A function $U \in C([0,T]; \bar{U} + L^1(\mathbb{R}^+; D))$ is a weak solution to problem (6.5), if $U(t) \in BV(\mathbb{R}^+; D)$, $\forall t \in [0,T]$, $T > 0$, satisfies the initial condition $U(x,0) = U_0(x)$, as well as the coupling condition at the junction, i.e., $\Phi(U(0^+,t)) = 0$, for a.e. $t > 0$. Furthermore, for all test functions $\varphi \in C_c^\infty(\mathbb{R}^+ \times (0,T); \mathbb{R})$ it holds*

$$\int_0^T \int_{\mathbb{R}^+} \left(U^{(i)} \partial_t \varphi + F^{\mathscr{E}_{k_i}}(U^{(i)}) \partial_x \varphi + G^{\mathscr{E}_{k_i}}(U^{(i)}) \varphi\right) dx dt = \int_0^T F(U^{(i)})(0^+,t) \varphi(0^+,t)\, dt$$

for all $i = 1,...,N,\ k_i \in \{1,2,3\}$. *The weak solution is entropic if for all non-negative* $\varphi \in C_c^\infty(\mathring{\mathbb{R}}^+ \times (0,T);\mathbb{R}^+)$ *and for all* $i = 1,...,N$ *it holds*

$$\int_0^T \int_{\mathbb{R}^+} \left(\nu^{\mathscr{E}_{k_i}}(U^{(i)})\partial_t\varphi + \psi^{\mathscr{E}_{k_i}}(U^{(i)})\partial_x\varphi + \partial_\nu G^{\mathscr{E}_{k_i}}(U^{(i)})\varphi \right) dxdt \geq 0,$$

with entropy-entropy flux pair $(\nu^{\mathscr{E}_k}, \psi^{\mathscr{E}_k})$, $k = 1,2,3$ *of models* $(\mathscr{E}_1)$-$(\mathscr{E}_3)$.

If all models are present on ingoing and outgoing pipes, i.e., $\mathbb{I}_i^{\mathscr{E}_k}, \mathbb{I}_o^{\mathscr{E}_k} \neq \emptyset$, $k = 1,2,3$, we extend our coupling conditions (5.8) to

$$\sum_{j=1}^N q_j(0^+,t) = 0,\ t > 0 \qquad \text{(conservation of mass)} \tag{6.6a}$$

$$h_j(0^+,t) = h_*(t),\ t > 0 \qquad \text{(equality of enthalpy)}, \tag{6.6b}$$

$$s_j(0^+,t) = s_*(t),\ j \in \mathbb{I}_o^{\mathscr{E}_1},\ t > 0 \qquad \text{(entropy mixture)}, \tag{6.6c}$$

with $h_*(t)$ as parameter. Function $s_*(t)$ in (6.6c) is defined by

$$s_*(t) = \frac{1}{\sum_{j\in\mathbb{I}_i} q_j(0^+,t)} \sum_{j\in\mathbb{I}_i} (q_j s_j)(0^+,t). \tag{6.7}$$

In (6.7), one sees the necessity of introducing the sets $D_\pm^{\mathscr{E}_k}$, $k = 2,3$, since entropy s_i of models $(\mathscr{E}_2)$ and $(\mathscr{E}_3)$ is needed on ingoing pipes as well.

If $\mathbb{I}_o^{\mathscr{E}_1} = \emptyset$, i.e., there is no pipe with model $(\mathscr{E}_1)$ present at the junction, the coupling conditions are reduced to equations (6.6a) and (6.6b). These are also used, for all other cases as long as $\mathbb{I}_o^{\mathscr{E}_1} = \emptyset$ and coincide with coupling conditions in [37, 38]. The well-posedness of both cases is shown separately.

Analogously to section 5, we formulate the generalized homogeneous Riemann problem at a junction first.

Definition 6.3. *The generalized homogeneous Riemann problem at a junction with N pipes is defined through the set of equations*

$$\begin{cases} \partial_t U^{(i)} + \partial_x F^{(k)}(U^{(i)}) &= 0, & (x,t) \in \mathbb{R}^+ \times \mathbb{R}^+, \\ \Phi\left(U^{(1)}(0^+,t),...,U^{(N)}(0^+,t)\right) &= \bar{\Pi}, & t \in \mathbb{R}^+, \\ U^{(i)}(x,0) &= \bar{U}_0^{(i)}, & x \in \mathbb{R}^+ \end{cases} \tag{6.8}$$

for $i \in \mathbb{I}_i \cup \mathbb{I}_o$, *where* $\bar{U}_0^{(1)},...,\bar{U}_0^{(N)}$ *are constant thermodynamic states in* D, $F^{(k)}$, $k = 1,2,3$ *are the flux functions of underlying models* $(\mathscr{E}_1)$-$(\mathscr{E}_3)$ *and* $\bar{\Pi} \in \mathbb{R}^d$ *is a constant.*

First, we assume $\mathbb{I}_i^{\mathscr{E}_k}, \mathbb{I}_o^{\mathscr{E}_k} \neq \emptyset,\ k = 1,2,3$. Based on the construction of the network one has

$$-\mathscr{L}_1^{\mathscr{E}_k}\left(\sigma, \bar{U}\big|_{-\bar{q}}\right) = \mathscr{L}_2^{\mathscr{E}_k}(\sigma, \bar{U}), \quad -\lambda_1^{\mathscr{E}_k}\left(\bar{U}\big|_{-\bar{q}}\right) = \lambda_2^{\mathscr{E}_k}(\bar{U}),$$

for $k = 2,3$ as well as

$$-\mathscr{L}_1^{\mathscr{E}_1}\left(\sigma, \bar{U}\big|_{-\bar{q}}\right) = \mathscr{L}_3^{\mathscr{E}_1}(\sigma, \bar{U}), \quad -\lambda_1^{\mathscr{E}_k}\left(\bar{U}\big|_{-\bar{q}}\right) = \lambda_3^{\mathscr{E}_k}(\bar{U}),$$

with $\bar{U} \in D$. This will simplify certain notations later on.

Coupling conditions (6.6) can now be expressed by means of Lax curves. Since the junction is located along $x = 0,\ t > 0$ the sought states $U_*^{(j)},\ j \in \mathbb{I}_i^{\mathscr{E}_k} \cup \mathbb{I}_o^{\mathscr{E}_k},\ k = 2,3$ of the isentropic and simplified isentropic Euler equations lie in the star region between L and R, while $U_*^{(j)},\ j \in \mathbb{I}_i^{\mathscr{E}_1} \cup \mathbb{I}_o^{\mathscr{E}_1}$ of the full Euler equations lie in L_*, see figure 17. This consideration is crucial for the composition of Lax-curves.

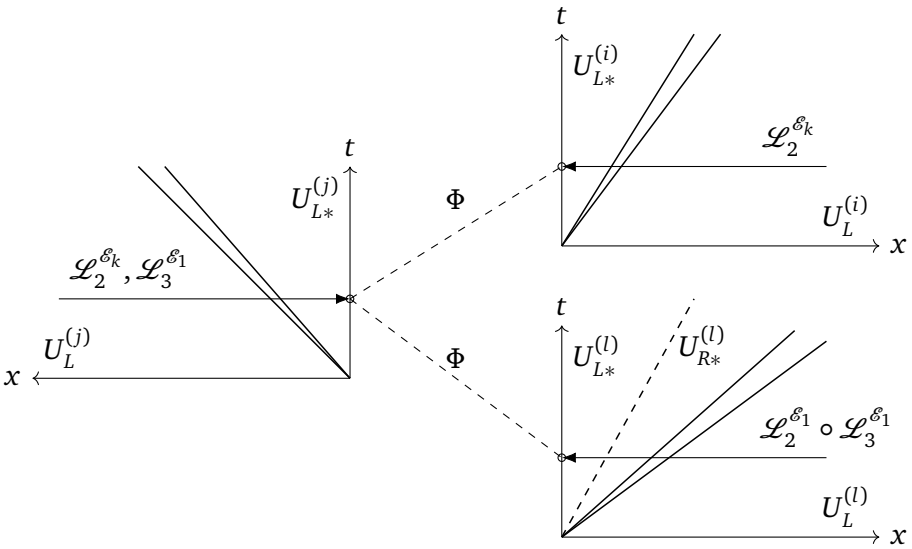

Figure 17: Schematic presentation of the coupling composed with Lax-curves at a junction.

Consequently, *ingoing* states are expressed by

$$U_*^{(j)} = \mathscr{L}_2^{\mathscr{E}_k}\left(\sigma_j, \bar{U}^{(j)}\right),\ \bar{U}^{(j)} \in D_-^{\mathscr{E}_k},\ j \in \mathbb{I}_i^{\mathscr{E}_k},\ k = 2,3, \tag{6.9a}$$

$$U_*^{(j)} = \mathscr{L}_3^{\mathscr{E}_1}\left(\sigma_j, \bar{U}^{(j)}\right),\ \bar{U}^{(j)} \in D_-^{\mathscr{E}_1},\ j \in \mathbb{I}_i^{\mathscr{E}_1}, \tag{6.9b}$$

whereas *outgoing* states are represented through

$$U_*^{(j)} = \mathscr{L}_2^{\mathscr{E}_k}\left(\sigma_j, \bar{U}^{(j)}\right),\ \bar{U} \in D_+^{\mathscr{E}_k},\ j \in \mathbb{I}_o^{\mathscr{E}_k},\ k = 2,3, \tag{6.10a}$$

$$U_*^{(j)} = \mathscr{L}_2^{\mathscr{E}_1}\left(\tau_j, \mathscr{L}_3^{\mathscr{E}_1}\left(\sigma_j, \bar{U}^{(j)}\right)\right),\ \bar{U}^{(j)} \in D_+^{\mathscr{E}_1},\ j \in \mathbb{I}_o^{\mathscr{E}_1}. \tag{6.10b}$$

Given formulations (6.9) and (6.10), the coupling condition (6.6) reads

$$\bar{\Pi} = \Phi\left(\left(U_*^{(j)}\right)_{j=1}^N\right). \tag{6.11}$$

For sake of a compact presentation in our main theorem, we introduce analogously to [32] the following notation

$$\begin{aligned}
f_j(\tau_j,\sigma_j) &= f_j\left(\mathscr{L}_2^{\mathscr{E}_1}\left(\tau_j,\mathscr{L}_3^{\mathscr{E}_1}\left(\sigma_j,\bar{U}^{(j)}\right)\right)\right),\ \bar{U}^{(j)} \in D_+^{\mathscr{E}_1},\ j = 1,\dots,N_1,\\
f_j(\sigma_j) &= f_j\left(\mathscr{L}_3^{\mathscr{E}_1}\left(\sigma_j,\bar{U}^{(j)}\right)\right),\ \bar{U}^{(j)} \in D_-^{\mathscr{E}_1},\ j = N_1+1,\dots,N_2,\\
f_j(\sigma_j) &= f_j\left(\mathscr{L}_2^{\mathscr{E}_2}\left(\sigma_j,\bar{U}^{(j)}\right)\right),\ \bar{U}^{(j)} \in D_-^{\mathscr{E}_2},\ j = N_2+1,\dots,N_3,\\
f_j(\sigma_j) &= f_j\left(\mathscr{L}_2^{\mathscr{E}_3}\left(\sigma_j,\bar{U}^{(j)}\right)\right),\ \bar{U}^{(j)} \in D_-^{\mathscr{E}_3},\ j = N_3+1,\dots,N_4,\\
f_j(\sigma_j) &= f_j\left(\mathscr{L}_2^{\mathscr{E}_2}\left(\sigma_j,\bar{U}^{(j)}\right)\right),\ \bar{U}^{(j)} \in D_+^{\mathscr{E}_2},\ j = N_4+1,\dots,N_5,\\
f_j(\sigma_j) &= f_j\left(\mathscr{L}_2^{\mathscr{E}_3}\left(\sigma_j,\bar{U}^{(j)}\right)\right),\ \bar{U}^{(j)} \in D_+^{\mathscr{E}_3},\ j = N_5+1,\dots,N,
\end{aligned}$$

with $f_j \in \{q_j, \hat{h}_j, s_j\}$, where $\hat{h}_j$ is given by

$$\hat{h}_j = \begin{cases} (E_j + p_j)/\rho_j, & j \in \mathbb{I}_i^{\mathscr{E}_1} \cup \mathbb{I}_o^{\mathscr{E}_1},\\ \gamma/(\gamma-1)\rho_j^\gamma + u_j^2/2, & j \in \mathbb{I}_i^{\mathscr{E}_2} \cup \mathbb{I}_o^{\mathscr{E}_2},\\ \gamma/(\gamma-1)\rho_j^\gamma, & j \in \mathbb{I}_i^{\mathscr{E}_3} \cup \mathbb{I}_o^{\mathscr{E}_3}, \end{cases}$$

and s_* defined through

$$s_*(\sigma_{N_1+1},\dots,\sigma_{N_4}) = \frac{1}{\sum_{j=N_1+1,\dots,N_4} q_j(\sigma_j)} \sum_{j=N_1+1,\dots,N_4} (q_j s_j)(\sigma_j). \tag{6.14}$$

The coupling function (6.15) can now be written as

$$\bar{\Pi} \stackrel{!}{=} \Phi(\sigma,\tau) = \begin{pmatrix} \sum_{j=1}^{N_1} q(\tau_j,\sigma_j) + \sum_{j=N_1+1}^{N} q(\sigma_j) \\ \hat{h}_{N_1+1}(\sigma_{N_1+1}) - \hat{h}_1(\tau_1,\sigma_1) \\ \vdots \\ \hat{h}_{N_1+1}(\sigma_{N_1+1}) - \hat{h}_{N_1}(\tau_{N_1},\sigma_{N_1}) \\ \hat{h}_{N_1+1}(\sigma_{N_1+1}) - \hat{h}_{N_2+1}(\sigma_{N_2+1}) \\ \vdots \\ \hat{h}_{N_1+1}(\sigma_{N_1+1}) - \hat{h}_N(\sigma_N) \\ s(\tau_1,\sigma_1) - s_*(\sigma_{N_1+1},\dots,\sigma_{N_4}) \\ \vdots \\ s(\tau_{N_1},\sigma_{N_1}) - s_*(\sigma_{N_1+1},\dots,\sigma_{N_4}) \end{pmatrix}. \tag{6.15}$$

Remark 6.4. *At this point we like to mention, that the summation in* (6.14) *incorporates also the isentropic models* $(\mathscr{E}_2)$ *and* $(\mathscr{E}_3)$*, even if the entropy on the corresponding ingoing pipes is constant. Again, equation* (6.14) *can be understood as convex combination of information, which enters a junction.*

With all preliminaries at hand, our main theorem of this section can be formulated next.

Theorem 6.5. *Let* $\mathbb{I}_i, \mathbb{I}_o \neq \emptyset$ *and* Φ *defined through* (6.6)*. Assume constant initial states* $\bar{U}^{(i)} \in D_-, i \in \mathbb{I}_i$ *and* $\bar{U}^{(i)} \in D_+, i \in \mathbb{I}_o$ *with* $\Phi(\bar{U}) = \bar{\Pi}$ *are given. Then there exist positive constants* δ *and* K *such that for all* $\tilde{U} \in \Omega$ *with* $\sum_{j=1,\dots,N} \|\tilde{U}^{(j)} - \bar{U}^{(j)}\| < \delta$*, the generalized homogeneous Riemann problem* (6.8) *admits a unique entropy solution* $U(x,t) = \mathscr{R}^{\Phi}(\bar{U})$ *satisfying* $\Phi(U(0^+,t)) = 0$ *and*

$$\|\mathscr{R}^{\Phi}(\tilde{U}) - \mathscr{R}^{\Phi}(\bar{U})\|_{\mathrm{L}^\infty(\Omega)} \leq K \sum_{j=1}^{N} \|\tilde{U}^{(j)} - \bar{U}^{(j)}\|. \tag{6.16}$$

proof. The techniques in this proof are similar to those in [32, Thm 2.1], which rely on an application of the implicit function theorem. Accordingly, the required Jacobian $J\Phi$ of (6.11), is evaluated in $\bar{\tau} = 0$ and $\bar{\sigma} = (\bar{p}_1, \dots, \bar{p}_{N_2}, \bar{\rho}_{N_2+1}, \dots, \bar{\rho}_N)$.

$$J\Phi(\bar{\tau},\bar{\sigma}) = \left(\begin{array}{ccc|ccc|ccc} q_{\tau_1} & \cdots & q_{\tau_{N_1}} & q_{\sigma_1} & \cdots & q_{\sigma_{N_1}} & q_{\sigma_{N_1+1}} & \cdots & q_{\sigma_N} \\ \hline & & & & & & \hat{h}_{\sigma_{N_1+1}} & -\hat{h}_{\sigma_{N_1+2}} & \\ & 0 & & & 0 & & \vdots & \ddots & \\ & & & & & & \hat{h}_{\sigma_{N_1+1}} & & -\hat{h}_{\sigma_N} \\ \hline -\hat{h}_{\tau_1} & & & -\hat{h}_{\sigma_1} & & & \hat{h}_{\sigma_{N_1+1}} & & \\ & \ddots & & & \ddots & & \vdots & 0 \cdots 0 & \\ & & -\hat{h}_{\tau_{N_1}} & & & -\hat{h}_{\sigma_{N_1}} & \hat{h}_{\sigma_{N_1+1}} & & \\ \hline & & & s_{\tau_{N_1}} & & & -s^*_{\sigma_{N_1+1}} & -s^*_{\sigma_{N_1+2}} \cdots & -s^*_{\sigma_N} \\ & 0 & & & \ddots & & \vdots & & \vdots \\ & & & & & s_{\tau_{N_1}} & -s^*_{\sigma_{N_1+1}} & -s^*_{\sigma_{N_1+2}} \cdots & -s^*_{\sigma_N} \end{array}\right) \tag{6.17}$$

Here, the short notation $f_\omega = \partial_\omega f$ for $f = q, \hat{h}, s, s^*$ and $\omega = \sigma, \tau$ is used. We want to remind that $\bar{U} = U(\bar{\tau},\bar{\sigma})$ fulfills the coupling condition (6.6) by assumption. Due to the structure of the Jacobian it appears that (6.17) is regular if and only if the following matrices are regular

$$A_j := \begin{pmatrix} q_{\tau_j} & q_{\sigma_j} & q_{\sigma_{N_1+1}} \\ -\hat{h}_{\tau_j} & -\hat{h}_{\sigma_j} & \hat{h}_{\sigma_{N_1+1}} \\ 0 & s_{\tau_j} & -s^*_{\sigma_{N_1+1}} \end{pmatrix},\ j = 1, \dots, N_2,$$

$$B_j := \begin{pmatrix} q_{\sigma_j} & q_{\sigma_{N_1+1}} \\ -\hat{h}_{\sigma_j} & \hat{h}_{\sigma_{N_1+1}} \end{pmatrix},\ j = N_2+1, \dots, N.$$

With some minor changes, the regularity of A_i, has already been proven in section 6, see also [32, Thm. 2.1]. For the remaining matrices B_i, it suffices to provide some derivatives

$$\hat{h}_{\sigma_i}(\bar{U}^{(j)}) = \begin{cases} \lambda_3^{\mathscr{E}_1}(\bar{U}^{(i)})/(\bar{\rho}_i\bar{c}_i) > 0, & i \in \mathbb{I}_i^{\mathscr{E}_1} \cup \mathbb{I}_o^{\mathscr{E}_1}, \\ \lambda_2^{\mathscr{E}_2}(\bar{U}^{(i)})\bar{c}_i/\bar{\rho}_i > 0, & i \in \mathbb{I}_i^{\mathscr{E}_2} \cup \mathbb{I}_o^{\mathscr{E}_2}, \\ \lambda_2^{\mathscr{E}_3}(\bar{U}^{(i)})\bar{c}_i/\bar{\rho}_i > 0, & i \in \mathbb{I}_i^{\mathscr{E}_3} \cup \mathbb{I}_o^{\mathscr{E}_3}, \end{cases} \tag{6.18a}$$

$$q_{\sigma_i}(\bar{U}^{(i)}) = \begin{cases} \lambda_3^{\mathscr{E}_1}(\bar{U}^{(i)})/\bar{c}_i^2 > 0, & i \in \mathbb{I}_i^{\mathscr{E}_1} \cup \mathbb{I}_o^{\mathscr{E}_1}, \\ \lambda_2^{\mathscr{E}_2}(\bar{U}^{(i)}) > 0, & i \in \mathbb{I}_i^{\mathscr{E}_2} \cup \mathbb{I}_o^{\mathscr{E}_2}, \\ \lambda_2^{\mathscr{E}_3}(\bar{U}^{(i)}) > 0, & i \in \mathbb{I}_i^{\mathscr{E}_3} \cup \mathbb{I}_o^{\mathscr{E}_3}. \end{cases} \tag{6.18b}$$

Under consideration of the signs in (6.18a) and (6.18b), the determinant of B_j reads

$$\det(B_j) = q_{\sigma_j}\hat{h}_{\sigma_{N_1+1}} + q_{\sigma_{N_1+1}}\hat{h}_{\sigma_j} > 0,$$

and states the proof for the case $\mathbb{I}_i^{\mathscr{E}_k}, \mathbb{I}_o^{\mathscr{E}_k} \neq \emptyset,\ k = 1,2,3$. If $\mathbb{I}_o^{\mathscr{E}_1} = \emptyset$ the Jacobian (6.17) is reduced to

$$J\Phi(\bar{\sigma}) = \left(\begin{array}{cccc|ccc|ccc} q_{\sigma_{N_1+1}} & \cdots & \cdots & q_{\sigma_{N_2}} & q_{\sigma_{N_2+1}} & \cdots & q_{\sigma_{N_3}} & q_{\sigma_{N_3+1}} & \cdots & q_{\sigma_N} \\ h_{\sigma_{N_1+1}} & -h_{\sigma_{N_1+2}} & & & & & & & & \\ \vdots & & \ddots & & & & & & & \\ h_{\sigma_{N_1+1}} & & & -h_{\sigma_{N_2}} & & & & & & \\ \hline h_{\sigma_{N_1+1}} & & & & -h_{\sigma_{N_2+1}} & & & & & \\ \vdots & & & & & \ddots & & & & \\ h_{\sigma_{N_1+1}} & & & & & & -h_{\sigma_{N_3}} & & & \\ \hline h_{\sigma_{N_1+1}} & & & & & & & -h_{\sigma_{N_3+1}} & & \\ \vdots & & & & & & & & \ddots & \\ h_{\sigma_{N_1+1}} & & & & & & & & & -h_{\sigma_N} \end{array}\right). \tag{6.19}$$

Matrix (6.19) is regular, which is proven by contradiction. Since $q_{\sigma_i}, h_{\sigma_i} >$, the matrix (6.19) has full rank if and only if the first column is linear independent to all other columns. Due to the structure of (6.19), it would request that $q_{\sigma_{N_1+1}} = \alpha_2 q_{\sigma_{N_1+1}} + \ldots + \alpha_N q_{\sigma_N}$ with $\alpha_i = -h_{\sigma_{N_1+1}}/h_{\sigma_i}$, which contradicts $q_{\sigma_i} > 0$. Therefore, $\det(D_{(\sigma,\tau)}\Phi(\sigma_0,\tau_0))$, $\det(D_\sigma\Phi(\sigma_0,\tau_0)) \neq 0$ and by the implicit function theorem, there exist $\delta > 0$, a neighborhood $\mathscr{U}(v_0)$ of $v_0 = (\sigma_0,\tau_0)$, as well as a function $\varphi : B(\bar{U},\delta) \to \mathscr{U}(v_0)$ such that $\varphi(\bar{U}) = v_0$ and $\Phi(v;U) = 0$ if and only if $v = \varphi(U)$ for all $U \in B(\bar{U},\delta)$. Solution $U(x,t) = \mathscr{R}^\Phi(\tilde{U})$ can be identified by the restriction to $x \in \mathbb{R}^+$ of the solution to the standard Riemann problem 6.3 with

$$U_*^{(i)} = \mathscr{L}_3(\varphi(\tilde{U}),\tilde{U}),\ i \in \mathbb{I}_i, \tag{6.20}$$

$$U_*^{(i)} = \mathscr{L}_2(\phi(\tilde{U})_{i+|\mathbb{I}_i|}, \mathscr{L}_3(\varphi(\tilde{U})_i,\tilde{U})),\ i \in \mathbb{I}_o. \tag{6.21}$$

The Lipschitz estimate (5.16) follows by C^1-regularity of the coupling condition Φ and becomes crucial for the Cauchy problem (5.3) in section 8.

□

Remark 6.6. *We like to mention, that in the proofs of theorems 5.4 and 5.4, the a priori knowledge about flow direction on the pipes is necessary for the construction of condition* (5.8c) *only. However, this a priori knowledge does not affect well-posedness. In section 9 we pose an algorithm to overcome this assumption.*

7 Well-posedness of Compressor Coupling

In this section, we examine the well-posedness of the compressor models (2.6) and (2.7), if coupled with our gas models $(\mathscr{E}_1)$-$(\mathscr{E}_3)$. The proceeding is analogously to the work of Gugat, Herty, Klar, Leugering and Schleper in [28] as well as Colombo, Guerra, Herty and Schleper in their work [16], i.e., a coupling problem is posed as generalized homogeneous Riemann problem, in which all Riemann states are described by Lax curves. Afterwards, the resulting mapping is proven to be well posed by an application of the implicit function theorem, compare also sections 5 and 6.

First, we consider, similar to sections 5 and 6, the region of subsonic flow only, i.e.,

$$\begin{aligned}
D_+^{\mathscr{E}_1} &= \{U=(\rho,\rho u,E)\in \mathring{\mathbb{R}}^+\times\mathbb{R}\times\mathring{\mathbb{R}}^+ \colon \lambda_1^{\mathscr{E}_1}(U)<0<\lambda_2^{\mathscr{E}_1}(U)<\lambda_1^{\mathscr{E}_1}(U)\},\\
D_-^{\mathscr{E}_1} &= \{U=(\rho,\rho u,E)\in \mathring{\mathbb{R}}^+\times\mathbb{R}\times\mathring{\mathbb{R}}^+ \colon \lambda_1^{\mathscr{E}_1}(U)<\lambda_2^{\mathscr{E}_1}(U)<0<\lambda_1^{\mathscr{E}_1}(U)\},\\
D_+^{\mathscr{E}_k} &= \{U=(\rho,\rho u)\in \mathring{\mathbb{R}}^+\times\mathbb{R} \colon \lambda_1^{\mathscr{E}_k}(U)<0<u<\lambda_2^{\mathscr{E}_k}(U)\},\\
D_-^{\mathscr{E}_k} &= \{U=(\rho,\rho u)\in \mathring{\mathbb{R}}^+\times\mathbb{R} \colon \lambda_1^{\mathscr{E}_k}(U)<u<0<\lambda_2^{\mathscr{E}_k}(U)\},
\end{aligned}$$

for $k=2,3$, on which the coupling of $(\mathscr{E}_1)$-$(\mathscr{E}_3)$ with compressor equations (2.6) and (2.7) will be investigated. Now, the generalized homogeneous Riemann problem for compressor models (2.6) and (2.7) can be formulated.

Definition 7.1. *The homogeneous generalized Riemann problem at a compressor with one ingoing and outgoing pipe is defined through the set of equations*

$$\begin{cases}
\partial_t U^{(i)}+\partial_x F^{(k)}(U^{(i)}) &= 0, & (x,t)\in\mathbb{R}^+\times\mathbb{R}^+,\ k\in\{1,2,3\},\ i=1,2,\\
\Phi\left(U^{(1)}(0^+,t),U^{(2)}(0^+,t)\right) &= \bar{\Pi}, & t\in\mathbb{R}^+,\\
U^{(i)}(x,0) &= \bar{U}_0^{(i)}, & x\in\mathbb{R}^+,\ i=1,2,
\end{cases} \tag{7.1}$$

where $\bar{U}_0^{(1)}\in D_-^{\alpha_2}$, $\alpha_2\in\{\mathscr{E}_1,\mathscr{E}_2,\mathscr{E}_3\}, U_0^{(2)}\in D_+^{\alpha_1}$, $\alpha_1\in\{\mathscr{E}_1,\mathscr{E}_2,\mathscr{E}_3\}$ *are constant thermodynamic states,* $F^{(k)}$, $k\in\{1,2,3\}$ *are the flux function of models* $(\mathscr{E}_1)$-$(\mathscr{E}_3)$, $\bar{\Pi}\in\mathbb{R}^d$ *is a constant, and* Φ *is either defined by* (2.6) *or* (2.7).

We like to remark, that due to simplification purposes in our further proceeding, ingoing states $U\in D_-^{\mathscr{E}_k}$ are labeled with index 2, while outgoing $U\in D_+^{\mathscr{E}_k}$ receive index 1, see also figure 18. for some intuition. Under consideration of the above setup, the main theorem of this section can be stated.

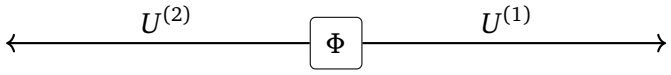

Figure 18: Schematic presentation of the compressor network. Here, $U^{(2)} \in D_-^{\alpha_2}$ and $U^{(1)} \in D_+^{\alpha_1}$ with $\alpha_k \in \{\mathscr{E}_1, \mathscr{E}_2, \mathscr{E}_3\},\ k = 1,2,3$. Furthermore, the ingoing pipe has negative sign, due to the orientation of a network at junctions.

Theorem 7.2. *Let $N = 2$ and Φ defined through (2.6). Assume constant initial states $\bar{U}^{(1)} \in D_+^{\alpha_1}$ and $\bar{U}^{(2)} \in D_-^{\alpha_2}$ with $\alpha_1, \alpha_2 \in \{\mathscr{E}_1, \mathscr{E}_2, \mathscr{E}_3\}$ such that $\Phi(\bar{U}) = \bar{\Pi}$ are given. Then there exist positive constants δ and K such that for all $\tilde{U} \in \Omega$ with $\|\tilde{U}^{(j)} - \bar{U}^{(j)}\| < \delta,\ j = 1,2$, the Riemann problem 6.3 admits a unique solution $U(x,t) = \mathscr{R}^{\Phi}(\bar{U})$ satisfying $\Phi(U(0^+,t)) = 0$ and*

$$\|\mathscr{R}^{\Phi}(\tilde{U}) - \mathscr{R}^{\Phi}(\bar{U})\|_{\mathrm{L}^\infty(\Omega)} \leq K\left(\|\tilde{U}^{(1)} - \bar{U}^{(1)}\| + \|\tilde{U}^{(2)} - \bar{U}^{(2)}\|\right). \tag{7.2}$$

If compressor (2.7) is chosen, one needs compression, i.e., $p_1(0^+,t) \geq p_2(0^+,t)$, additionally to the above assumptions, to ensure all results.

Proof. In the first part of our proof, compressor model (2.6) is considered. Like already mentioned in section 2, the last equation in compressor models (2.6) and (2.7) is neglected, if $\alpha_2 \neq \mathscr{E}_1$, i.e, the isentropic and simplified isentropic gas equations are posed on the outgoing pipe. Therefore, we investigate Φ with $\alpha_2 \in \{\mathscr{E}_1, \mathscr{E}_2, \mathscr{E}_3\}$ and $\alpha_2 = \mathscr{E}_1$ first. Similar to sections 5 and 6, all states at the coupling node are described by an utilization of Lax-curves in subsection 4.2.2. On the ingoing pipe, one has

$$\begin{aligned} f(\sigma_2) &= f\left(\mathscr{L}_2^{\mathscr{E}_k}(\sigma_2, \bar{U}^{(2)})\right),\ k = 2,3, \\ f(\sigma_2) &= f\left(\mathscr{L}_3^{\mathscr{E}_1}(\sigma_2, \bar{U}^{(2)})\right), \end{aligned}$$

while on the outgoing pipe we receive

$$\begin{aligned} f(\sigma_1) &= f\left(\mathscr{L}_2^{\mathscr{E}_k}(\sigma_2, \bar{U}^{(2)})\right),\ k = 2,3, \\ f(\tau_1, \sigma_1) &= \left(\mathscr{L}_2^{\mathscr{E}_1}\left(\tau_1, \mathscr{L}_3^{\mathscr{E}_1}(\sigma_1, \bar{U}^1)\right)\right) \end{aligned}$$

with functions $f = q, p, \mathsf{T}, s$. Consequently, compressor equation (2.6) can be reformulated in means of parameters $\tau_1, \sigma_1, \sigma_2$, i.e.,

$$\Phi = \begin{pmatrix} \Phi_1(\tau_1,\sigma_1,\sigma_2) \\ \Phi_2(\tau_1,\sigma_1,\sigma_2) \\ \Phi_3(\tau_1,\sigma_1,\sigma_2) \end{pmatrix} = \begin{pmatrix} q(\tau_1,\sigma_1) + q(\sigma_2) \\ C\mathsf{T}(\sigma_2)\left(\left(\frac{p(\tau_1,\sigma_1)}{p(\sigma_2)}\right)^{\frac{\gamma-1}{\gamma}} - 1\right) \\ s(\tau_1,\sigma_1) - s(\sigma_2) \end{pmatrix} \overset{!}{=} \begin{pmatrix} 0 \\ H \\ 0 \end{pmatrix}. \tag{7.3}$$

where $C = R\gamma/(\gamma-1)$, Now, one proceeds analogously to sections 5.2 and 6 by deriving all necessary derivatives, followed by an application of the implicit function theorem. Since it suffices to solve $\Phi = \begin{pmatrix} 0 & H & 0 \end{pmatrix}^T$, the second equation can be multiplied by R/C, without changing well-posedness, resulting in

$$\hat{\mathsf{T}}(\sigma_2)q(\sigma_1)\left(\left(\frac{p(\tau_1,\sigma_1)}{p(\sigma_2)}\right)^{\frac{\gamma-1}{\gamma}}-1\right)-HR/C=0, \tag{7.4}$$

where $\hat{\mathsf{T}} = p/\rho$ and $\hat{H} = HR/C$. This simplifies certain calculations later on. Next, we give all necessary derivatives in dependence of $\alpha_1, \alpha_2 \in \{\mathscr{E}_1, \mathscr{E}_2, \mathscr{E}_3\}$, to examine Φ in more detail. For this purpose, let $f_\mu = \partial_\mu f(\bar{U})$, $\mu = \tau_1, \sigma_1, \sigma_2$ be a short notation. The derivative of $q_\mu(\bar{U})$, $\mu \in \{\tau_1, \sigma_1, \sigma_2\}$ has already been evaluated in (6.18), but is given down below for the reader's convenience

$$\begin{array}{lcll}
q_{\tau_1}(\bar{U}^{(1)}) & = & \bar{u}_1 & > 0, \quad \alpha_1 = \mathscr{E}_1, \\
q_{\sigma_1}(\bar{U}^{(1)}) & = & \begin{cases} \lambda_3^{\alpha_1}(\bar{U}^{(1)})/\bar{c}_1^2 & > 0, \quad \alpha_1 = \mathscr{E}_1, \\ \lambda_2^{\alpha_1}(\bar{U}^{(1)}) & > 0, \quad \alpha_1 = \mathscr{E}_2, \mathscr{E}_3, \end{cases} \\
q_{\sigma_2}(\bar{U}^{(2)}) & = & \lambda_3^{\alpha_2}(\bar{U}^{(2)})/\bar{c}_2^2 & < 0, \quad \alpha_1 = \mathscr{E}_1, \mathscr{E}_2, \mathscr{E}_3, \\
\hline
p_{\tau_1}(\bar{U}^{(1)}) & & & = 0 \quad \alpha_1 = \mathscr{E}_1, \\
p_{\sigma_j}(\bar{U}^{(j)}) & = & \begin{cases} 1 & > 0, \quad \alpha_j = \mathscr{E}_1, \\ \gamma\bar{\rho}_j^{\gamma-1} & > 0, \quad \alpha_j = \mathscr{E}_2, \mathscr{E}_3, \end{cases} \\
\hline
\mathsf{T}_{\sigma_2}(\bar{U}^{(2)}) & = & \begin{cases} (\gamma-1)/(\gamma\bar{\rho}_2) & > 0, \quad \alpha_2 = \mathscr{E}_1, \\ (\gamma-1)\bar{\rho}_2^{\gamma-2} & > 0, \quad \alpha_2 = \mathscr{E}_2, \mathscr{E}_3, \end{cases} \\
\hline
s_{\tau_1}(\bar{U}^{(1)}) & = & -(c_v\gamma)/\bar{\rho}_1 & < 0, \quad \alpha_1 = \mathscr{E}_1, \\
s_{\sigma_j}(\bar{U}^{(j)}) & & & = 0, \quad \alpha_j = \mathscr{E}_1, \mathscr{E}_2, \mathscr{E}_3,
\end{array} \tag{7.5}$$

for $j = 1, 2$. Under consideration of $\alpha_1 = \mathscr{E}_1$, $\alpha_2 \in \{\mathscr{E}_1, \mathscr{E}_2, \mathscr{E}_3\}$ and utilizing (7.5), one finds in particular for the gradient of Φ_2 the expression

$$\partial_{\tau_1}\Phi_2(\bar{U}) = \left(\frac{\gamma-1}{\gamma}\right)\frac{\bar{\hat{\mathsf{T}}}_2 p_{\tau_1}}{\bar{p}_1}\left(\frac{\bar{p}_1}{\bar{p}_2}\right)^{\frac{\gamma-1}{\gamma}} = 0, \tag{7.6a}$$

$$\partial_{\sigma_1}\Phi_2(\bar{U}) = \left(\frac{\gamma-1}{\gamma}\right)\frac{\bar{\hat{\mathsf{T}}}_2 p_{\sigma_1}}{\bar{p}_1}\left(\frac{\bar{p}_1}{\bar{p}_2}\right)^{\frac{\gamma-1}{\gamma}} > 0, \tag{7.6b}$$

$$\partial_{\sigma_2}\Phi_2(\bar{U}) = \left(\frac{\bar{p}_1}{\bar{p}_2}\right)^{\frac{\gamma-1}{\gamma}}\left(\mathsf{T}_{\sigma_2} - \left(\frac{\gamma-1}{\gamma}\right)\frac{\bar{\hat{\mathsf{T}}}_2 p_{\sigma_2}}{\bar{p}_2}\right) - \mathsf{T}_{\sigma_2}. \tag{7.6c}$$

However, for all gas models on the outgoing pipe, i.e., $\alpha_1 \in \{\mathscr{E}_1, \mathscr{E}_2, \mathscr{E}_3\}$, we conclude that

$$\left(\mathsf{T}_{\sigma_2} - \left(\frac{\gamma - 1}{\gamma} \right) \frac{\bar{\hat{\mathsf{T}}}_2 p_{\sigma_2}}{\bar{p}_2} \right) = 0,$$

and accordingly it remains $\partial_{\sigma_2} \Phi_2(\bar{U}) = -\mathsf{T}_{\sigma_2}$. Now, due to the derivatives in (7.5) we seek the estimate

$$\partial_{\sigma_2} \Phi_2(\bar{U}) < 0. \tag{7.7}$$

Altogether, the determinant of $D\Phi(\bar{U})$ with $\alpha_2 \in \{\mathscr{E}_1, \mathscr{E}_2, \mathscr{E}_3\}$ can be expressed as

$$\det(\nabla \Phi(\bar{U})) = \begin{cases} s_{\tau_1}(q_{\sigma_1} \partial_{\sigma_2} \Phi_2 - q_{\sigma_2} \partial_{\sigma_1} \Phi_2) > 0, & \alpha_1 = \mathscr{E}_1, \\ q_{\sigma_1} \partial_{\sigma_2} \Phi_2 - q_{\sigma_2} \partial_{\sigma_1} \Phi_2 < 0, & \alpha_1 \neq \mathscr{E}_1. \end{cases} \tag{7.8}$$

Consequently, an application of the implicit function theorem states well-posedness of problem (7.1), if equipped with compressor model (2.6).

Next, model (2.7) is investigated. Similar to section 2, its function is denoted by $\tilde{\Phi}$. However, since both compressor models (2.6) and (2.7) differ in the second function component of Φ, respectively $\tilde{\Phi}$, only, it suffices to examine the gradient of $\tilde{\Phi}_2$. First, suppose gas model ($\mathscr{E}_1$) is stated on the outgoing pipe, i.e., $\alpha_1 = \mathscr{E}_1$, while $\alpha_2 \in \{\mathscr{E}_1, \mathscr{E}_2, \mathscr{E}_3\}$. Furthermore, we like to remind, that in case of compressor model (2.7), compression is assumed, i.e., $p_1 \geq p_2$. Hence

$$\partial_{\tau_1} \tilde{\Phi}_2(\bar{U}) = \bar{\hat{\mathsf{T}}}_2 q_{\tau_1} \left(\frac{\bar{p}_1}{\bar{p}_2} \right)^{\frac{\gamma-1}{\gamma}} \geq 0, \tag{7.9a}$$

$$\partial_{\sigma_1} \tilde{\Phi}_2(\bar{U}) = \bar{\hat{\mathsf{T}}}_2 \left(\frac{\bar{p}_1}{\bar{p}_2} \right)^{\frac{\gamma-1}{\gamma}} \left(q_{\sigma_1} + \left(\frac{\gamma - 1}{\gamma} \right) \frac{\bar{q}_1 p_{\sigma_1}}{\bar{p}_1} \right) - \bar{\hat{\mathsf{T}}}_2 q_{\sigma_1}, \tag{7.9b}$$

$$\partial_{\sigma_2} \tilde{\Phi}_2(\bar{U}) = \bar{q}_1 \left(\frac{\bar{p}_1}{\bar{p}_2} \right)^{\frac{\gamma-1}{\gamma}} \left(\mathsf{T}_{\sigma_2} - \left(\frac{\gamma - 1}{\gamma} \right) \frac{\bar{\mathsf{T}}_2 p_{\sigma_2}}{\bar{p}_2} \right) - \mathsf{T}_{\sigma_2} \bar{q}_1. \tag{7.9c}$$

If $\alpha_1 \in \{\mathscr{E}_2, \mathscr{E}_3\}$, the first derivative $\delta_{\tau_1} \Phi_2(\bar{U})$ is simply neglected. The remaining signs in (7.9c) can be concluded due to

$$\bar{\hat{\mathsf{T}}}_2 \left(\frac{\bar{p}_1}{\bar{p}_2} \right)^{\frac{\gamma-1}{\gamma}} \left(q_{\sigma_1} + \left(\frac{\gamma - 1}{\gamma} \right) \frac{\bar{q}_1 p_{\sigma_1}}{\bar{p}_1} \right) \geq \bar{\hat{\mathsf{T}}}_2 q_{\sigma_1}, \qquad \left(\mathsf{T}_{\sigma_2} - \left(\frac{\gamma - 1}{\gamma} \right) \frac{\bar{\hat{\mathsf{T}}}_2 p_{\sigma_2}}{\bar{p}_2} \right) = 0,$$

for all models on ingoing and outgoing pipes. Therefore one receives the estimates

$$\partial_{\sigma_1} \tilde{\Phi}_2(\bar{U}) < 0, \quad \partial_{\sigma_2} \tilde{\Phi}_2(\bar{U}) > 0. \tag{7.10}$$

Altogether, the determinant of $D\tilde{\Phi}(\bar{U})$ with $\alpha_2 \in \{\mathscr{E}_1, \mathscr{E}_2, \mathscr{E}_3\}$ can be expressed as

$$\det(\nabla\Phi(\bar{U})) = \begin{cases} s_{\tau_1}(q_{\sigma_1}\partial_{\sigma_2}\tilde{\Phi}_2 - q_{\sigma_2}\partial_{\sigma_1}\tilde{\Phi}_2) > 0, & \alpha_1 = \mathscr{E}_1, \\ q_{\sigma_1}\partial_{\sigma_2}\tilde{\Phi}_2 - q_{\sigma_2}\partial_{\sigma_1}\Phi_2 < 0, & \alpha_1 \neq \mathscr{E}_1. \end{cases} \tag{7.11}$$

Now, by an application of the implicit function theorem, both compressor models (2.6) and (2.7) are proven to be well-defined, if connected to our gas models $(\mathscr{E}_1)$-$(\mathscr{E}_3)$ and under consideration of piecewise constant initial data. □

In our next section, all Riemann problems of sections 5-7 are extended to Cauchy problems and proven to be well-posed under suitable initial data.

8 The Cauchy Problem

In this section, we will extend well-posedness of the generalized homogeneous Riemann problems on networks in sections 5-7 to well-posedness of generalized homogeneous Cauchy problems on networks.

We start with these problems on a single pipe first. Here, the initial data U_0 of the Cauchy problem is replaced by a piecewise constant approximation $\bar{U}_0$. Therefore, the Cauchy problem is reduced to *local* Riemann problems. Now, latter problems can be solved locally and prolonged in time until two discontinuities of different Riemann solutions interact and produce a new Riemann problem, which is solved again, until the next interaction occurs. With some effort, one can prove, that this method produces a sequence of solutions, so called *ϵ-solutions*, which converge for $\|U_0 - \bar{U}_0\|_{L^1} < \epsilon$, $\epsilon \to 0$ to the entropy solution. The algorithm just mentioned was originally introduced by Bressan and can be found in more detail in his work [5]. Furthermore, we recommend the work of Dafermos [19, Sect. 14.2], Holden [30, Sect. 6.1] and Smoller [43, Sect. 19 §A].

Regarding the prove of convergence, the building block is the definition of a suitable functional $t \mapsto \Upsilon(t)$, which incorporates the sum of the magnitudes of all Lax curves as well as an interaction functional Q. Because the sum of all magnitudes might increase over time, this increase is compensated by the latter functional Q, resulting in a non-increase of $t \mapsto \Upsilon(t)$. Since every solution is uniformly bounded and Υ is equivalent to the total variation of the solution, it follows by Helly's embedding theorem [5, Thm. 2.3] the existence of the sequence's limit.

However, for our purposes, we give an overview to the front tracking algorithm only, while discussing some components in more detail, if they are necessary for an adaption to Cauchy problems on networks. Moreover, the adaption to networks relies mainly on our results for Riemann problems at junctions in sections 5-7. This includes convergence as well as stability.

8.1 Front Tracking on $\mathbb{R}$

In this subsection, we want to give an overview of the front tracking algorithm [5], which is used to state well-posedness of hyperbolic systems of conservation laws on $\mathbb{R}$. Therefore, consider the problem

$$\begin{cases} U_t + F(U)_x &= 0, \\ U(x,0) &= U_0(x) \end{cases} \tag{8.1}$$

with $U : \mathbb{R} \times \mathbb{R}_+ \to D \subseteq \mathbb{R}^n$, $F \in C^1(D;\mathbb{R}^n)$, $U_0 \in L^1(\mathbb{R}^n)$ and $TV\{U_0\} < \delta$. Assume that problem (8.1) has eigenvalues $\lambda_1 < \ldots < \lambda_n$, which are either genuinely nonlinear or linear degenerated, compare definition 4.2. The k-th shock and rarefaction parameterizations are denoted by S_k and R_k, respectively.

We begin by describing the functionality of the algorithm and provide some illustrations, see also [5, Sect. 7.2]. First, the initial data U_0 is approximated by a piecewise constant function $\bar{U}_0$, such that $TV\{\bar{U}_0\} < \delta$ and $\|\bar{U}_0 - U_0\|_{L^1} < \epsilon$. In subsection 4.2, we have seen that such an approximation $\bar{U}_0$ can be achieved through the finite volume approach. Consequently, local Riemann problems are produced, since $\bar{U}_0$ is piecewise constant. If a rarefaction wave is a solution of a local Riemann problem, it will be replaced by an piecewise constant function as well. We call this approximation a *rarefaction fan*, see figure 19.

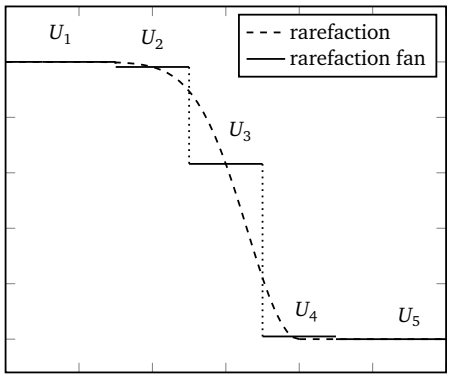

(a) Schematic presentation of the rarefaction fan at time t.

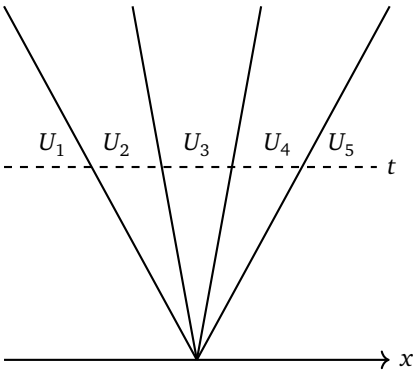

(b) Schematic presentation of the rarefaction fan in the x-t-axis.

Figure 19: Approximation of a rarefaction wave by a piecewise constant function at time t.

Now, the approximated solution to a Riemann problem consists of piecewise constant functions only. Let all discontinuities be located along the lines $\{x_\alpha\}_\alpha$ with speed $\dot{x}_\alpha$. The above described procedure will be encoded in an *approximated Riemann solver* $\theta = \theta_1 \circ ... \circ \theta_n$, in which θ_{k_α}, $k_\alpha \in \{1, ..., n\}$ connects U_L and U_R through the k_α-characteristic x_α, i.e.,

$$\theta_{k_\alpha}(v_{k_\alpha}) = \begin{cases} S_{k_\alpha}(v_{k_\alpha}), & v_{k_\alpha} \leq 0 \\ R_{k_\alpha}(v_{k_\alpha}), & v_{k_\alpha} > 0. \end{cases} \tag{8.2}$$

Unfortunately without further adjustment, this algorithm might produce infinitely many discontinuities after finite time, so called *cluster points* [10, Sect 4.2], see for example figure 21a. To overcome this difficulty, a non-physical wave, with characteristic speed greater than the largest eigenvalue, is introduced and added to the approximated Riemann solver, i.e., $\theta = \theta_1 \circ ... \circ \theta_n \circ \theta_{n+1}$. Here, θ_{n+1} parameterizes a non-physical contact discontinuity of fixed speed $\hat{\lambda} > \lambda_n$, connecting U_R with the n-th Riemann state, compare figure 20. Now, the cluster point in figure 21b is resolved. A detailed description of this

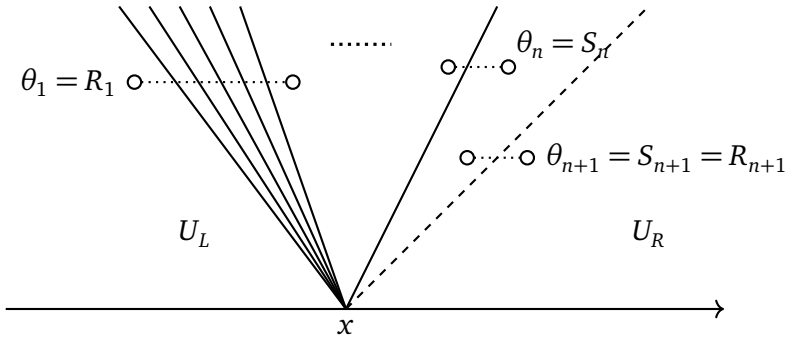

Figure 20: Schematic presentation of the approximated Riemann solver $\theta = \theta_1 \circ ... \circ \theta_n \circ \theta_{n+1}$. Here, lines — are shock waves or rarefaction fans, while —— is a non-physical wave.

procedure can be found in [5, Sect. 7.2]. All together, this technique is called front tracking algorithm.

In [5, section 7] it has been shown, that an application of the front tracking algorithm produces an *ϵ-solution*, which is defined next.

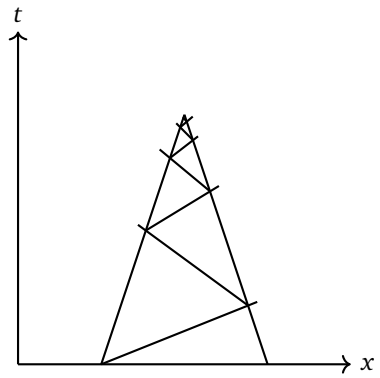

(a) Appearance of infinitely many interactions after a finite time, so called cluster points.

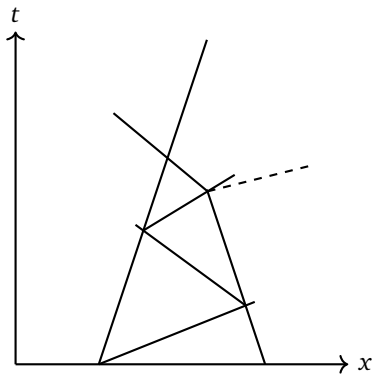

(b) Prevention of a cluster point by introducing a non-physical wave ——.

Figure 21: Schematic presentation of an introduced non-physical wave to prevent cluster points.

Definition 8.1 (ϵ-solution)**.** *For $\epsilon > 0$ a function $U : [0, \infty[\to L^1_{loc}(\mathbb{R}^n)$ is called ϵ-solution to the problem* (8.1)*, if it has following properties:*

1. *U is piecewise constant in the x-t plane, consisting of finitely many jumps along straight lines $x_\alpha(t)$, i.e., no occurrence of cluster points, and consisting of shocks, contact discontinuities, rarefaction fans and non-physical waves only.*

2. *Along each shock or contact discontinuity $x_\alpha(t)$, separating U^+ and U^-, it holds*

$$U^+ = S_{k_\alpha}(\nu_{k_\alpha})(U^-),\ \nu_{k_\alpha} \le 0, \tag{8.3a}$$
$$|\dot{x}_\alpha - \lambda_{k_\alpha}(U^+, U^-)| \le \epsilon \tag{8.3b}$$

   for some genuinely nonlinear family $k_\alpha \in \{1, ..., n\}$.

3. *Along each rarefaction fan $x_\alpha(t)$, $\alpha \in \mathscr{R}$, separating U^+ and U^-, one has*

$$U^+ = R_{k_\alpha}(\nu_{k_\alpha})(U^-),\ \nu_{k_\alpha} \in (0, \epsilon], \tag{8.4a}$$
$$|\dot{x}_\alpha - \lambda_{k_\alpha}(U^+, U^-)| \le \epsilon \tag{8.4b}$$

   for some genuinely nonlinear family $k_\alpha \in \{1, ..., n\}$. Here, $\mathscr{R}$ denotes the set of all rarefaction fans.

4. *All non-physical fronts x_α, $\alpha \in \mathscr{NP}$ have the same speed $\hat{\lambda} \equiv \dot{x}_\alpha > \lambda_n$. Furthermore, the total strength of all non-physical fronts remain uniformly small, i.e.,*

$$\sum_{\alpha \in \mathscr{NP}} |U(x_\alpha+, t) - U(x_\alpha-, t))| \le \epsilon,\ \forall t \ge 0, \tag{8.5}$$

   where $\mathscr{NP}$ is the set of all non-physical fronts.

5. *For the initial state $U(\cdot,0)$ and a piecewise constant function $\bar{U}$ it holds*

$$\|U(\cdot,0)-\bar{U}\|_{L^1} < \epsilon. \tag{8.6}$$

Next, we give an overview of necessary steps, which show, that the *limit* of ϵ-solutions solves problem (8.1). In more detail, let $\{\epsilon_\nu\}_\nu \subseteq \mathbb{R}_+$ such that $\epsilon_\nu \to 0$ for $\nu \to \infty$ and $\{U^{\epsilon_\nu}\}_\nu$ be a sequence of ϵ_ν-solutions, constructed by the front tracking algorithm. Now, from the embedding theorem below, one concludes the existence of the limit $U = \lim_{\nu\to\infty} U^{\epsilon_\nu}$, if $\{U^{\epsilon_\nu}\}_\nu$ fulfills the assumptions therein.

Theorem 8.2 (Helly). *Consider a sequence of functions $U_\nu\colon \mathbb{R}\times[0,\infty)\to\mathbb{R}^n$ with the following properties*

$$TV\{U_\nu(\cdot,t)\} \le C,\ \forall t, \tag{8.7a}$$

$$|U_\nu(x,t)| \le M,\ \forall t,x, \tag{8.7b}$$

$$\int_{\mathbb{R}} |U_\nu(x,t)-U_\nu(x,s)|\,dx \le L|t-s|,\ \forall t,s\ge 0 \tag{8.7c}$$

for some constants $C,M,L>0$. Then there exists a subsequence $\{U_\mu\}_\mu$, which converges to some function $U\in L^1_{loc}(\mathbb{R}\times[0,\infty);\mathbb{R}^n)$. This limit satisfies

$$TV\{U(\cdot,t)\} \le C,\ \forall t, \tag{8.8a}$$

$$|U(x,t)| \le M,\ \forall x,t, \tag{8.8b}$$

$$\int_{\mathbb{R}} |U(x,t)-U(x,s)|\,dx \le C|t-s|,\ \forall t,s\ge 0. \tag{8.8c}$$

Proof. [5, p. 15]. □

Now, we investigate properties of ϵ-solutions to the problem (8.1).

Lemma 8.3. *Let U be an ϵ-solution of problem (8.1). Moreover, let ν and ψ be an entropy-entropy flux pair, according to definition 3.4 and define*

$$E_\alpha = \big(F(U^+)-F(U^-)\big)-\dot{x}_\alpha(U^+-U^-),$$
$$E'_\alpha = \big(\psi(U^+)-\psi(U^-)\big)-\dot{x}_\alpha(\nu(U^+)-\nu(U^-)),$$

where x_α denotes a discontinuity, which separates U into left and right states U^- and U^+, respectively. Let v_{k_α} be a parameter of the k_α-family. Then it holds:

1. *At a rarefaction front*

$$E_\alpha = \mathcal{O}(1)\epsilon|v_{k_\alpha}|,\quad E'_\alpha = \mathcal{O}(1)\epsilon|v_{k_\alpha}|. \tag{8.9}$$

2. *At a shock*

$$E_\alpha = \mathcal{O}(1)\epsilon|\nu_{k_\alpha}|, \quad E'_\alpha \leq \mathcal{O}(1)\epsilon|\nu_{k_\alpha}|. \tag{8.10}$$

3. *At a non-physical front*

$$E_\alpha = \mathcal{O}(1)|\nu_{k_\alpha}|, \quad E'_\alpha = \mathcal{O}(1)|\nu_{k_\alpha}|. \tag{8.11}$$

Proof. [5, Lemma 7.1]. □

We want to remind, that all models $(\mathcal{E}_1)$-$(\mathcal{E}_3)$ have an entropy-entropy flux pair (ν, ψ), see section 3 and the references therein.

Remark 8.4. *From lemma 8.3, one concludes existence of an entropic weak solution to problem* (8.1)*, compare [5, Sect. 7.4]. Furthermore, it does not depend on the underlying geometry and can therefore be used for networks as well.*

Theorem 8.5. *Consider the hyperbolic partial differential system* (8.1)*. Then there exists a constant $\delta_0 > 0$, such that for every initial data $U_0 \in L^1$ with $TV\{U_0\} \leq \delta_0$, the Cauchy problem* (8.1) *has a weak solution $U = U(x,t)$, defined for all $t \geq 0$. In addition, if system* (8.1) *admits an entropy-entropy flux pair, $U = U(x,t)$ is an entropic weak solution.*

Proof. The proof can be found in [5, Section 7.4]. □

Consequently, it only suffices to show, that front tracking produces an ϵ-solution.

We want to remind, that in definition 8.1, it can be assumed without loss of generality, that $\nu \leq 0$ for shock waves and $\nu > 0$ for rarefaction fans, see theorem 4.7. Also, the hidden assumption $\nu_{k_\alpha} \in (0, \epsilon]$, $\alpha \in \mathcal{R}$, might be constructible right after the initialization of a rarefaction fan, but needs to be proven for every additional interaction.

For simplicity, an interaction of at most two waves is considered in our further proceeding only. This restriction is justified by the fact $|\dot{x}_\alpha - \lambda_{k_\alpha}| < \epsilon$, due to the properties in definition 8.1. Consequently, the front speed $\dot{x}_\alpha$ can be adjusted such that a situation of multiple interaction is avoided. This becomes useful in later calculations.

Below, all steps, which are necessary to ensure the existence of an ϵ-solution, together with the assumptions in Helly's embedding theorem, are enumerated for the reader's convenience:

1. The ϵ-solution is piecewise constant without any cluster points, i.e., point 1. in definition 8.1.
2. States, which are separated by shocks, rarefaction fans, contact discontinuities or non-physical waves, are connected through an approximated Riemann solver. Furthermore, lines of discontinuities differ from eigenvalues not more than $\epsilon > 0$, i.e., points 2. and 3. in definition 8.1.
3. The ϵ-solution is stable in time, i.e., (8.7c)
4. Parameters of rarefaction fans are bounded by $\epsilon > 0$, i.e., (8.4).
5. The sum of all non-physical parameters is bounded by $\mathcal{O}(1)\epsilon$, i.e., (8.5), where $\mathcal{O}(1)$ is a uniformly bounded constant.

6. Total variation is non-increasing, which fulfills (8.7a).

7. The constructed piecewise solution is bounded in L_∞, i.e., (8.7b).

By the construction of the approximated Riemann solver on networks, the first two properties are already fulfilled. The third point has been proven in [5, Sect. 7], independent of the underlying geometry. Point 4. has already been shown in [18], while point 5. can be neglected, since non-physical waves are *ignored* at the junction, see subsection 8.3 and [18]. For problem (8.1), we show the last two properties in more detail only, since these points are relevant for the extension to networks.

First, we give some basic estimates, which are helpful later on. Next lemma will be a building block in the proof of existence here, and with some changes, it becomes useful for the stability theory in subsection 8.3.2 as well.

Lemma 8.6. *1. Let v_i', v_j' be two colliding fronts and $v_1, ..., v_n$ resulting fronts after the interaction. Then the following estimate holds*

$$|v_i - v_i'| + |v_j - v_j'| + \sum_{k \neq i,j} |v_k| \leq \mathcal{O}(1)|v_i' v_j'|. \tag{8.12}$$

2. Let v_i', v_i'' be two colliding fronts of the same family i and $v_1, ..., v_n$ resulting fronts after the interaction. Then the following estimate holds

$$|v_i - v_i' - v_i''| + \sum_{k \neq i} |v_k| \leq \mathcal{O}(1)|v_i' v_i''|(|v_i'| + |v_i''|). \tag{8.13}$$

Proof. [5, Lemma 7.2]. □

The original lemma [5, Lemma 7.2] contains two more estimates, that are related to non-physical waves. However, these estimates are not relevant for our theory and are therefore omitted.

Remark 8.7. *For sufficiently small ingoing waves σ', lemma 8.6 states additionally, that all signs remain invariant through any interaction.*

8.2 Bounds on the Total Variation

In this subsection, we give an idea, why total variation of an ϵ-solution is bounded, compare [5, Sect. 7]. For this purpose, the definition of *approaching waves* is introduced next.

Definition 8.8 (Approaching Waves)**.** *Consider two fronts $v_{k_\alpha}, v_{k_\beta}$ of families $k_\alpha, k_\beta \in \{1, ..., n\}$, which are located at $x_\alpha < x_\beta$, respectively. These waves are called approaching, if $k_\alpha > k_\beta$ or $k_\alpha = k_\beta$ and at least one wave is a genuinely nonlinear shock.*

The set of approaching waves at a given point in time t is denoted by $\mathcal{A}$. Consequently, if v_{k_α} and v_{k_β} approach each other, we write $(\alpha, \beta) \in \mathcal{A}$. See also figure 22 for some intuition. With definition 8.8

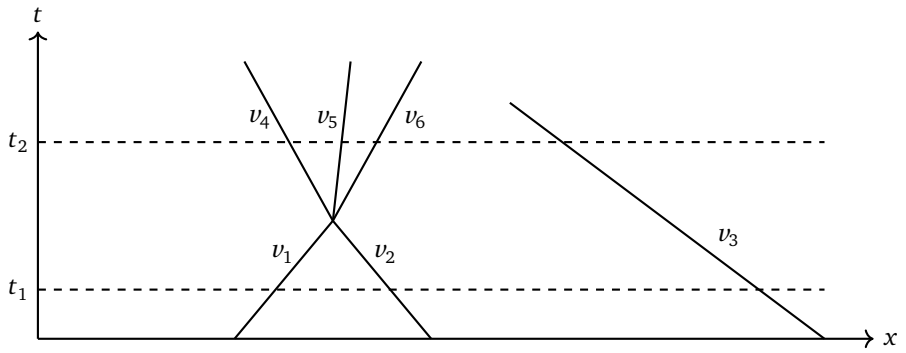

Figure 22: In this example, it holds $(1,2),(1,3) \in \mathscr{A}$, at time t_1, while after interaction at time t_2, we have $(3,5),(3,6) \in \mathscr{A}$.

at hand, the following functionals are introduced

$$\mathsf{V}(U)(t) = \sum_{\alpha} |v_{k_\alpha}|, \quad \mathsf{Q}(U)(t) = \sum_{(\alpha,\beta)\in\mathscr{A}} |v_{k_\alpha} v_{k_\beta}|, \quad \Upsilon(U)(t) = \mathsf{V}(U)(t) + C_0 \mathsf{Q}(U)(t), \tag{8.14}$$

with $C_0 > 0$. Here, $\mathsf{V}(U)(t)$ is the sum of all discontinuities of U at fixed time t, while $\mathsf{Q}(U)(t)$ is the so called *interaction functional* and sums up all approaching wave fronts of U at time t.

For the sake of compact presentation, we neglect the input U in the functionals Υ, V and Q. However, the we come back to the original definition in subsection 8.3.2 when a reference to U becomes crucial.

In appearance of two colliding fronts v', v'' at time t, consider the following cases:

1. $v' = v_i'$ and $v'' = v_j''$, $i \neq j$. Then

$$\mathsf{V}(t+) - \mathsf{V}(t-) = \sum_{k=1}^{n} |v_k| - |v_i'| - |v_j''| \leq |v_i| - |v_i'| + |v_j| - |v_j''| + \sum_{k\neq i,j} |v_k| \leq \mathscr{O}(1)|v_i'||v_j''|$$

2. $v' = v_i'$ and $v'' = v_i''$. Then

$$\begin{aligned}\mathsf{V}(t+) - \mathsf{V}(t-) &= \sum_{k=1}^{n} |v_k| - |v_i'| - |v_i''| \leq |v_i| - |v_i'| - |v_j''| + \sum_{k\neq i} |v_k| \leq \mathscr{O}(1)|v_i'||v_i''|\big(|v_i'| + |v_i''|\big) \\ &\leq \mathscr{O}(1)|v_i'||v_i''|\end{aligned}$$

The estimates, where non-physical fronts are considered, have been neglected here, since they are not relevant for our theory at the junction.

Again, lemma 8.6 states, that all signs of the approaching fronts v', v'' do not change after collision. Therefore, every approaching wave, which is not part of the wave interaction at time t, is still approaching the incoming fronts v', v'' *after* time t. This observation is important in regard of $t \mapsto \Delta\mathsf{Q}$. We consider only two waves v_α, v_β outside of an interaction, see figure 23. The case with more than two

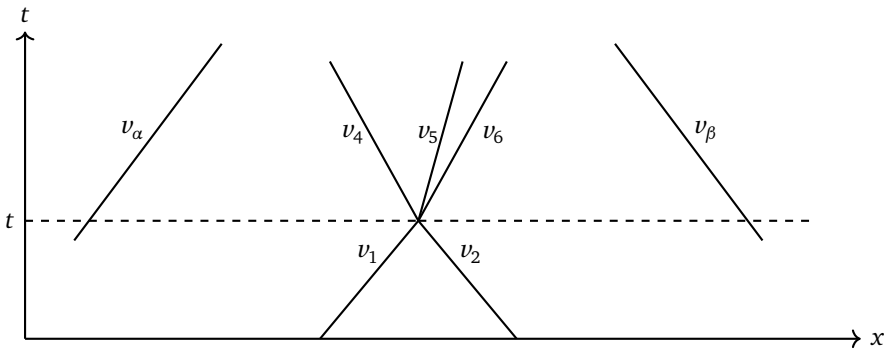

Figure 23: Example of approaching waves before and after an interaction to demonstrate the proof of $t \mapsto \Delta \mathsf{Q}(t)$ non-increasing .

waves is straight forward and can be obtained by induction. With this setup, we conclude

$$\begin{aligned}
\Delta \mathsf{Q}(t) = \mathsf{Q}(t+) - \mathsf{Q}(t-) &= \left(\sum_{k=1}^{k_\alpha} |v_k v_\alpha| + \sum_{k=k_\alpha+1}^{n} |v_k v_\beta| \right) - \left(|v_i' v_j''| + |v_i' v_\beta| + |v_j'' v_\alpha| \right) \\
&\leq \sum_{\gamma \in \{\alpha,\beta\}} \sum_{k \neq i,j} |v_k v_\gamma| - |v_i' \sigma_j''| + |v_\beta| \underbrace{|v_j - v_j''|}_{\leq \mathscr{O}(1)|v_i' v_j''} + |v_\alpha| \underbrace{|v_i - v_i''|}_{\leq \mathscr{O}(1)|v_i' v_j''} \\
&\leq \underbrace{\sum_{\gamma \in \{\alpha,\beta\}} |v_\gamma|}_{\leq V(t-)} \underbrace{\sum_{k \neq i,j} |v_k|}_{\leq \mathscr{O}(1)|v_i' v_j''|} - |v_i' v_j''| + \mathscr{O}(1) \underbrace{\big(|v_\beta| + |v_\alpha| \big)}_{\leq V(t-)} |v_i' v_j''| \\
&\leq \mathscr{O}(1) V(t-) |v_i' v_j''| - |v_i' v_j''|.
\end{aligned}$$

Here, the above incorporated estimates

$$|v_j - v_j''| \leq \mathscr{O}(1)|v_i' v_j''|, \quad |v_i - v_i'| \leq \mathscr{O}(1)|v_i' v_j''|, \quad \sum_{k \neq i,j} |v_k| \leq \mathscr{O}(1)|v_i' v_j''|$$

are immediate results from lemma 8.6. Due to the fact, that v_α, v_β are not part of an interaction at time t, it holds $|v_\alpha| + |v_\beta| \leq \mathsf{V}(t-)$. Case $v' = v'' = v_i$ is treated analogously. If the variation functional $\mathsf{V}(t-)$ is small enough, we receive

$$\mathsf{Q}(t+) - \mathsf{Q}(t-) \leq -\mathscr{O}(1) \frac{|v' v''|}{2}. \tag{8.15}$$

Since V increases at most of $\mathscr{O}(1)|v' v''|$ and Q decreases by $\mathscr{O}(1)|v' v''|$, one can find a constant $C_0 > 0$ and $\delta_2 \in]0, \delta_1]$: $\mathsf{V}(t-) \leq \delta_2$, such that the functional $t \mapsto \Upsilon(t) = \mathsf{V}(t) + C_0 \mathsf{Q}(t)$ is non-increasing in time. Now, let $C_1 > 0$ such that

$$\frac{1}{C_1} TV\{U(\cdot, t)\} \leq \mathsf{V}(t) \leq C_1 TV\{U(\cdot, t)\}, \tag{8.16}$$

as well as $\delta_3 > 0$: $C_1^2\delta_3 + C_0C_1^3\delta_3 \leq \delta_2$. Then, we achieve for $TV\{U(\cdot,0)\} \leq \delta_3$ the estimate

$$\begin{aligned} TV\{U(\cdot,t)\} &\leq C_1\mathsf{V}(t) \\ &\leq C_1[\mathsf{V}(t) + C_0\mathsf{Q}(t)] \\ &\leq C_1[\mathsf{V}(0) + C_0\mathsf{Q}(0)] \\ &\leq C_1[C_1TV\{U(\cdot,0)\} + C_0\mathsf{V}(0)^2] \\ &\leq C_1[C_1\delta_3 + C_0(C_1\delta_3)^2] \\ &\leq \delta_2. \end{aligned}$$

Because U is piecewise constant and $TV\{U(\cdot,t)\} \leq \delta_2$, it follows $|U(x,t)| \leq M$, $\forall x,t$. Since the wave speed of U is finite, it follows by [5, Sect. 7] the Lipschitz continuity in time. Together with the bounded total variation of U and the uniform boundednes, Helly's embedding theorem 8.2 is applicable.

For L^1-stability of the front tracking algorithm in pipes only, we refer to [5, Sect. 8]. However, for our purpose L^1-stability of ϵ-solutions on networks is treated in subsection 8.3.2.

8.3 The Cauchy problem at the Junction

In this subsection, the front tracking algorithm from our previous section is extended to networks with a single junction, on which gas dynamics are described by models $(\mathscr{E}_1)$-$(\mathscr{E}_3)$. Consequently, the generalized homogeneous Cauchy problem of section 6 is repeated here for the reader's convenience

Definition 8.9. *The generalized homogeneous Cauchy problem at a junction with N pipes and equipped with models $(\mathscr{E}_1)$-$(\mathscr{E}_3)$, is defined through the set of equations*

$$\begin{cases} \partial_t U^{(i)} + \partial_x F^{(k_i)}(U^{(i)}) &= 0, & (x,t) \in \mathbb{R}^+ \times \mathbb{R}^+, \\ \Phi\left(U^{(1)}(0^+,t), \ldots, U^{(N)}(0^+,t)\right) &= \Pi(t), & t \in \mathbb{R}^+, \\ U^{(i)}(x,0) &= U_0^{(i)}, & x \in \mathbb{R}^+ \end{cases} \tag{8.17}$$

for $i \in \mathbb{I}_i \cup \mathbb{I}_o$, where $U_0^{(1)}, \ldots, U_0^{(N)}$ are thermodynamic states in $D = \bigtimes_{i\in\mathbb{I}_i} D_- \times \bigtimes_{i\in\mathbb{I}_o} D_+$, with domains $D_\pm$ and index sets $\mathbb{I}_i$, $\mathbb{I}_o$ defined in section 6. Furthermore, $F^{(k)}$, $k \in \{1,2,3\}$ are flux functions of underlying models $(\mathscr{E}_1)$-$(\mathscr{E}_3)$, and $\Pi\colon \mathbb{R}_+ \to \mathbb{R}^d$ is a function at the junction.

We claim the next theorem.

Theorem 8.10. *Assume problem* (8.17) *and constant thermodynamic states $\bar{U}^{(i)} \in D_+$, $i \in \mathbb{I}_i$ and $\bar{U}^{(i)} \in D_-$, $i \in \mathbb{I}_o$, which fulfill the coupling conditions* (6.6)*, i.e., $\Phi(\bar{U}) = \bar{\Pi}$, with $\bar{\Phi}$ constant. Furthermore, let $t \mapsto \Pi(t)$ be of bounded total variation. Then, there exist a domain $\mathscr{D}$, positive constants δ, K, and a uniformly Lipschitz semi-group $S\colon \mathbb{R}_+ \times \mathscr{D} \to \mathscr{D}$ with properties:*

1. $cl_{L^1}\{U \in \bar{U} + L^1(\mathbb{R}_+; D)\colon TV\{U\} \leq \delta\} \subseteq \mathscr{D}$.
2. $S_0 = id$ *and* $S_sS_t = S_{t+s}$.

3. *For all $U \in \mathscr{D}$, the map $t \mapsto S_t(U)$ is the weak entropic solution to the Cauchy problem* (8.17).

4. *For $\hat{U}, \tilde{U} \in \mathscr{D}$ and $s, t \geq 0$ it holds*

$$\|S_t(\hat{U}) - S_s(\tilde{U})\|_{L^1} \leq K\left(\|\hat{U} - \tilde{U}\|_{L^1} + |t-s|\right) \tag{8.18}$$

5. *If $U \in \mathscr{D}$ is piecewise constant and $t > 0$ sufficiently small, then $S_t(U)$ coincides with the juxtaposition of solutions to Riemann problems centered at points of jumps.*

The proof of theorem 8.10 is divided into subsections 8.3.1 and 8.3.2. In the first subsection, we adapt the front tracking algorithm of subsection 8.1 to networks, consisting of a single junction and show existence of an ϵ-solution there. From remark 8.4, we already know, that ϵ-solutions converge to weak entropic solutions for $\epsilon \to 0$, which states 3. From the construction of the front tracking algorithm, we conclude 2. and 5. The first point in theorem 8.10 is due to extensions of the functionals $\mathsf{V}, \mathsf{Q}, \Upsilon$ to networks, which are examined in subsection 8.3.1. The remaining point 4. is proven in subsection 8.3.2.

8.3.1 Consistency

In order to prove the existence of an ϵ-solution on a network, we need to extend functionals $\mathsf{V}, \mathsf{Q}, \Upsilon$ from subsection 8.1 and prove the non-increase of $t \mapsto \Upsilon(t)$. Afterwards, an embedding into L^1 follows by theorem 8.2. Furthermore, it has to be proven, that the magnitude of all rarefaction fan parameters is smaller than $\epsilon > 0$. However, this was already done in [18] and is neglected here. Additionally, it has to be proven, that the sum of all non-physical waves is smaller than ϵ, if the junction is passed. But since we ignore non-physical waves at junctions, this proof falls back to the inner of a pipe, see herefore [5].

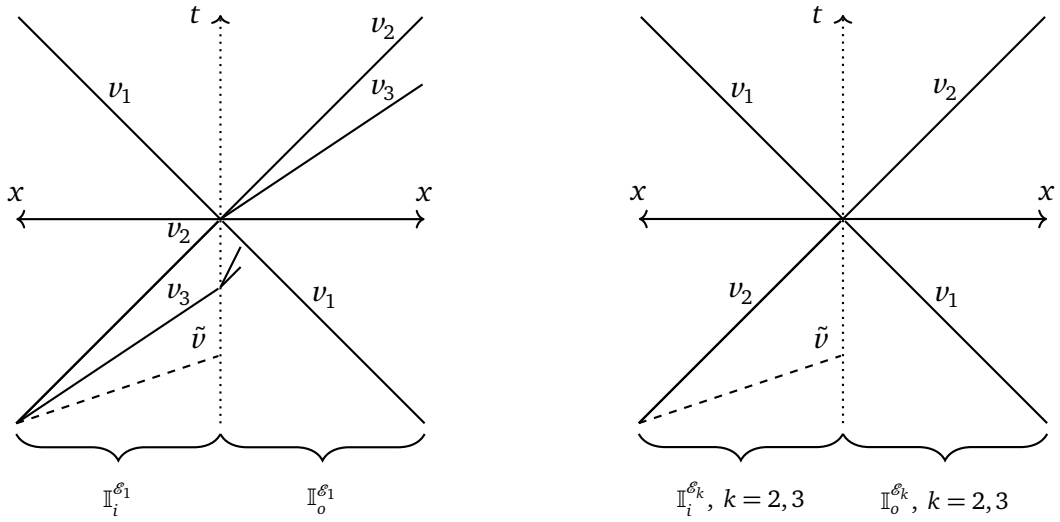

(a) In this figure, interactions between waves of model $(\mathscr{E}_1)$ and the junction are presented, as well as produced waves after the interaction.

(b) In this figure, interactions between waves of models $(\mathscr{E}_2)$, $(\mathscr{E}_3)$ with the junction are presented, as well as produced waves after the interaction.

Figure 24: Interaction at the junction of the models $(\mathscr{E}_1)$ and $(\mathscr{E}_3)$. Non-physical waves $\tilde{v}$ are ignored at both junctions, in case of an interaction.

We start by posing a lemma, which relates wave fronts before and after an interaction at a junction.

Lemma 8.11. *Consider a network, equipped with models* $(\mathscr{E}_1)$*-*$(\mathscr{E}_3)$ *and an interaction time* t*, at which a shock or rarefaction fan hits the junction. All involved parameters before the interaction time* t *are denoted by* v^-*. The occurring Riemann problem at time* t *is solved, by our exact Riemann solver from section 6, with parameters* v^+*. Then, it holds the following estimate*

$$\sum_i \|v_i^+\| \leq K_J \sum_i \|v_i^-\|. \tag{8.19}$$

Before continuing with the proof, we want to remind, that if an underlying pipe of model $(\mathscr{E}_1)$ *is outgoing, the corresponding parameter is given by* $v = (\sigma, \tau)$ *with norm* $\|v\| = |\sigma| + |\tau|$*. For all other cases, parameters are given by* $v = \sigma$ *with* $\|v\| = |\sigma|$*, see for example the proofs of theorems 5.4, 6.5 and 7.2.*

Proof. In the proof of theorem 6.5, we showed existence of an invertible and differentiable function $\varphi : B(\bar{U}, \delta) \to \mathscr{U}(v_0)$ such that $\varphi(U) = v$ and $\varphi(\bar{U}) = v_0$. Due to the properties of φ, we get

$$\|U - \tilde{U}\| = \|\varphi^{-1} \circ \varphi(U) - \varphi^{-1} \circ \varphi(\tilde{U})\| \leq \sup_{v \in \mathscr{U}(v_0)} \|D\varphi^{-1}(v)\| \|\varphi(U) - \varphi(\tilde{U})\| \leq \sup_{v \in \mathscr{U}(v_0)} \|D\varphi^{-1}(v)\| \|v - \tilde{v}\|$$

as well as

$$\|v - \tilde{v}\| \leq \sup_{U \in \varphi^{-1}(\mathscr{U}(v_0))} \|D\varphi(U)\| \|\varphi^{-1}(v) - \varphi^{-1}(\tilde{v})\| = \sup_{U \in \varphi^{-1}(\mathscr{U}(v_0))} \|D\varphi(U)\| \|U - \tilde{U}\|.$$

With definition

$$C := \max \left\{ \sup_{v \in \mathscr{U}(v_0)} \|D\varphi^{-1}(v)\|, \sup_{U \in \varphi^{-1}(\mathscr{U}(v_0))} \|D\varphi(U)\| \right\} < \infty,$$

it follows

$$\frac{1}{C} \|v - \tilde{v}\| \leq \|U - \tilde{U}\| \leq C \|v - \tilde{v}\|. \tag{8.20}$$

Now, let denote the stationary state and the states before and after interaction by $\bar{U}$, U^- and U^+, respectively. With an application of theorem 4.7, these states have parameters $\bar{v} = 0$, v^- and v^+. From (8.20), (6.16) in combination with φ, it follows

$$\frac{1}{C} \|v^+ - \bar{v}\| \leq \|U^+ - \bar{U}\| = \|\mathscr{R}^\phi(U^-) - \mathscr{R}^\phi(\bar{U})\| \leq K \|U^- - \bar{U}\| \leq KC \|v^- - \bar{v}\|$$

and since $\bar{v} = 0$, we conclude

$$\|v^+\| \leq K_J \|v^-\|$$

with $K_J = KC^2$ and $\|v^\pm\| = \sum_i \|v_i^\pm\|$. □

Similar to [12, 18], extensions of $\mathsf{V}, \mathsf{Q}, \Upsilon$ in (8.14) are given through

$$\mathsf{V}(t) = \sum_{l=1}^{n} \mathsf{V}_l(t), \quad \mathsf{V}_l(t) = \sum_{\alpha \in J_l} C_l(v_{k_\alpha}) |v_{k_\alpha}|, \tag{8.21}$$

$$\mathsf{Q}(t) = \sum_{l=1}^{n} \mathsf{Q}_l(t), \quad \mathsf{Q}_l(t) = \sum_{(\alpha,\beta) \in \mathscr{A}_l} |v_{k_\alpha} v_{k_\beta}|, \tag{8.22}$$

$$\Upsilon(t) = \mathsf{V}(t) + \tilde{K}_J \mathsf{Q}(t), \tag{8.23}$$

with $\tilde{K}_J > 0$, J_l the set of discontinuities of U on the l-th pipe and weights

$$C_l(v) := \begin{cases} 1, & l \in \mathbb{I}_o^{\mathscr{E}_1} \text{ and } v \text{ belongs to 2- or 3-family,} \\ 1, & l \in \mathbb{I}_i^{\mathscr{E}_1} \text{ and } v \text{ belongs to 1-family,} \\ 2K_J, & l \in \mathbb{I}_o^{\mathscr{E}_1} \text{ and } v \text{ belongs to 1-family,} \\ 2K_J, & l \in \mathbb{I}_i^{\mathscr{E}_1} \text{ and } v \text{ belongs to 2- or 3-family,} \\ 1, & l \in \mathbb{I}_o^{\mathscr{E}_2} \text{ and } v \text{ belongs to 2-family,} \\ 1, & l \in \mathbb{I}_i^{\mathscr{E}_2} \text{ and } v \text{ belongs to 1-family,} \\ 2K_J, & l \in \mathbb{I}_o^{\mathscr{E}_2} \text{ and } v \text{ belongs to 1-family,} \\ 2K_J, & l \in \mathbb{I}_i^{\mathscr{E}_2} \text{ and } v \text{ belongs to 2-family,} \\ 1, & l \in \mathbb{I}_o^{\mathscr{E}_3} \text{ and } v \text{ belongs to 2-family,} \\ 1, & l \in \mathbb{I}_i^{\mathscr{E}_3} \text{ and } v \text{ belongs to 1-family,} \\ 2K_J, & l \in \mathbb{I}_o^{\mathscr{E}_3} \text{ and } v \text{ belongs to 1-family,} \\ 2K_J, & l \in \mathbb{I}_i^{\mathscr{E}_3} \text{ and } v \text{ belongs to 2-family.} \end{cases} \tag{8.24}$$

The constant $\tilde{K}_J$ in (8.23) will be defined later.

Lemma 8.12. *Given definitions* (8.21)-(8.23) *and* $\mathsf{V}(0) \le \delta$. *Then, the map* $t \mapsto \Upsilon(t) = \mathsf{V}(t) + \tilde{K}_J \mathsf{Q}(t)$ *is non-increasing for a suitable* $\tilde{K}_J > 0$.

Proof. By an utilization of index sets $\mathbb{I}_i^{\mathscr{E}_k}, \mathbb{I}_o^{\mathscr{E}_k}, k = 1, 2, 3$, we rewrite functional V as follows

$$\mathsf{V}(t) = \left(\sum_{l \in \mathbb{I}_i^{\mathscr{E}_1}} + \sum_{l \in \mathbb{I}_o^{\mathscr{E}_1}} \right) \mathsf{V}_l(t) + \left(\sum_{l \in \mathbb{I}_i^{\mathscr{E}_2}} + \sum_{l \in \mathbb{I}_o^{\mathscr{E}_2}} \right) \mathsf{V}_l(t) + \left(\sum_{l \in \mathbb{I}_i^{\mathscr{E}_3}} + \sum_{l \in \mathbb{I}_o^{\mathscr{E}_3}} \right) \mathsf{V}_l(t).$$

Accordingly, we can estimate the change of V, at an interaction time t, by studying $\Delta\mathsf{V}$ for models $\mathscr{E}_k$, $k = 1, 2, 3$ separately, i.e.,

$$\Delta\mathsf{V}(t) = \Delta\mathsf{V}^{\mathscr{E}_1}(t) + \Delta\mathsf{V}^{\mathscr{E}_2}(t) + \Delta\mathsf{V}^{\mathscr{E}_3}(t),$$

with summands

$$\Delta \mathsf{V}^{\mathscr{E}_1}(t) = \mathsf{V}^{\mathscr{E}_1}(t+) - \mathsf{V}^{\mathscr{E}_1}(t-) = \left(\sum_{l \in \mathbb{I}_o^{\mathscr{E}_1}} (|v_{l,2}^{\mathscr{E}_1,+}| + |v_{l,3}^{\mathscr{E}_1,+}|) + \sum_{l \in \mathbb{I}_i^{\mathscr{E}_1}} |v_{l,1}^{\mathscr{E}_1,+}| \right) - \left(\sum_{l \in \mathbb{I}_o^{\mathscr{E}_1}} 2K_J |v_{l,1}^{\mathscr{E}_1,-}| + \sum_{l \in \mathbb{I}_i^{\mathscr{E}_1}} 2K_J (|v_{l,2}^{\mathscr{E}_1,-}| + |v_{l,3}^{\mathscr{E}_1,-}|) \right),$$

$$\begin{aligned}
\Delta \mathsf{V}^{\mathscr{E}_2}(t) &= \mathsf{V}^{\mathscr{E}_2}(t+) - \mathsf{V}^{\mathscr{E}_2}(t-), \\
&= \left(\sum_{l \in \mathbb{I}_o^{\mathscr{E}_2}} |v_{l,2}^{\mathscr{E}_2,+}| + \sum_{l \in \mathbb{I}_i^{\mathscr{E}_2}} |v_{l,1}^{\mathscr{E}_2,+}| \right) - \left(\sum_{l \in \mathbb{I}_o^{\mathscr{E}_2}} 2K_J |v_{l,1}^{\mathscr{E}_2,-}| + \sum_{l \in \mathbb{I}_i^{\mathscr{E}_2}} 2K_J |v_{l,2}^{\mathscr{E}_2,+}| \right), \\
\Delta \mathsf{V}^{\mathscr{E}_3}(t) &= \mathsf{V}^{\mathscr{E}_3}(t+) - \mathsf{V}^{\mathscr{E}_3}(t-) \\
&= \left(\sum_{l \in \mathbb{I}_o^{\mathscr{E}_3}} |v_{l,2}^{\mathscr{E}_3,+}| + \sum_{l \in \mathbb{I}_i^{\mathscr{E}_3}} |v_{l,1}^{\mathscr{E}_3,+}| \right) - \left(\sum_{l \in \mathbb{I}_o^{\mathscr{E}_3}} 2K_J |v_{l,1}^{\mathscr{E}_3,-}| + \sum_{l \in \mathbb{I}_i^{\mathscr{E}_3}} 2K_J |v_{l,2}^{\mathscr{E}_3,+}| \right).
\end{aligned}$$

By using estimate (8.19), it follows

$$\begin{aligned}
\Delta \mathsf{V}^{\mathscr{E}_1}(t) &\leq -K_J \left(\sum_{l \in \mathbb{I}_i^{\mathscr{E}_1}} |v_{l,1}^{\mathscr{E}_1,-}| + \sum_{l \in \mathbb{I}_o^{\mathscr{E}_1}} (|v_{l,2}^{\mathscr{E}_1,-}| + |v_{l,3}^{\mathscr{E}_1,-}|) \right) = -K_J \mathsf{V}^{\mathscr{E}_1}(t-), \\
\Delta \mathsf{V}^{\mathscr{E}_2}(t) &\leq -K_J \left(\sum_{l \in \mathbb{I}_i^{\mathscr{E}_2}} |v_{l,1}^{\mathscr{E}_2,-}| + \sum_{l \in \mathbb{I}_o^{\mathscr{E}_2}} |v_{l,2}^{\mathscr{E}_2,+}| \right) = -K_J \mathsf{V}^{\mathscr{E}_2}(t-), \\
\Delta \mathsf{V}^{\mathscr{E}_3}(t) &\leq -K_J \left(\sum_{l \in \mathbb{I}_i^{\mathscr{E}_3}} |v_{l,1}^{\mathscr{E}_3,-}| + \sum_{l \in \mathbb{I}_o^{\mathscr{E}_3}} |v_{l,2}^{\mathscr{E}_3,+}| \right) = -K_J \mathsf{V}^{\mathscr{E}_3}(t-),
\end{aligned}$$

and therefore $\Delta \mathsf{V}(t) \leq -K_J \mathsf{V}(t-)$. Consequently, $t \mapsto \mathsf{V}(t)$ is non-increasing at the junction. In regard of $\Delta Q(t)$, we proceed analogously to [12, 18], i.e.,

$$\Delta \mathsf{Q}(t) = \mathsf{Q}(t+) - \mathsf{Q}(t-) \leq \mathsf{Q}(t+) = \sum_{l=1}^{N} \sum_{(\alpha,\beta) \in \mathscr{A}_l} |v_\alpha v_\beta| \leq \mathsf{V}(t+)^2 \leq \mathsf{V}(t-)^2. \tag{8.25}$$

With $\Delta\mathsf{V}$ and $\Delta\mathsf{Q}$ at hand, one receives for $\Delta\Upsilon(t) = \Delta\mathsf{V}(t) + \tilde{K}_J\Delta\mathsf{Q}(t)$ the following inequality

$$\Delta\Upsilon(t) = \Delta\mathsf{V}(t) + \tilde{K}_J\Delta\mathsf{Q}(t) \leq (\tilde{K}_J\mathsf{V}(t-) - K_J)\mathsf{V}(t-) \leq (\tilde{K}_J\mathsf{V}(0) - K_J)\mathsf{V}(t-).$$

Now, $\tilde{K}_J$ has to be chosen, such that $\tilde{K}_J \leq K_J/\mathsf{V}(0)$, from which it follows $t \mapsto \Upsilon(t)$ is non-increasing. □

Based on this result, we can state the next proposition.

Proposition 8.13. *Let U^ϵ be an ϵ-solution for the homogeneous Cauchy problem* (8.38) *constructed by the front tracking algorithm with $\mathsf{V}(0) \leq \delta$. Then there exist constants $C, M > 0$, such that $TV\{U^\epsilon\} \leq C$ and $|U^\epsilon(x,t)| \leq M,\ \forall x, t$.*

Proof. First, we conclude from subsection 8.1 together with lemma 8.12, that $t \mapsto \Upsilon(t)$ is non-increasing on the whole network. Additionally, it holds equivalence between V and TV, i.e.,

$$\frac{1}{\kappa}TV\{U^\epsilon(t)\} \leq \mathsf{V}(t) \leq \kappa TV\{U^\epsilon(t)\} \tag{8.26}$$

for a constant $\kappa > 0$ independent of U^ϵ. Therefore,

$$TV\{U^\epsilon(t)\} \leq \mathsf{V}(t) \leq \kappa\Upsilon(t) \leq \kappa\Upsilon(0) \leq \kappa\delta + K_J\delta^2.$$

Consequently, all ϵ-solutions are well-defined, if the initial data U_0 fulfills

$$U_0 \in D_\delta(\bar{U}) = \{U \in \bar{U} + L^1(\mathbb{R}_+;\mathbb{R}^d)\colon TV\{U\} \leq \delta\}. \tag{8.27}$$

We like to remind, that the stationary state $\bar{U}$ in (8.27) results from theorem 6.5, which was used in our above construction at the junction. There, the Riemann problem is well-defined in a neighborhood of the stationary state $\bar{U}$.

Boundedness of U^ϵ follows from the fact, that U^ϵ is piecewise constant and has a bounded total variation $TV(U^\epsilon) < \delta$, see also figure 25 for some intuition. Assume the j-th pipe and the set $\{x_i\}_{i\in\mathbb{N}}$ on which an ϵ-solution U^ϵ has discontinuities. Then, for $x \in (x_{i-1}, x_i]$, it holds

$$\begin{aligned}
|U^\epsilon(x,t)| &\leq |U^\epsilon(x_i,t) - U^\epsilon(x_{i-1},t)| + |U^\epsilon(x_{i-1},t)| \\
&\leq TV\{U^\epsilon(t)\} + |U^\epsilon(0+,t)| \\
&\leq TV\{U^\epsilon(t)\} + K_J|\Phi(t)| \\
&\leq TV\{U^\epsilon(t)\} + K_J TV\{\bar{\Pi}\} + |\bar{\Pi}(0)| \\
&\leq \kappa\delta + K_J\delta + |\bar{\Pi}(0)|.
\end{aligned}$$

□

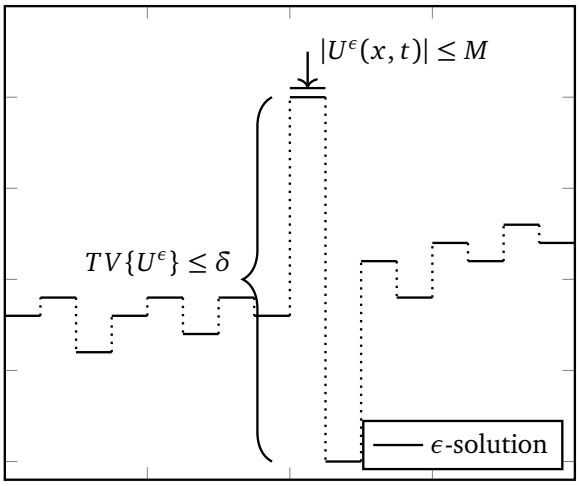

Figure 25: Every ϵ-solution is bounded due to the boundedness of it's total variation.

From proposition 8.13, an application of theorem 8.2 is immediate, i.e., let $\{U^{\epsilon_\nu}\}_\nu$ be a sequence of ϵ_ν-solutions, constructed by the front tracking algorithm on networks. By proposition 8.13 and theorem 8.2 this sequence converges for $\nu \to \infty$ to a function $U \in L^1_{loc}$, by remaining all properties of U^{ϵ_ν}. According to remark 8.4, the limit is a weak entropic solution to the Cauchy problem (8.38), and defines the desired semi-group S on domain $\mathscr{D} = cl_{L^1}(D_\delta(\bar{U}))$ in theorem 8.10. Due to theorem 8.2, the L^1-closure of D_δ does indeed exist. As mentioned before, the stability in regard of time, i.e., the second part in point 4. of theorem 8.10 has been proven in [5, Sect. 7]. Consequently, it only remains to proof the stability in regard of different initial conditions, i.e., the first part of point 4. in theorem 8.10, which will be done in the next subsection.

However, we want to close the current subsection with the next lemma, which examines the trackability of the junction trace. In more detail, it makes no difference if the trace is tracked from the sequence of ϵ-solutions or of their limit.

Lemma 8.14. *For a.e. $t > 0$, the trace $U(0+,t)$ of the solution at the junction exists and coincides with the traces of ϵ_ν-solutions in the limit $\epsilon_\nu \to 0$, i.e.,*

$$\lim_{x\to 0+}\lim_{\nu\to\infty} U^{\epsilon_\nu}(x,t) = \lim_{\nu\to\infty}\lim_{x\to 0+} U^{\epsilon_\nu}(x,t) \tag{8.28}$$

and satisfies coupling conditions (6.6).

Proof. [18, Proposition 4.5]. □

In the proof of lemma 8.14, one defines a sequence $\{\epsilon_\nu\}_\nu$ such that $\epsilon_\nu \to 0$ for $\nu \to \infty$ and constructs a sequence of ϵ_ν-solutions. Now, for every ϵ_ν, the corresponding ϵ_ν-solution is piecewise constant and solves the Riemann problem at the junction, from which the trace can be extracted for every $\epsilon_\nu \in \{\epsilon_\nu\}_\nu \subseteq \mathbb{R}_+$. Then, an application of [1] ensures the limit $\epsilon_\nu \to 0$, as well as the commutation in (8.28).

Additionally from [1], one concludes existence of the trace, when $\Pi\colon \mathbb{R}_+ \to \mathbb{R}^d$ is a given function at the junction, as long as $TV\{\Pi\} \leq \delta$, see also [16, Section 4.1].

However, for this purpose functional Υ in (8.23) has to be extended by an additional summand

$$\Upsilon(U,\Pi)(t) = \mathsf{V}(U)(t) + \tilde{K}_J \mathsf{Q}(U)(t) + \hat{K}_J\, TV\{\Pi(t)\}, \tag{8.29}$$

where $\hat{K}_J > 0$ has to be defined, such that $t \mapsto \Upsilon(U,\Pi)(t)$ is non-increasing, see [16, Sect. 4.1.2]. We like to remind, that in the proof of proposition 8.13, the extension (8.29) was not needed, since Π is not an externally defined function, but implicitly posed due to the solution of the Riemann problem at the junction.

Nonetheless, in appearance of a compressor, Π will be an externally given function and consequently Υ has to be stated according to (8.29). Since the proofs in [16, Sect. 4.1] are generic, our previous results are straight forward expendable.

8.3.2 Stability on Networks

In this section we like to give an overview of L^1-stability. The L^1-stability for the front tracking algorithm has first been introduced by Bressan and Colombo [6] for 2×2-conservation laws on $\mathbb{R}$, followed by an extension to $n\times n$-systems of conservation laws in Bressan [5]. Under some modifications, Amadori [1] as well as Donadello and Marson [22] showed L^1-stability for $n\times n$-systems of conservation laws with boundary. In Colombo, Guerra, Herty and Schleper [16] Colombo, Herty and Sachers [17] as well as Colombo and Mauri [18], an extension for isothermal Euler equations and the full Euler-equations ($\mathscr{E}_1$) on networks has been proven.

Here, we formulate the results in the latter literature in more detail and for our model coupling, presented in sections 6 and 7. For this purpose, one proceeds according to [16, 17, 18] and considers two ϵ-solutions $U^\epsilon(t)=S_t^\epsilon U_0$ and $V^\epsilon(t)=S_t^\epsilon V_0$, which have been constructed by the front tracking algorithm in the previous subsections, given the initial data U_0 and V_0. Our goal is to construct a functional $\Theta\colon D\times D\to\mathbb{R}$, with the following properties

$$\Theta(U^\epsilon(t),U^\epsilon(t))=0, \tag{8.30a}$$

$$\Theta(U^\epsilon(t),V^\epsilon(t))\le\Theta(U_0,V_0)+C\epsilon t, \tag{8.30b}$$

$$\frac{1}{\kappa}\|U^\epsilon(t)-V^\epsilon(t)\|_{L^1}\le\Theta(U^\epsilon(t),V^\epsilon(t))\le\kappa\|U^\epsilon(t)-V^\epsilon(t)\|_{L^1} \tag{8.30c}$$

where, $C,\kappa>0$ are constants. From (8.30) it follows that $\{S^\epsilon U_0\}_\epsilon$ is a Cauchy sequence, since

$$\|U^{\epsilon_2}-U^{\epsilon_1}\|_{L^1}\le\kappa\Theta(U^{\epsilon_2},U^{\epsilon_1})\le\kappa\Theta(U_0,U_0)+\kappa C(\epsilon_2-\epsilon_1)t=\kappa C(\epsilon_2-\epsilon_1)t,$$

with $\epsilon_2\ge\epsilon_1$. Furthermore, one has

$$\|U^\epsilon(t)-V^\epsilon(t)\|_{L^1}\le C\|U_0-V_0\|_{L^1}+C\epsilon t,$$

due to

$$\|U^\epsilon(t)-V^\epsilon(t)\|_{L^1}\le\kappa\Theta(U^\epsilon(t),V^\epsilon(t))\le\kappa\Theta(U_0,V_0)+C\epsilon t\le\kappa^2\|U_0-V_0\|_{L^1}+C\epsilon t,$$

see also [18]. We show, that property (8.30) is ensured, if the functional Θ is defined through

$$\begin{aligned}
\Theta(U^\epsilon,V^\epsilon) &= \textstyle\sum_{l=1}^N\Theta_l(U^\epsilon,V^\epsilon),\\
\Theta_l(U^\epsilon,V^\epsilon) &= \textstyle\sum_{i=1}^n\int_{\mathbb{R}_+}|q_{l,i}(x)|W_{l,i}(x)\,dx,\\
W_{l,1}(x) &= \check{K}\left(1+\kappa_1A_{l,1}(x)+\kappa_1\kappa_2(\Upsilon(U^\epsilon)(t)+\Upsilon(V^\epsilon)(t))\right),\\
W_{l,i}(x) &= 1+\kappa_1A_{l,i}(x)+\kappa_1\kappa_2(\Upsilon(U^\epsilon)(t)+\Upsilon(V^\epsilon)(t)),\ i\ge 2,
\end{aligned} \tag{8.31}$$

with $\kappa_1, \kappa_2 > 0$ and q implicitly given as solution of

$$V^\epsilon(t) = S_n(q_n(x)) \circ \ldots \circ S_1(q_1(x))(U^\epsilon(t)).$$

Constant $\check{K}$ in (8.31) is defined by

$$\check{K} = 1 + 2K_J \hat{\lambda}_l / \check{\lambda}_l \begin{cases} \max_l W_{l,3} & \text{if } \mathscr{E}_1 \text{ is given on the } l\text{-th pipe,} \\ \max_l W_{l,2} & \text{if } \mathscr{E}_k, k = 2,3 \text{ is given on the } l\text{-th pipe,} \end{cases} \tag{8.32}$$

where $\check{\lambda}_l \le \inf |\lambda_1^{\mathscr{E}_k}|$ for $k = 1,2,3$ and $\hat{\lambda}_l$ is given such that

$$\hat{\lambda}_l > \begin{cases} \sup \lambda_3^{\mathscr{E}_1}, & \text{if } \mathscr{E}_1 \text{ is given on the } l\text{-th pipe,} \\ \sup \lambda_2^{\mathscr{E}_k}, & \text{if } \mathscr{E}_k, k = 2,3 \text{ is given on the } l\text{-th pipe.} \end{cases} \tag{8.33}$$

Functions $A_{l,i}$ in (8.31) are stated as

$$A_{l,i} = A_{l,i}^{\mathscr{E}_1} \chi\{\mathscr{E}_1 \text{ is given on } l\text{-th pipe}\} + A_{l,i}^{\mathscr{E}_{2/3}} \chi\{\mathscr{E}_2 \text{ or } \mathscr{E}_3 \text{ is given on } l\text{-th pipe}\}, \tag{8.34}$$

with

$$\begin{aligned} A_{l,i}^{\mathscr{E}_1}(x) = \sum \left\{ |\sigma_{l,k_\alpha,\alpha}| \colon \begin{array}{l} \alpha \in J_l(U^\epsilon) \cup J_l(V^\epsilon) \\ x_\alpha < x,\ i < k_\alpha \le 3 \\ x_\alpha > x,\ 1 = k_\alpha < i \end{array} \right\} \\ + \begin{cases} \sum \left\{ |\sigma_{l,i,\alpha}| \colon \begin{array}{l} x_\alpha < x,\ \alpha \in J_l(U^\epsilon) \\ x_\alpha > x,\ \alpha \in J_l(V^\epsilon) \end{array} \right\}, & \text{if } q_{l,i}(x) < 0, \\ \sum \left\{ |\sigma_{l,i,\alpha}| \colon \begin{array}{l} x_\alpha < x,\ \alpha \in J_l(V^\epsilon) \\ x_\alpha > x,\ \alpha \in J_l(U^\epsilon) \end{array} \right\}, & \text{if } q_{l,i}(x) \ge 0, \end{cases} \end{aligned} \tag{8.35}$$

while for $k = 2,3$, $A_{l,i}^{\mathscr{E}_k}$ is given through

$$\begin{aligned} A_{l,i}^{\mathscr{E}_k}(x) = \sum \left\{ |\sigma_{l,k_\alpha,\alpha}| \colon \begin{array}{l} \alpha \in J_l(U^\epsilon) \cup J_l(V^\epsilon) \\ x_\alpha < x,\ i < k_\alpha \le 3 \\ x_\alpha > x,\ 1 = k_\alpha < i \end{array} \right\} \\ + \begin{cases} \sum_{i \ne 2} \left\{ |\sigma_{l,i,\alpha}| \colon \begin{array}{l} x_\alpha < x,\ \alpha \in J_l(U^\epsilon) \\ x_\alpha > x,\ \alpha \in J_l(V^\epsilon) \end{array} \right\}, & \text{if } q_{l,i}(x) < 0, \\ \sum_{i \ne 2} \left\{ |\sigma_{l,i,\alpha}| \colon \begin{array}{l} x_\alpha < x,\ \alpha \in J_l(V^\epsilon) \\ x_\alpha > x,\ \alpha \in J_l(U^\epsilon) \end{array} \right\}, & \text{if } q_{l,i}(x) \ge 0, \end{cases} \end{aligned} \tag{8.36}$$

where $J_l(U^\epsilon), J_l(V^\epsilon)$ are sets of discontinuities in U^ϵ and V^ϵ, respectively, see also [5, Sect. 8]. In the functions $A_{l,i}^{\mathscr{E}_k}$, $k = 1,2,3$ above, approaching waves are summed up essentially. However, these weights are the building block, in order to prove property (8.30).

Lemma 8.15. *With a suitable choice of $\kappa_1, \kappa_2 > 0$ in (8.31) and $\delta > 0$ such that $TV\{U_0\}$, $TV\{V_0\} \le \delta$, it holds $1 \le W_{l,i} \le \kappa$ $\forall i, l$.*

Proof. Since $\check{K} \ge 1$ and $A_{l,i} \ge 0$, the inequality $W_{l,i} \ge 1$ is immediate. From (8.35), one concludes $A_{l,i} \le \Upsilon(U^\epsilon)(t) + \Upsilon(V^\epsilon)(t)$ and consequently

$$\begin{aligned} W_{l,1} &\le \check{K}(1 + \kappa_1(\Upsilon(U^\epsilon)(t) + \Upsilon(V^\epsilon)(t)) + \kappa_1\kappa_2(\Upsilon(U^\epsilon)(t) + \Upsilon(V^\epsilon)(t))) \\ &= \check{K}(1 + (\Upsilon(U^\epsilon)(t) + \Upsilon(V^\epsilon)(t))(\kappa_1 + \kappa_1\kappa_2)) \\ &\le \check{K}(1 + 2\delta(\kappa_1 + \kappa_1\kappa_2)). \end{aligned} \tag{8.37}$$

The last inequality in (8.37) results from the fact, that $t \mapsto \Upsilon(U^\epsilon)(t)$ is non-increasing as well as $\Upsilon(U^\epsilon)(0), \Upsilon(V^\epsilon)(0) \le \delta$. For all remaining weights $W_{l,i}$, one proceeds analogously while neglecting coefficient $\check{K}$. Accordingly, $1 \le W_{l,i} \le \kappa$ holds for $\kappa = \check{K}(1 + 2\delta(\kappa_1 + \kappa_1\kappa_2))$. □

Remark 8.16. *More precisely, in regard of model $(\mathscr{E}_1)$ it holds $1 \le \check{K} \le W_{l,1} \le \kappa$ and $1 \le W_{l,i} \le 2$ for $i = 2,3$. If models $(\mathscr{E}_2)$ and $(\mathscr{E}_3)$ are considered, we get $1 \le \check{K} \le W_{l,1} \le \kappa$ and $1 \le W_{l,2} \le 2$.*

An immediate consequence of lemma 8.15 is estimate (8.30b). The proof of (8.30c) is more involved, and we show this property for the junction only, while for the pipes itself, this follows from [5, Sect. 8], see also [17].

Let $x_{\alpha_1}, x_{\alpha_2}, \ldots$ be points, where U^ϵ and V^ϵ have discontinuities in the l-th pipe at time t. By the divergence theorem it follows

$$\frac{d}{dt}\Theta_l(U^\epsilon(t), V^\epsilon(t)) = \sum\nolimits_j \sum\nolimits_i \left\{ |q_i(x_{\alpha_j}-)| W_{l,i}(x_{\alpha_j}-) - |q_i(x_{l,\alpha_j}+)| W_{l,i}(x_{\alpha_j}+) \right\} \dot{x}_{\alpha_j}.$$

Since U^ϵ and V^ϵ are constant on intervals $]x_{\alpha_{j-1}}, x_{\alpha_j}[$, one has

$$|q_{l,i}(x)| W_{l,i}(x) \lambda_{l,i}(x) = |q_{l,i}(x_{\alpha_{j-1}}+)| W_{l,i}(x_{\alpha_{j-1}}+) \lambda_{l,i}(x_{\alpha_{j-1}}+) = |q_{l,i}(x_{\alpha_j}-)| W_{l,i}(x_{\alpha_j}-) \lambda_{l,i}(x_{\alpha_j}-),$$

see also [5, Sect. 8], and we conclude

$$\begin{aligned} \frac{d}{dt}\Theta_l(U^\epsilon(t), V^\epsilon(t)) = &\sum\nolimits_i |q_{l,i}(0+)| W_{l,i}(0+) \lambda_{l,i}(0+) \\ &+ \sum\nolimits_j \sum\nolimits_i \left\{ |q_{l,i}(x_{\alpha_j}-)| W_{l,i}(x_{\alpha_j}-) \left[\dot{x}_{\alpha_j} - \lambda_i(x_{\alpha_j}-) \right] \right. \\ &\left. - |q_{l,i}(x_{\alpha_j}+)| W_{l,i}(x_{\alpha_j}+) \left[\dot{x}_{\alpha_j} - \lambda_i(x_{\alpha_j}+) \right] \right\}. \end{aligned}$$

Reference [5, Sect. 8] shows $\sum_j \sum_i \{...\} \leq C\epsilon$. Therefore

$$\frac{d}{dt}\Theta(U^\epsilon(t), V^\epsilon(t)) \leq \sum_l \sum_i |q_{l,i}(0+)|W_{l,i}(0+)\lambda_{l,i}(0+) + \sum_l C\epsilon.$$

Now, we consider model $(\mathscr{E}_1)$ on the l-th pipe and receive at the junction

$$\begin{aligned}\sum_i |q_{l,i}(0+)|W_{l,i}(0+)\lambda_{l,i}(0+) &\leq \{-|q_{l,1}(0+)|W_{l,1}\check{\lambda}_l + \left(|q_{l,2}(0+)|W_{l,2} + |q_{l,3}(0+)|W_{l,3}\right)\hat{\lambda}_l\} \\ &\leq \{-|q_{l,1}(0+)|\check{K}\check{\lambda}_l + 2\left(|q_{l,2}(0+)| + |q_{l,3}(0+)|\right)\hat{\lambda}_l\} \\ &\leq |q_{l,1}(0+)|\left(-\check{K}\check{\lambda}_l + 2K_J\hat{\lambda}_l\right) \\ &\leq 0.\end{aligned}$$

In the first inequality we used $\lambda_{l,1} < -\inf|\lambda_{l,1}| \leq -\check{\lambda}_l$ and $\hat{\lambda} > \sup|\lambda_i|, i = 2,3$. The second inequality follows from remark 8.16, i.e., $\check{K} \leq W_{l,1}$ and $W_{l,i} \leq 2$ for $i = 2,3$, while the third and last inequality hold true, since $\sum_l(|q_{l,2}| + |q_{l,3}|) \leq K_J \sum_l |q_{l,1}|$ and $\check{K} = 1 + 2\hat{\lambda}K_J/\check{\lambda}$, respectively. Models $(\mathscr{E}_2)$ and $(\mathscr{E}_3)$ are treated similarly. Altogether, this proofs the remaining point 4. in theorem 8.10.

Remark 8.17. *We like to mention, that the proof of theorem 8.10 point 4. breaks down, as soon as* $\check{\lambda} = 0$ *or* $\hat{\lambda} = \infty$. *But since* $\check{\lambda} = \inf|-c+u| < 0$ *and* $\hat{\lambda} = \sup|c+u| < \infty$, *these cases do not appear. In regard of a change in flow direction, i.e.,* $u = 0$ *at a certain point in time, it still holds* $\check{\lambda} = \inf|-c| < 0$ *as well as* $\hat{\lambda} = \sup|c| > \infty$. *Accordingly, a priori knowledge of flow direction, does not affect well-posedness of the Cauchy problem* (8.38).

8.4 Treatment of the Source Term

In this subsection we extend our generalized homogeneous Cauchy problems to generalized inhomogeneous Cauchy problems, i.e., the right hand side is not trivial anymore, and show well-posedness. Since well-posedness has already been achieved for homogeneous problems on networks in section 8, it seems natural to include these results. A possible way to do so, is the utilization of a splitting technique. Here, the homogeneous Cauchy problem is solved first, up to a certain point in time. Afterwards, this solution is posed as initial data for a system of ordinary differential equations, in which the right hand side incorporates all source terms of our network.

However, the theory, which shows well-posedness for these splitting techniques already exists, see for example Colombo and Guerra in [15, Thm. 2.5], and consequently, the assumptions therein have only to be checked. But, for the reader's convenience, we also like to give a brief overview of the theory itself, which is based on the work of Colombo and Guerra [14, 13] as well as Colombo, Guerra, Herty and Schleper [16].

The proceeding is as follows. First, some preliminaries are introduced as well as our main theorem and the theorem 2.5 of Colombo and Guerra in [15], which we like to apply. Latter theorem relies on a successively composition of *Euler steps*, the so called *Euler polynomial*. If the Euler polynomial is contractible in a suitable metric and the composition of Euler steps is always possible, the limit exists and solves the inhomogeneous Cauchy problem. However, a composition of Euler steps might break down

for a certain step size, and we need additional effort to overcome this issue. Nonetheless, if all conditions have been stated, such that the limit is ensured, our underlying domain is suitably restricted. For the reader's convenience, we again state the generalized inhomogeneous Cauchy problem from section 6.

Definition 8.18. *The generalized inhomogeneous Cauchy problem at a junction with N pipes equipped with models* $(\mathscr{E}_1)$-$(\mathscr{E}_3)$ *is defined through the set of equations*

$$\begin{cases} \partial_t U^{(i)} + \partial_x F^{(k_i)}(U^{(i)}) &= G^{(k_i)}(U^{(i)}), & (x,t) \in \mathbb{R}^+ \times \mathbb{R}^+, \\ \Phi\left(U^{(1)}(0^+,t), \dots, U^{(N)}(0^+,t)\right) &= \Pi(t), & t \in \mathbb{R}^+, \\ U^{(i)}(x,0) &= U_0^{(i)}, & x \in \mathbb{R}^+ \end{cases} \tag{8.38}$$

for $i \in \mathbb{I}_i \cup \mathbb{I}_o$, $k_i \in \{1,2,3\}$, *where* $U_0^{(1)}, \dots, U_0^{(N)}$ *are thermodynamic states in* $D = \bigtimes_{i\in\mathbb{I}_i} D_- \times \bigtimes_{i\in\mathbb{I}_o} D_+$, *with domains* $D^{\pm}$ *and index sets* $\mathbb{I}_i$, $\mathbb{I}_o$ *defined in section 6. Furthermore,* $F^{(k)}$, $k = 1,2,3$ *are flux functions of the underlying models* $(\mathscr{E}_1)$-$(\mathscr{E}_3)$, *and* $\Pi\colon \mathbb{R}_+ \to \mathbb{R}^d$ *is a function at the junction. Source terms* $G^{(k)}$, $k = 1,2,3$ *are given through* (2.4) *and* (2.5).

Analogously to [16], we introduce

$$\begin{aligned} X &= \left(\bar{U} + L^1(\mathbb{R}^+; D)\right) \times \left(\bar{\Pi} + L^1(\mathbb{R}^+; \mathbb{R}^n)\right), \\ d\left((U,\Pi),(\tilde{U},\tilde{\Pi})\right) &= \|U - \tilde{U}\|_{L^1} + \|\Pi - \tilde{\Pi}\|_{L^1}, \\ TV(p) &= TV(U) + TV(\Pi) + \|\Phi(U(0+)) - \Pi(0+)\|, \\ \mathscr{U}_\delta &= \{U \in \bar{U} + L^1(\mathbb{R}^+, \Omega)\colon TV(U) \le \delta\}, \end{aligned}$$

where (X,d) is a metric space, on which problem (8.38) is solved.

The approach in all before mentioned references relies on a splitting argument. Here, the network is solved in conservative form, up to time τ, first, i.e., we solve

$$\begin{cases} U_t + F(U)_x &= 0, \\ U(0,x) &= U_0(x), \\ \Phi(U) &= \Pi(t), \end{cases} \tag{8.39}$$

where, all flux functions are assumed to be encoded in $F(U) = \left(F^{(k_1)}(U^{(1)}) \ \cdots \ F^{(k_N)}(U^{(N)})\right)$. Afterwards, the resulting solution U at time τ is used as initial condition for an ordinary differential equations, of the form

$$\begin{cases} V_t &= G(V), \\ V(0) &= U(\tau). \end{cases} \tag{8.40}$$

with $G(U) = \left(G^{(k_1)}(U^{(1)}) \ \cdots \ G^{(k_N)}(U^{(N)})\right)$. Since our source terms (2.4) and (2.5) are piecewise differentiable and continuous, it follows by Picard Lindelöf, that (8.40) has at least locally a unique solution.

Based on this approach, *Euler polygonals* are constructed with step length $\epsilon > 0$, similar to the theory of ordinary differential equations, see [7]. For $\epsilon \to 0$, all trajectories coincide with the solution of (8.38).

The results of this subsection are formulated in the next theorem.

Theorem 8.19. *Let $\mathbb{I}_i, \mathbb{I}_o \neq \emptyset$ and Φ given by either (6.6), (2.6) or (2.7). Assume constant initial data $\bar{U}^{(i)}$, $i = 1, ..., N$ with $\Phi(\bar{U}) = 0$ are given. Then there exist positive constants δ, δ', K, domains D_t for $t \in [0, T]$ and a map*

$$\mathscr{E}: \{(\tau, t_0, p): t_0 \in [0, T),\ \tau \in [0, T - t_0],\ p \in D_{t_0}\} \to D^{\delta}: (\tau, t_0, p) \mapsto \mathscr{E}(\tau, t_0)p$$

with $\mathscr{E}(\tau, t_0)p = (U(t_0 + \tau), \mathscr{T}_{\tau + t_0}\Pi(t_0))$ and $\mathscr{T}_t\Pi(t_0) = \Pi(t + t_0)$ the right shift operator, such that

1. *$D^{\delta'} \subseteq D_t \subseteq D^{\delta}(\bar{U})$ for all $t \in [0, T]$,*
2. *$\mathscr{E}(0, T_0)p = p$ for all $t_0 \in [0, T]$, $p \in D_t$,*
3. *$\mathscr{E}(\tau, t_0)D_{t_0} \subseteq D_{t_0 + \tau}$ for all $t_0 \in [0, T]$, $\tau \in [0, T - t_0]$,*
4. *for all $t_0 \in [0, T]$, $\tau_1, \tau_2 \geq 0$ with $\tau_1 + \tau_2 \in [0, T - t_0]$ it holds*

$$\mathscr{E}(\tau_2, t_0 + \tau_1) \circ \mathscr{E}(\tau_1, t_0) = \mathscr{E}(\tau_1 + \tau_2, t_0),$$

5. *$\mathscr{E}$ is a tangent to the Euler polygonal in the sense that for all $t_0 \in [0, T)$ and for all $(U_0, \Pi) \in D_{t_0}$ there holds*

$$\lim_{t \to 0} \frac{1}{t} \| U(t) - (S_t(U_0, \Pi) + tG(U_0)) \|_{L^1} = 0,$$

6. *for all $t_0 \in [0, T)$, $\tau \in [0, T - t_0]$ and for all $p, \tilde{p} \in D_{t_0}$*

$$\| \mathscr{E}(\tau, t_0)p - \mathscr{E}(\tau, t_0)\tilde{p} \|_{L^1} \leq L \| U - \tilde{U} \|_{L^1} + L \int_{t_0}^{t_0 + \tau} \| \Pi(t) - \tilde{\Pi}(t) \| \, dt. \tag{8.41}$$

Here, we set $D^{\delta} = cl_{L^1}\{p \in X : TV(p) < \delta\}$, which is an extension of $\mathscr{D} = cl_{L^1}(D_{\delta}(\bar{U})) = \{U \in D : TV(U) < \delta\}$ in subsection 8.3.2. From point 5 in theorem 8.19 it follows that $U(t)$ is a weak entropic solution to problem 8.18, by utilizing [13]. For simplification purposes, define

$$\Xi = \{(\tau, t_0, p): t_0 \in [0, T),\ \tau \in [0, T - t_0],\ p \in D_{t_0}\}. \tag{8.42}$$

At this point, we like to remark, that D_t from theorem 8.19 is used in definition 8.42, without even knowing, if it exists. However, it will be specified in the further proceeding.

Next, the *Euler step function* is introduced

$$F(t, t_0)p = \big(S_t U(t_0) + tG(S_t U(t_0)), \mathscr{T}_t \Pi(t_0)\big), \tag{8.43}$$

as well as the *ϵ-Euler polygonal*

$$F^{\epsilon}(t,t_0)p = F(t-k\epsilon t_0+k\epsilon)\circ\bigcirc_{j=0}^{k-1}F(\epsilon,t_0+h\epsilon)p, \tag{8.44}$$

with $k=\lfloor t/\epsilon\rfloor$. Like already mentioned, we want to take the limit $\epsilon\to 0$ in (8.44), in order to discover a process, which solves problem 8.18. This process is defined next, see also [15, Def. 2.4].

Definition 8.20. *Consider a family of domains $D_{t_0}\subseteq D$ for all $t_0\in I$. A global process on X is a map $P\colon \Xi\to X$ such that, for all t_0,t_1,t_2,p satisfying $t_1,t_2\geq 0,\ t_0+t_1+t_2\in I$, and $p\in D_{t_0}$, which satisfies*

$$P(0,t_0)p = p, \tag{8.45a}$$
$$P(t_1,t_0)p\in D_{t_0+t_1}, \tag{8.45b}$$
$$P(t_2,t_0+t_1)\circ P(t_1,t_0)p = P(t_2+t_1,t_0)p. \tag{8.45c}$$

Furthermore, we introduce the definition of a *local flow*, according to [15, Def. 2.1].

Definition 8.21. *Given a closed subset $D\subseteq X$, a local flow is a continuous map $F\colon[0,\delta]\times I\times D\to X$, such that $F(0,t_0)p=p$ for any $(t_0,p)\in I\times D$, and which is Lipschitz in its first and third component and uniformly in its second, i.e., there exists a $L>0$ such that for all $\tau,\tau'\in[0,\delta]$ and $p,p'\in D$, it holds*

$$d\left(F(\tau,t_0)p,F(\tau',t_0)p'\right)\leq L\left(d(p,p')+|\tau-\tau'|\right). \tag{8.46}$$

Now, [15, Thm 2.5] can be stated.

Theorem 8.22. *The local flow F is such that there exists*

1. *a non-decreasing map $\omega\colon[0,\delta]\mapsto\mathbb{R}_+$ with $\int_0^\delta w(\tau)/\tau\,d\tau<\infty$ such that*

$$d\left(F(k\tau,t_0+\tau)\circ F(\tau,t_0)p,F((k+1)\tau,t_0)p\right)\leq k\tau w(\tau) \tag{8.47}$$

   whenever $\tau\in[0,\delta]$, $k\in\mathbb{N}$ and the left hand side above is well defined;

2. *a positive constant L such that*

$$d\left(F^{\epsilon}(t,t_0)p,F^{\epsilon}(t,t_0)p'\right)\leq L\,d(p,p') \tag{8.48}$$

   whenever $\epsilon\in[0,\delta]$, $p,p'\in D$, $t\geq 0$, $t_0,t_0+t\in I$ and the left hand side above is well defined.

Then, together with domain

$$D_{t_0}^3=\left\{p\in D\colon \begin{array}{l} F^{\epsilon_3}(t_3,t_0+t_1+t_2)\circ F^{\epsilon_2}(t_2,t_0+t_1)\circ F^{\epsilon_1}(t_1,t_0)p \\ \text{is in } D \text{ for all } \epsilon_1,\epsilon_2,\epsilon_3\in(0,\delta] \text{ and all} \\ t_1,t_2,t_3\geq 0 \text{ such that } t_0+t_1+t_2+t_3\in I \end{array}\right\} \tag{8.49}$$

there exists a family of sets D_{t_0}, $t_0 < T$ and a unique global process $P : \Xi \to X$ with following properties

1. *$D^3_{t_0} \subseteq D_{t_0}$ for any $t_0 \in I$.*
2. *P is Lipschitz in (t, t_0, U).*
3. *P is tangent to F in the sense that for all $p \in D_{t_0}$, for all t such that $t \in (0, \delta]$ and $t_0 + t \in I$, it holds*

$$\frac{1}{t} d\left(P(t,t_0)p, F(t,t_0)p\right) \leq \frac{2L}{ln(2)} \int_0^t \frac{w(\xi)}{\xi}\, d\xi. \tag{8.50}$$

As soon as assumptions in theorem 8.22 are verified, points 2.-4., 6. in theorem 8.19 can be concluded immediately from theorem 8.22 with $P = \mathscr{E}$.

However, the first conclusion in theorem 8.22 needs some additional treatment, since $D^3_{t_0}$ might become empty for $\epsilon \to 0$ and will be examined in more detail later on.

Next, we show that F in (8.43) is a local flow, according to definition 8.21. $F(0, t_0)p = p$ follows due to construction of F. Estimate (8.46) is proven in [16, Prop. 4.8]. A proof of estimates (8.47) and (8.48) can be found in [16, Prop. 4.9].

Now, the first conclusion in theorem 8.22 is investigated in more detail. In the limit $\epsilon \to 0$, it is not clear, if domain $D^3_{t_0}$ might become empty, and therefore $\Xi = \emptyset$, on which the global process is defined. This happens for example, if images and domains of $F^{\epsilon_3}(t_3, t_0 + t_1 + t_2)$, $F^{\epsilon_2}(t_2, t_0 + t_1)$, $F^{\epsilon_1}(t_1, t_0)$ do not match anymore, for $\epsilon_j \to 0$, $j = 1, 2, 3$. In order to overcome this problem, we extend all functionals $\mathsf{V}, \mathsf{Q}, \Upsilon$ in (8.21)-(8.23) onto X in consideration of a boundary term Π, according to (8.29), i.e.,

$$\begin{aligned}
\mathsf{V}(U)(t) &= \sum_{l=1}^{n} \mathsf{V}_l(U)(t), \quad \mathsf{V}_l(U)(t) = \sum_{\alpha \in J_l} C_l(v_{k_\alpha}) |v_{k_\alpha}|, \\
\mathsf{Q}(U)(t) &= \sum_{l=1}^{n} \mathsf{Q}_l(U)(t), \quad \mathsf{Q}_l(t) = \sum_{(\alpha,\beta) \in \mathscr{A}_l} |v_{k_\alpha} v_{k_\beta}|, \\
\Upsilon(p)(t) &= \mathsf{V}(U)(t) + \tilde{K}_J \mathsf{Q}(U)(t) + \hat{K}_J TV\{\Pi(t)\}.
\end{aligned}$$

Here, constants $\tilde{K}_J$, $\hat{K}_J > 0$ correspond to lemma 8.12 and (8.29), respectively, from which we conclude $t \mapsto \Upsilon(p)(t)$ is non-increasing. The stability functional Θ in (8.31) can be extended onto X as well

$$\hat{\Theta}(p, \tilde{p}) = \Theta(U, \tilde{U}) + \hat{K}_J \|\Pi - \tilde{\Pi}\|_{L^1} = \sum_{l=1}^{N} \Theta_l(U, \tilde{U}) + \hat{K}_J \|\Pi - \tilde{\Pi}\|_{L^1},$$

with Θ and Θ_l defined through (8.31), see also [16]. Analogously to [16, Prop 4.6], we formulate our next proposition.

Proposition 8.23. *Let G be weak differentiable for all $p \in D$ and $t_0 \in [0, T]$. Then the following estimates hold for $\tau > 0$ sufficiently small*

$$\Upsilon(F(\tau, t_0)p) \leq \Upsilon(p) + C\tau \tag{8.51}$$

$$\Theta(F(\tau, t_0)p, F(\tau, t_0)\tilde{p}) \leq (1 + \tilde{C}\tau)\Theta(p, \tilde{p}), \tag{8.52}$$

The proof of (8.51) can be found in [16]. The second estimate (8.52) however is slightly different to the one, given in [16, Prop. 4.6] and will therefore be shown here.

Proof. Consider $U, \tilde{U} \in \mathscr{U}_\delta$. Then, it suffices to show that

$$\Theta(U + \tau G(U), \tilde{U} + \tau G(\tilde{U})) \leq (1 + \tilde{C}\tau)\Theta(S_\tau U, S_\tau \tilde{U}) \tag{8.53}$$

since

$$\begin{aligned}
\hat{\Theta}(F(\tau, t_0)p, F(\tau, t_0)\tilde{p}) &= \Theta(U(t_0) + \tau G(U(t_0)), \tilde{U}(t_0) + \tau G(\tilde{U}(t_0))) + \hat{K}_J \|\Pi - \tilde{\Pi}\|_{L^1} \\
&\leq (1 + \tilde{C}\tau)\Theta(U(\tau), \tilde{U}(\tau)) + \hat{K}_J \|\Pi - \tilde{\Pi}\|_{L^1} \\
&= (1 + \tilde{C}\tau)\Theta(S_\tau U(t_0), S_\tau \tilde{U}(t_0)) + \hat{K}_J \|\Pi - \tilde{\Pi}\|_{L^1} \\
&\leq (1 + \tilde{C}\tau)\hat{\Theta}(p, \tilde{p})
\end{aligned}$$

in which (8.53) and (8.30b) have been used in the first and second inequality, respectively.

Regarding the proof of (8.53), we partly utilize some estimates in [14, Proof of Lemma 2.3]. Therefore, let $\Theta_l(t) = \Theta_l(U + tG(U), \tilde{U} + tG(\tilde{U}))$ be a short notation. By an application of [14, Lem 3.1], we receive on the l-th pipe

$$\begin{aligned}
\frac{d}{dt}\Theta_l(t) \leq & \int_{\mathbb{R}^+} \sum_{i=1}^{n} \left\{ |q_i^+(x)| - |q_i^-(x)| \right\} dx \\
& + \mathscr{O}(1)\tau\delta \int_{\mathbb{R}^+} \sum_{i=1}^{n} |q_i^-(x)| dx + \mathscr{O}(1)\tau\delta \int_{\mathbb{R}^+} \|G(U)(x) - G(\tilde{U})(x)\| dx \\
\leq & \mathscr{O}(1)\tau \sum_{i=1}^{n} \int_{\mathbb{R}^+} |q_i^-(x)| dx + \mathscr{O}(1)\tau \int_{\mathbb{R}^+} \|G(U)(x) - G(\tilde{U})(x)\| dx \\
& + \mathscr{O}(1)\tau\delta \int_{\mathbb{R}^+} \sum_{i=1}^{n} |q_i^-(x)| dx + \mathscr{O}(1)\tau\delta \int_{\mathbb{R}^+} \|G(U)(x) - G(\tilde{U})(x)\| dx \\
\leq & \mathscr{O}(1)\tau(1+\delta) \sum_{i=1}^{n} \int_{\mathbb{R}^+} |q_i(x)| dx + \mathscr{O}(1)\tau \|DG\|_{L^\infty(\mathscr{U}_\delta)} \int_{\mathbb{R}^+} \|U(x) - \tilde{U}(x)\| dx \\
\leq & \tau\mathscr{O}(1)[(1+\delta) + \|DG\|_{L^\infty(\mathscr{U}_\delta)}] \sum_{i=1}^{n} \int_{\mathbb{R}^+} |q_i^-(x)| dx
\end{aligned}$$

where $\mathscr{O}(1)$ is an uniformly bounded constant. Given definitions of $W_{l,i}$ in (8.31), we know $|W_{l,i}| \geq 1$ due to lemma 8.15. This implies

$$\sum_{i=1}^{n} \int_{\mathbb{R}^+} |q_i^-(x)| dx \leq \Theta(U, \tilde{U})$$

and consequently

$$\Theta(U + \tau G(U), \tilde{U} + \tau G(\tilde{U})) \leq (1 + \tilde{C}\tau)\Theta(U, \tilde{U})$$

with constant $\tilde{C} = \mathcal{O}(1)[(1+\delta) + \|DG\|_{L^\infty(\mathcal{U}_\delta)}]$, stating the proof. □

Now, consider the domain

$$\hat{D}_t^M = \left\{ p \in X : \begin{array}{lcl} \Upsilon(p) & \leq & \delta - C(T-t) \\ \Theta(p,\bar{p}) & \leq & M - C(T-t) \end{array} \right\} \subseteq D^\delta \tag{8.54}$$

with $M, T > 0$ and $\bar{p} = (\bar{U}, \bar{\Pi})$ as stationary state. Here, $M > 0$ has to be chosen, such that $M - C(T-t) > 0, \forall t \geq T$. Based on estimates (8.51) and (8.52), it follows $F(t, t_0, p)\hat{D}_{t_0}^M \subseteq \hat{D}_{t_0+t}^M$. Accordingly, domains and images of all single Euler steps in the ϵ-Euler polygonal match and we receive the lower bound $\hat{D}_{t_0}^M \subseteq D_{t_0}^3 \subseteq D_{t_0}$, which ensures $\Xi \neq \emptyset$, see also [15, **(D)**]. In theorem 8.19, one identifies $D^\delta = \hat{D}_{t_0}^M$.

In the next subsection, a proof towards existence of an optimal control at the junction is given.

8.5 Existence of an Optimal Control

Due to theorem 8.19, where L^1-stability of the solution to problem (8.38) in dependence of the initial and junction data has been proven, it becomes natural to built an optimal control theory upon these results. This has already been done in Colombo, Guerra, Herty and Schleper [16, Prop. 2.4]. But for convenience of the reader, we like to formulate the proof in more detail.

Theorem 8.24. *Consider the generalized inhomogeneous Cauchy problem* (8.38) *and the functional*

$$J(\Pi) = J_0(\Pi) + \int_0^T J_1(\mathscr{E}(\tau, 0)(U_0, \Pi))\, d\tau \tag{8.55}$$

with

$$J_0 \colon \left\{ \Pi\big|_{[0,T]} \colon \Pi \in (\bar{\Pi} + L^1(\mathbb{R}_+; \mathbb{R}^n)) \text{ and } (U_0, \Pi) \in \mathscr{D}^\delta \right\} \to \mathbb{R}_+, \qquad J_1 \colon \mathscr{D}^\delta \to \mathbb{R}_+.$$

Let J_0 and J_1 be lower semi-continuous with respect to the L^1-norm. Then J has a minimum on

$$\mathscr{M} = \left\{ \Pi\big|_{[0,T]} \colon \Pi \in (\bar{\Pi} + L^1(\mathbb{R}_+; \mathbb{R}^n)) \text{ and } (U_0, \Pi) \in \mathscr{D}^\delta \right\}. \tag{8.56}$$

Proof. Since $\mathscr{M}$ contains L^1 functions Π with bounded total variation on the intervall $[0, T]$, i.e., $(U_0, \Pi) \in \mathscr{D}^\delta$, it follows that $\mathscr{M}$ is compactly embedded in L^1. By an application of the Weierstrass theorem, the existence of a minimum on $\mathscr{M}$ follows immediately for any lower semi-continuous func-

tional in regard of the underlying metric. Towards the semi-continuity of J, it suffices to study the second summand only, since J_0 is already lower semi-continuous, with respect to L^1, by assumption.

$$\begin{aligned} \int_0^T J_1(\mathscr{E}(\tau,0)(U_0,\hat{\Pi}))\,d\tau &= \int_0^T J_1\left(\lim_{\|\Pi-\hat{\Pi}\|_{L^1}\to 0}\mathscr{E}(\tau,0)(U_0,\Pi)\right)d\tau \\ &\leq \int_0^T \liminf_{\|\Pi-\hat{\Pi}\|_{L^1}\to 0} J_1(\mathscr{E}(\tau,0)(U_0,\Pi))\,d\tau \\ &\leq \liminf_{\|\Pi-\hat{\Pi}\|_{L^1}\to 0}\int_0^T J_1(\mathscr{E}(\tau,0)(U_0,\Pi))\,d\tau \end{aligned} \tag{8.57}$$

The first equation in (8.57) is a consequence of (8.41), which states continuity of $\mathscr{E}$ in Π. The first inequality in (8.57) is due to the lower semi-continuity of J_1, while the second inequality holds by an application of Fatou's lemma, which states the proof. □

9 Numerics

This section is concerned with the numerical treatment of gas dynamics on networks as well as their optimization. In our first subsection 9.1, we give an overview of numerical algorithms, based on the finite volume approach in subsection 4.2. Subsection 9.2 is concerned with the boundary and junction treatment, based on our results in sections 5 and 6. In subsection 9.3, an algorithm is introduced to handle changing flow directions in our coupling conditions (6.6).

Since, we also like to give an optimal control technique, the functional (8.55) is examined from a numerical point of view in subsection 9.4. In order to solve the occurring optimal control problem numerically, a Gauss-Newton algorithm is briefly presented in subsection 9.5, and applied in subsection 9.6. The last subsection 9.7 is concerned with some numerical illustrations as well as an optimization example.

9.1 Finite Volume Methods

In this subsection, we introduce some methods, based on the finite volume approach in subsection 4.2, in order to treat systems of hyperbolic partial differential equations on networks. However, up to the current date it is unclear, whether these methods create a series of numerical solutions, that converge to the solution of the hyperbolic problem. Nonetheless, for scalar conservation and balance laws, this issue can be answered positively. Compare for example the work of LeVeque in [33, Sect. 12.7].

We start with the following system of hyperbolic partial differential equations

$$\begin{cases} U_t + F(U)_x &= G(U), \\ U(x,0) &= U_0(x) \end{cases} \tag{9.1}$$

with $U\colon \mathbb{R}\times\mathbb{R}_+ \supseteq \Omega_x\times\Omega_t \to D \subseteq \mathbb{R}^n$, $F\in C^1(D;\mathbb{R}^n)$ and $G\in L^1(D;\mathbb{R}^n)$. By an application of the *finite volume method*, U_0 is approximated by a piecewise constant function $\tilde{U}_0$ on intervals $I_i = [x_{i-\frac{1}{2}}, x_{i+\frac{1}{2}}]$ with length $\Delta x_i = x_{i+\frac{1}{2}} - x_{i-\frac{1}{2}}$. Furthermore, the time axis $\mathbb{R}_+$ is divided into intervals $J_j = [t_j, t_{j+1}]$ with length $\Delta t_j = t_{j+1} - t_j$ as well. For sake of simplicity, all intervals are assumed to be equidistant, i.e., $\Delta t = \Delta t_j$ and $\Delta x = \Delta x_i$. Now, problem (9.1) is integrated over boxes $I_i \times J_j$, resulting in

$$\begin{aligned} \int_{I_i} U(x,t_{j+1}) - U(x,t_j)\,dx \;+\; & \int_{J_j} F(U(x_{i+\frac{1}{2}},t)) - F(U(x_{i+\frac{1}{2}},t))\,dt \\ = \; & \int_{J_j\times I_i} G(U(x,t))\,d(x,t). \end{aligned} \tag{9.2}$$

By multiplying equation (9.2) with $1/\Delta x$, we receive

$$\tilde{U}_i(t_{j+1}) - \tilde{U}_i(t_j) + \frac{\Delta t}{\Delta x}\left(F_{i+\frac{1}{2}} - F_{i-\frac{1}{2}}\right) - G_{i,j} = 0. \tag{9.3}$$

where

$$\bar{U}_i(t) = 1/\Delta x \int_{I_i} U(x,t)\,dx,$$
$$F_{i+\frac{1}{2}}(u) = 1/\Delta t \int_{J_j} F(u(x_{i+\frac{1}{2}},t))\,dt,$$
$$G_{i,j} = 1/\Delta x \int_{J_j \times I_i} G(u(x,t))\,d(x,t).$$

Terms $\bar{U}$ and $F_{i+\frac{1}{2}}$ are called *cell volume* and *cell flux*, respectively.

Since, $F_{i+\frac{1}{2}}$ and $G_{i,j}$ depend on the solution U for $t \in J_j$ itself, which is unknown, these integrals have to be approximated by functions $\hat{F}_{i+\frac{1}{2}}$ and $\hat{G}_{i,j}$. Former is called *numerical flux function* or *numerical flux*.

By neglecting the source term in (9.6), i.e., $G \equiv 0$, we observe, that a change in $\bar{U}$ is due to the cell flux $F_{i+\frac{1}{2}}$ at cell boundaries ∂I_i only, and one rediscovers the conservation property in definition 2.1. See also figure 26. Consequently, the numerical flux $\hat{F}_{i\pm\frac{1}{2}}$ will be made dependent on $U(x_{i+\frac{1}{2}}\pm, t)$, i.e.,

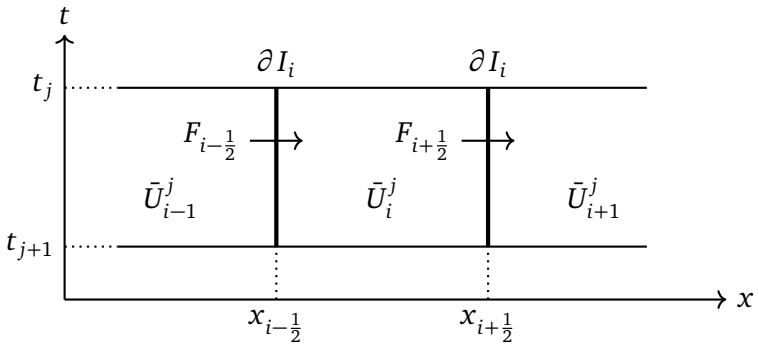

Figure 26: Schematic presentation of temporal change in $\bar{U}$ due to the flux $F_{i\pm\frac{1}{2}}$ at cell boundary ∂I_i.

$$\hat{F}_{i+\frac{1}{2}}(t) = \hat{F}_{i+\frac{1}{2}}\Big(U(x_{i+\frac{1}{2}}+,t), U(x_{i+\frac{1}{2}}-,t)\Big). \tag{9.4}$$

This expression becomes crucial for spatial approximations of higher order in-particular. Several numerical fluxes with property (9.4) can be found in [33, Sect. 4]. A common approximation is the so called *Lax-Friedrich flux*

$$\hat{F}_{i+\frac{1}{2}} = \frac{1}{2}(F(U_i) + F(U_{i+1})) + \frac{\Delta x}{2\Delta t}(U_i - U_{i+1}). \tag{9.5}$$

For $\hat{G}_{i,j}$, one might choose a quadrature. In this work, $G_{i,j}$ is simply approximated through $G_{i,j} \approx \hat{G}_{i,j} = \Delta t G(U_i^j)$. Under consideration of $\hat{F}_{i+\frac{1}{2}}$ and $\hat{G}_{i,j}$, a numerical approximation of (9.3) is provided by

$$\mathrm{PDE}(U^{j+1}, U^j)_i := U_i^{j+1} - U_i^j + \frac{\Delta t}{\Delta x}\Big(\hat{F}_{i+\frac{1}{2}} - \hat{F}_{i+\frac{1}{2}}\Big) - \hat{G}_{i,j} = 0. \tag{9.6}$$

Now, PDE(U^{j+1}, U^j) has to be solved for $\{U_i^{j+1}\}_i \approx \{\bar{U}_i(t_{j+1})\}_i$, given the data $\{U_i^j\} \approx \{\bar{U}_i(t_j)\}_i$. It remains the question, how to approximate the boundary values $U(x_{i+\frac{1}{2}}\pm, t)$, on intervals $I_i = [x_{i-\frac{1}{2}}, x_{i+\frac{1}{2}}]$. One possible approach is

$$U(x_{i+\frac{1}{2}}\pm, t) \approx U_i^j, \ \forall t \in [t_j, t_{j+1}). \tag{9.7}$$

Scheme (9.6) equipped with (9.7) is then called *time explicit*. By choosing

$$U(x_{i+\frac{1}{2}}\pm, t) \approx U_i^{j+1}, \ \forall t \in [t_j, t_{j+1}). \tag{9.8}$$

expression (9.6) becomes *time implicit*. Another possible approximation of the boundary values $U(x_{i+\frac{1}{2}}, t)$ is achieved by the so called *weighted essentially non-oscillatory* method of order k, or short k-WENO. Here, polynomials are constructed from staggered stencils, consisting of cell-volumes $\{U_i^j\}$. Afterwards, a convex combination of these polynomials is build, in which coefficients become zero, if a discontinuity appears in $\{U_i^j\}$. This approach results in higher order approximation of $U(x_{i+\frac{1}{2}}, t)$, if $\{U_i^j\}$ is sufficiently smooth, but captures shocks if necessary. For more details see [42].

9.2 Implementation Details

In this subsection, we like to give some insight information regarding our implementation of gas dynamics on networks.

A network topology $\mathcal{G} = (\mathcal{A}, \mathcal{V})$ is initialized by an incidence matrix $B = (b_{l,k})_{l,k}$, $b_{l,k} \in \{-1, 0, 1\}$, $l = 1, ..., M_{\mathcal{V}}$, $k = 1, ..., M_{\mathcal{A}}$, with $M_{\mathcal{V}} = |\mathcal{V}|$ and $M_{\mathcal{A}} = |\mathcal{A}|$, see [4] for more details on its definition. A node v_l, which is connected to v_k due to a pipe $e_{l,k}$, is called *ingoing*, if $b_{k,l} = 1$ and *outgoing*, if $b_{k,l} = -1$. Furthermore, v_l is a boundary node, if $b_{k,\hat{l}} = 0, \forall \hat{l} \neq l$. In figure 27, an example network is provided as well as its incidence matrix.

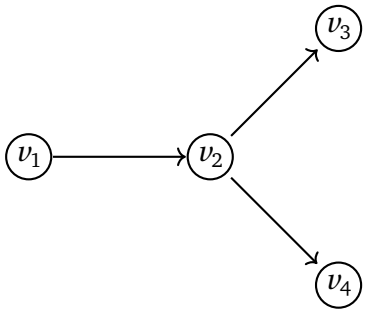

$$B = \begin{pmatrix} -1 & 0 & 0 \\ 1 & -1 & -1 \\ 0 & 1 & 0 \\ 0 & 0 & 1 \end{pmatrix}$$

Figure 27: Example for a network formulation, based on the incidence matrix B. Here, v_1 is an entry node, v_3, v_4 are exit nodes and v_2 is a junction.

After identifying all junctions and boundary nodes, every pipe $e_{l,k}$ is discretized by a predefined mesh size Δx_k, generating $M_{l,k}$ spatial points. On these discretized pipes we use the numerical scheme (9.6), receiving spatial and temporal approximations $U_k^j = \{U_{k,i}^j\}_i$ on the k-th pipe at time t_j.

In order to treat boundary nodes and junctions, we introduce auxiliary points x_*^{in} and x_*^{out} at the ends of every pipe, on which Riemann states U_*^j of time t_j are located, compare sections 5, 6, 7. Now, the total vector of unknowns at time t_j is defined through $\mathbf{U}^j = [U^j, U_*^j]$.

Figure 28: Schematic presentation of the dependence between boundary nodes □ and inner nodes ∘.

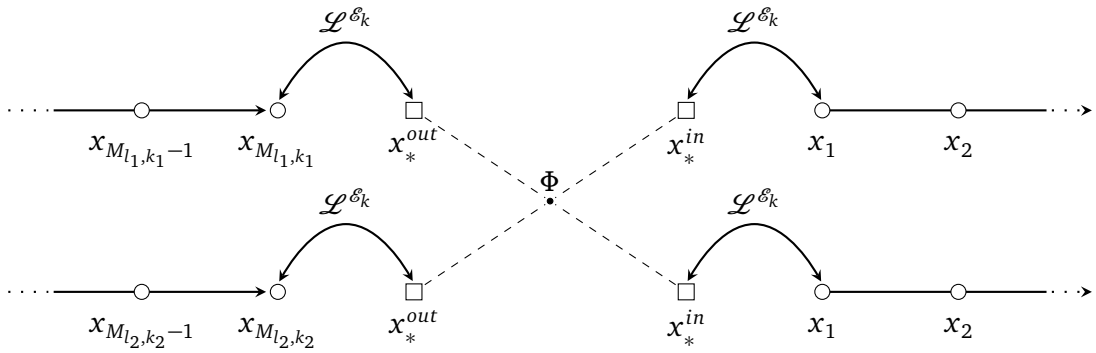

Figure 29: Schematic presentation of the numerical construction at a junction. Here, Φ is a coupling function.

Since for all mesh sizes Δx_k, boundary points x_*^{in} and x_*^{out} have Lebesgue measure zero, all source terms $G^{(k)}$, $k = 1,2,3$ of models $(\mathscr{E}_1)$-$(\mathscr{E}_3)$ are neglected there. Consequently, boundaries can be treated as homogeneous Riemann problems and are solved by an utilization of Lax-curves $\mathscr{L}^{\mathscr{E}_k}$, $k = 1,2,3$, which have been introduced in subsection 4.2.2. Again, these curves are a link between the piecewise constant states U_i^j on pipes and Riemann states U_*^j on boundaries, see figure 28. In regard of an ingoing boundary, one component of U_*^j needs to be posed in order to match the degree of freedom in $\mathscr{L}_1^{\mathscr{E}_k}$, $k = 1,2,3$. At outgoing nodes, one component of U_*^j has to be stated in the presence of $\mathscr{L}_2^{\mathscr{E}_k}$, $k = 2,3$; and two components, if the underlying model is $\mathscr{E}_1$. In appearance of a junction, all belonging Riemann states have to fulfill our coupling conditions (6.6), (2.6) and (2.7), see also figure 29. By denoting $\texttt{LAX}(U^{j+1}, U_*)$ and $\texttt{CPLNG}(U_*^{j+1})$ the collection of Lax curves and coupling functions (6.15), (2.6), (2.7), respectively, the complete function to solve, reads

$$\mathscr{F}(\mathbf{U}^{j+1}, \mathbf{U}^j, \texttt{data}) = \begin{bmatrix} \texttt{PDE}(U^{j+1}, U^j) \\ \texttt{CPX}(U^{j+1}, U_*^{j+1}) \end{bmatrix} \stackrel{!}{=} 0, \tag{9.9}$$

in which the short notation $\texttt{CPX} := \texttt{CPLNG}circ\texttt{LAX}$ has been used. Furthermore, `data` stands for initial, boundary or compressor values. Afterwards, equation (9.9) is solved by an application of Newton's method.

Lemma 9.1. *The Jacobian $D\mathscr{F}$ of function* (9.9) *exists and is invertible.*

Proof. Since both functions PDE and CPX, are continuously differentiable in U^{j+1}, U_*^{j+1}, we receive

$$D_{\mathbf{U}^{j+1}}\mathscr{F} = \begin{bmatrix} D_{U^{j+1}}\texttt{PDE} & 0 \\ D_{U^{j+1}}\texttt{CPX} & D_{U_*^{j+1}}\texttt{CPX} \end{bmatrix} \tag{9.10}$$

From theorems 6.5, 7.2 and [31], one concludes $\det(D_{U_*^{j+1}}\mathtt{CPX})$, $\det(D_{U^{j+1}}\mathtt{PDE}) \neq 0$ respectively. Consequently $\det(D_{\mathbf{U}^{j+1}}\mathscr{F}) = \det(D_{U^{j+1}}\mathtt{PDE})\det(D_{U_*^{j+1}}\mathtt{CPX}) \neq 0$, which states the proof. □

The Jacobian $D\mathscr{F}$ will be reused in subsection 9.4, where a compressor control is optimized.

In the next subsection, we give a numerical algorithm, in order to treat changing flow directions on networks.

9.3 Change of Flow Direction

This subsection is concerned with a change of flow direction on a network. The network consists of a single junction and at least one outgoing pipe, equipped with model $(\mathscr{E}_1)$.

A possible scenario for a change in flow direction is depicted in figure 30. There, the flow in pipe e_4 might change its sign, depending on the flow along the pipes e_2, e_5 and e_3, e_6.

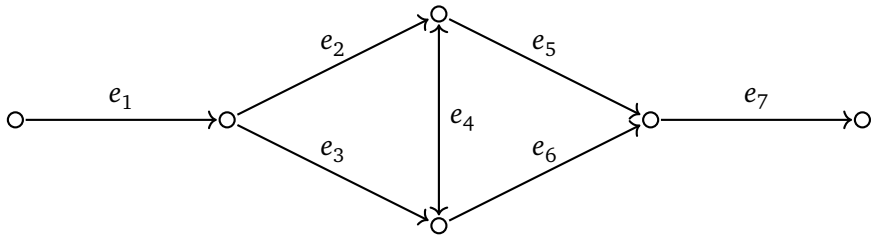

Figure 30: Network topology with changing flux sign on edge e_4.

Our main results in sections 5 and 6 needed an a priori knowledge about flow directions $\operatorname{sign}(q_i)$, in order to built the entropic coupling conditions (6.6c). All remaining coupling conditions (6.6a), (6.6b) are not affected by the flow direction. Consequently, if models $(\mathscr{E}_2)$, $(\mathscr{E}_3)$ are considered only, a change of flow direction can be performed without further adjustment.

We want to remind, that the number of ingoing and outgoing pipes at a junction are contained in the index sets $\mathbb{I}_i = \mathbb{I}_i^{\mathscr{E}_1} \cup \mathbb{I}_i^{\mathscr{E}_2} \cup \mathbb{I}_i^{\mathscr{E}_3}$ and $\mathbb{I}_o = \mathbb{I}_o^{\mathscr{E}_1} \cup \mathbb{I}_o^{\mathscr{E}_2} \cup \mathbb{I}_o^{\mathscr{E}_3}$, respectively.

However, well-posedness of Riemann and Cauchy problems in sections 5.2-8.3, is independent of $\mathbb{I}_i$, $\mathbb{I}_o$ and consequently holds truth for variable sets $\mathbb{I}_i(t)$, $\mathbb{I}_o(t)$, $t > 0$.

Nonetheless, regarding coupling condition (6.6c), which will be denoted by Φ_S, a changing number of ingoing and outgoing pipes becomes a hindrance, since it affects the number of equations. Therefore, we provide a numerical algorithm to overcome this difficulty.

First, coupling condition (6.6c) is extended, such that it contains *all* pipes, i.e.,

$$\tilde{\Phi}_S := \begin{pmatrix} \chi_{\{q_1>0\}}(s^* - q^* s_1) \\ \vdots \\ \chi_{\{q_N>0\}}(s^* - q^* s_N) \end{pmatrix} \stackrel{!}{=} 0, \tag{9.11}$$

with $N = |\mathbb{I}_i^{\mathscr{E}_1}| + |\mathbb{I}_o^{\mathscr{E}_1}|$ and terms

$$s^* = \sum_{i=1}^{N} \max\{0, q_i\} s_i, \qquad q^* = \sum_{i=1}^{N} \max\{0, q_i\}. \tag{9.12a}$$

The indicator function $\chi_{\{q_i>0\}}$ in (9.11) ignores all pipes of ingoing flow into the junction, by setting them to zero. If all resulting zeros in (9.11) are neglected, one regains coupling condition (6.6c) again

$$\tilde{\Phi}_S = \begin{pmatrix} s^* - q^* s_1 \\ \vdots \\ s^* - q^* s_{|\mathbb{I}_o^{\mathscr{E}_1}|} \\ 0 \\ \vdots \\ 0 \end{pmatrix} = \begin{pmatrix} \Phi_S \\ 0 \end{pmatrix}. \tag{9.13}$$

For simplicity, entries in (9.13) have been sorted. Let mass and enthalpy coupling conditions in (6.6) be denoted by Φ_M and Φ_H, respectively. Altogether, we have to solve

$$\tilde{\Phi} = \begin{pmatrix} \Phi_M \\ \Phi_H \\ \tilde{\Phi}_S \end{pmatrix} (q,h,s) \stackrel{!}{=} 0 \tag{9.14}$$

for q,h,s. Due to the additional equations in (9.13), expression (9.14) becomes underdetermined. In order to solve (9.14), a least square Newton approach is applied. Let $J\tilde{\Phi}$ denote the Jacobian of $\tilde{\Phi}$, which has a zero block in its lower half, i.e.,

$$J\tilde{\Phi} = \begin{pmatrix} J\Phi \\ 0 \end{pmatrix}, \tag{9.15}$$

In (9.15) $J\Phi$ is the Jacobian of Φ. Given the k-th iteration vector $y_k = (q_k, h_k, s_k)$ and a tolerance $tol > 0$ a least squares Newton approach reads

while $\|\tilde{\Phi}(y_k)\| > tol$ **do**
  solve $[J\tilde{\Phi}(y_k)^T J\tilde{\Phi}(y_k)]\delta y = J\tilde{\Phi}(y_k)^T \tilde{\Phi}(y_k)$;
  set $y_{k+1} = y_k + \delta y \quad k+1 \to k$;
end

Algorithm 1: Schematic presentation of a least squares Newton algorithm for solving coupling conditions (9.14) with flow change.

Proposition 9.2. *Algorithm 1 is equivalent to Newton's algorithm used for coupling conditions* (6.6).

Proof. Due to the zeros in $\tilde{\Phi}$ and $J\tilde{\Phi}$ we receive

$$\begin{aligned} &[J\tilde{\Phi}(y_k)^T J\tilde{\Phi}(y_k)]\delta y = J\tilde{\Phi}(y_k)^T \tilde{\Phi}(y_k) \\ &\Leftrightarrow [\begin{pmatrix} J\Phi(y_k)^T & 0 \end{pmatrix} \begin{pmatrix} J\Phi(y_k) \\ 0 \end{pmatrix}]\delta y = \begin{pmatrix} J\Phi(y_k)^T & 0 \end{pmatrix} \begin{pmatrix} \Phi(y_k) \\ 0 \end{pmatrix} \\ &\Leftrightarrow [J\Phi(y_k)^T J\Phi(y_k)]\delta y = J\Phi(y_k)^T \Phi(y_k), \end{aligned}$$

and since $J\Phi(y_k)$ is invertible, the last equation is equivalent to $J\Phi(y_k)\delta y = \Phi(y_k)$, which is the k-th Newton step for coupling conditions (6.6). □

Remark 9.3. *Due to proposition 9.2, expression* (9.13) *can be composed with Lax curves in order to solve a Riemann problem at a junction under consideration of a change in flow direction.*

9.4 Optimization

This subsection is concerned with the optimal control of compressors located in a network. Thereby, a predefined boundary profile at outgoing nodes shall be tracked. In section 8, well-posedness of our model coupling at junctions, compressor models, as well as the existence of an optimal control has been proven for Cauchy data.

However, these results are based on pipes of infinitely length, namely $\mathbb{R}_+$. Up to the current date, well-posedness of nonlinear hyperbolic systems has not been proven for intervals $[a, b] \subset \mathbb{R}$ in context of nonlinear Cauchy problems.

Accordingly, we have to assume the existence of a solution and its uniqueness, if models $(\mathscr{E}_1)$-$(\mathscr{E}_3)$ are coupled on a network, equipped with pipes of *finite* length. Same assumptions have to be made for our optimal control. Nonetheless, if the juxtaposition of Riemann problems is considered only, i.e., $\Delta x \not\to 0$, the existence and uniqueness of solutions is ensured even on bounded intervals $[a, b] \subset \mathbb{R}$.

We begin with our optimization problem. Consider a network topology $\mathscr{G} = (\mathscr{A}, \mathscr{V})$ equipped with models $(\mathscr{E}_1)$-$(\mathscr{E}_3)$, predefined initial data and boundary data as well as a single compressor, which influences at least one exit node. Again, any posed boundary data has to match the degree of freedom, inflicted by characteristics, entering and leaving the network, see subsections 5 and 6. Let $\Pi(t) \in \mathbb{R}$ denote the compressor control, see subsection 8.5.

Now, assume $v_1, ..., v_K$ to be exit nodes, where a further data profile, *additional* to the boundary data, has to be fulfilled. Obviously, the system becomes underdetermined, resulting in an optimization problem, which might be posed as follows

$$\min_{\Pi \in \mathscr{M}} J(\Pi) := \frac{1}{2} \sum_{\nu=1}^{K} \int_0^T J_1(U(\Pi))^2(v_\nu, t)\, dt + \frac{\alpha}{2} \|\Pi(\cdot)\|^2_{H^1(0,T)}. \tag{9.16}$$

Here, U is the entropic solution of the underlying network, $\mathscr{M}$ has been defined in (8.56) and J_1 is a non-negative lower-semicontinuous functional. In regard of theorem 8.24, we further identify $J_0(\Pi) = \alpha/2\|\Pi(\cdot)\|^2_{H^1(0,T)}$. However, these functionals are not semi-continuous with respect to L^1 but to L^2. This choice is motivated by an application of a Gauss-Newton algorithm, which turns out to be suitable for our problem and is explained in more detail later in subsection 9.5. However, to regain the semi-continuity of J_0 and J_1 with respect to the L^1-norm, $\mathscr{M}$ will be intersected with a domain of piecewise polynomial functions $\mathscr{P}$, i.e., $\mathscr{M}' = \mathscr{M} \cap \mathscr{P}$. Since $\mathscr{P}$ is dense in $L^p([0, T])$, $1 \leq p < \infty$, one has $\mathscr{P} \cap \mathscr{M} \neq \emptyset$. Now, on $\mathscr{M}'$, the inverse estimate theorem can be utilized, and results in our desired semi-continuity with respect to L^1. The objective function reads then

$$\min_{\Pi \in \mathscr{M}'} J(\Pi) := \frac{1}{2} \sum_{\nu=1}^{K} \int_0^T J_1(U(\Pi))^2(x = v_\nu, t)\, dt + \frac{\alpha}{2} \|\Pi(\cdot)\|^2_{H^1(0,T)} \tag{9.17}$$

In order to evaluate (9.17), a discretization is applied

$$\min_{\mathbf{\Pi}} \tilde{J}(\mathbf{\Pi}) := \frac{\Delta t}{2} \sum_{\nu=1}^{K} \langle J_1(\mathbf{U}(\mathbf{\Pi})), J_1(\mathbf{U}(\mathbf{\Pi})) \rangle (v_{\nu,*}^{out}) + \frac{\alpha}{2} \langle (I+D)\mathbf{\Pi}, (I+D)\mathbf{\Pi} \rangle. \tag{9.18}$$

with identity matrix I, discrete time derivative operator D, Euclidean scalar product $\langle \cdot, \cdot \rangle$, N_T the number of discrete time points, $\mathbf{\Pi} = \left[\Pi(t_0) \cdots \Pi(t_{N_T-1}) \right]^T$ and $\mathbf{U} = \left[\mathbf{U}^0 \cdots \mathbf{U}^{N_T} \right]^T$, where $\mathbf{U}^j = [U^j, U_*^j]^T$.

9.5 Gauss-Newton Algorithm

Due to the special structure of (9.18), it suffices to study problems of the form

$$\min_{\Pi \in \Omega} J(\Pi) := \frac{1}{2} \langle F(\Pi), F(\Pi) \rangle. \tag{9.19}$$

with $\Omega \subset \mathbb{R}^n$ compact and $F : \Omega \to \mathbb{R}^m$ differentiable. Assume $\hat{\Pi}$ to be a local minimum of (9.19). Then, one has $\nabla J(\hat{\Pi}) = 0$ and the Hessian $HJ(\hat{H})$ is positive definite. In order to solve $\nabla J(\hat{\Pi}) = 0$ for $\hat{\Pi}$, we like to apply Newton's method. The gradient can be written as $\nabla J = \langle F', F \rangle$. For its Hessian, one receives $HJ(\Pi) = \langle F', F' \rangle + \langle F'', F \rangle$. But since a derivation of F'' might coincide with great effort, HJ is approximated by $HJ \approx \langle F', F' \rangle$. Accordingly, $\nabla J(\Pi) = 0$ is solved with a *quasi* Newton's method, i.e.,

$$\Pi_{k+1} := \Pi_k - \langle F'(\Pi_k), F(\Pi_k) \rangle^{-1} \nabla J(\Pi_k), \; k = 1, 2, \ldots \tag{9.20}$$

However, the quasi Newton solver (9.20) will be utilized in our further proceeding to solve optimization problems of the form (9.17) on networks.

9.6 Application on Networks

In this subsection, we apply the quasi Newton solver 2 on expression (9.18). Therefore, an evaluation of the gradient $\nabla \tilde{J}$ needs to be done first, i.e.,

$$\nabla \tilde{J}(\mathbf{\Pi}) = \Delta t \sum_{\nu=1}^{K} \left\langle \nabla J_1(\mathbf{U}(\mathbf{\Pi})) \dot{\mathbf{U}}(\mathbf{\Pi}), \mathbf{U}(\mathbf{\Pi}) \right\rangle (v_{\nu,*}^{out}) + \alpha (I+D)^T (I+D) \mathbf{\Pi}. \tag{9.21}$$

In order to receive $\dot{\mathbf{U}}(\mathbf{\Pi})$ in (9.21), we store equation (9.9) in a vector for all time steps t_j, i.e.,

$$\mathbb{F}(\mathbf{U}, \mathbf{\Pi}) = \begin{bmatrix} \mathscr{F}(\mathbf{U}^1, \mathbf{U}^0, \Pi_0) \\ \vdots \\ \mathscr{F}(\mathbf{U}^{N_T}, \mathbf{U}^{N_T-1}, \Pi_{N_T-1}) \end{bmatrix}. \tag{9.22}$$

Now, a differentiation of (9.22) with respect to $\mathbf{\Pi}$ results in $0 = d/d\mathbf{\Pi}\,\mathbb{F} = d_1\mathbb{F}\,\dot{\mathbf{U}}(\mathbf{\Pi}) + d_2\mathbb{F}$ and consequently

$$\dot{\mathbf{U}}(\mathbf{\Pi}) = -d_1\mathbb{F}^{-1}d_2\mathbb{F}. \tag{9.23}$$

With $\nabla\tilde{J}$ and $\dot{\mathbf{U}}(\mathbf{\Pi})$ at hand, we get the approximated Hessian matrix $H\tilde{J}(\mathbf{\Pi})$ as follows

$$H\tilde{J}(\mathbf{\Pi}) \approx \tilde{H}\tilde{J}(\mathbf{\Pi}) := \left[\nabla J_1(\mathbf{U}(\mathbf{\Pi}))\dot{\mathbf{U}}(\mathbf{\Pi}))\right]^T\left[\nabla J_1(\mathbf{U}(\mathbf{\Pi}))\dot{\mathbf{U}}(\mathbf{\Pi}))\right] + \alpha(I+D). \tag{9.24}$$

Given the expressions (9.21), (9.22), (9.23) and (9.24) as well as a predefined tolerance $tol > 0$, we can formulate the complete Gauss Newton algorithm for problem (9.18) next.

while $\|\nabla\tilde{J}(\mathbf{\Pi}_k)\| > tol$ **do**
  solve $d_1\mathbb{F}(\mathbf{U}_k, \mathbf{\Pi}_k)\dot{\mathbf{U}}(\mathbf{\Pi})_k = -d_2\mathbb{F}(\mathbf{U}_k, \mathbf{\Pi}_k)$;
  solve $\tilde{H}\tilde{J}(\dot{\mathbf{U}}, \mathbf{\Pi}_k)\delta\mathbf{\Pi} = -\nabla\tilde{J}(\mathbf{\Pi}_k)$;
  set $\mathbf{\Pi}_{k+1} := \mathbf{\Pi}_k + \delta\mathbf{\Pi}$;
  solve $\mathbb{F}(\mathbf{U}_{k+1}, \mathbf{\Pi}_{k+1}) = 0$;
  set $k+1 \to k$;
end

Algorithm 2: Schematic presentation of a Gauss Newton algorithm for solving expression (9.18).

The last operation in algorithm 2, i.e., *solve* $\mathbb{F}(\mathbf{U}_{k+1}, \mathbf{\Pi}_{k+1}) = 0$, determines the new iterative solution $\mathbf{U}_{k+1}$, depending on the new control $\mathbf{\Pi}_{k+1}$.

In subsection 9.7, we provide some numerical experiments and illustrations, based on the before mentioned theory and algorithms. All calculations are done with the time implicit Lax-Friedrichs scheme and 3-WENO reconstruction on pipes, while at junctions, our exact Riemann solvers from sections 5 and 6 are utilized.

9.7 Numerical Experiments and Illustrations

In this section, some numerical examples are given. For simplicity, all models $(\mathscr{E}_1)$-$(\mathscr{E}_3)$ are made dimensionless, using techniques in [46, Sect. 14.4].

In our first numerical illustration, we simulate two closed networks to demonstrate the change of energy, in dependence of the underlying coupling conditions (5.8a)-(5.9c).

Therefore, consider the network topology, depicted in figure 31, with pipes $e_j = [0,1]$, $j = 1,2,3$, which are equipped with the homogeneous Euler equations $(\mathscr{E}_1)$, i.e., $G \equiv 0$. In subsection 5.1, it has been shown, that mass and energy are preserved over time. Latter is ensured due to equality of enthalpy (5.8b) at the junction. However, energy is not conserved, if equality of pressure (5.9b) or equality of dynamic pressure (5.9c) are used instead of (5.8b). This is now demonstrated on the network in figure

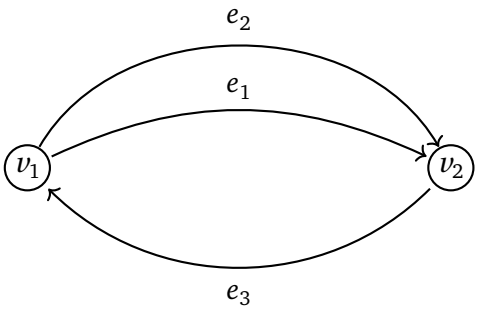

Figure 31: Network with junctions only

31. Accordingly, nodes v_1 and v_2 are equipped with three different coupling conditions C_1, C_2 and C_3, defined through

$$C_1 = \left\{ \begin{array}{c} \text{mass conserv. (5.8a)} \\ \text{equ. of enthalpy (5.8b)} \\ \text{entropy mix. (5.8c)} \end{array} \right\}, \; C_2 = \left\{ \begin{array}{c} \text{mass conserv. (5.8a)} \\ \text{equ. of pres. (5.9b)} \\ \text{entropy mix. (5.8c)} \end{array} \right\}, \; C_3 = \left\{ \begin{array}{c} \text{mass conserv. (5.8a)} \\ \text{equ. of dyn. pres. (5.9c)} \\ \text{entropy mix. (5.8c)} \end{array} \right\}. \tag{9.25}$$

All arcs $e_j,\ j = 1,2,3$ are discretized with an equidistant mesh of 60 inner spatial points,.i.e., $\Delta x = 1/61$. The boundary and junction points are treated seperately, see subsection 9.2. In order to create a feasible initial state, we pose

$$\begin{array}{rclrcl} \rho_0(x) & = & 2, & u_0(x) & = & 0.1 + 2\chi_{[0.25,0.75]}(x), \\ p_0(x) & = & \rho_0(x)^\gamma, & E_0(x) & = & p_0(x)/(\gamma-1) + (\rho_0 u_0^2)(x)/2, \\ q_0(x) & = & (\rho_0 u_0)(x) & & & \end{array} \tag{9.26}$$

for $x \in e_k,\ k = 1,...,5,\ \gamma = 1.4$ and make one time step of size $\Delta t = \Delta x/2$ with the simplified isentropic homogeneous Euler equations $(\mathscr{E}_3)$. The occurring results serve as initial data for model $(\mathscr{E}_1)$. Now, we perform a simulation for every coupling condition in (9.25) separately, as long as $t_j = j\Delta t \leq T = 2$. Therefore, let us define total energy and total entropy for one time step through

$$E_{total}(t) = \sum_{k=1}^{3} \sum_{x_i \in e_k} E(x_i,t)\Delta x, \quad s_{total}(t) = \sum_{k=1}^{3} \sum_{x_i \in e_k} s(x_i,t)\Delta x. \tag{9.27}$$

While performing the simulation in dependence of $C_j,\ j = 1,2,3$, both quantities in (9.27) are evaluated in every time step t_j, which are depicted in figures 32a and 32b. From 32a, we conclude, that total energy is conserved for C_1, while it is not for C_2 and C_3. Furthermore, total entropy $s_{total}(t)$ is increasing, see figure 32b, which states, that the all time steps, including the first step with model $(\mathscr{E}_3)$, produced a entropy solutions. Now, consider the closed network in figure 31 again. But this time with models $\mathscr{E}_1$, $(\mathscr{E}_2)$ and $(\mathscr{E}_3)$ on pipes $e_j = [0,1],\ j = 1,2,3$, respectively. Similar to our previous numerical illustration, we like also to demonstrate the change of energy in dependence of coupling conditions $C_j,\ j = 1,2,3$ in (9.25) here. For this purpose, we keep the initial data (9.26), as well as temporal and

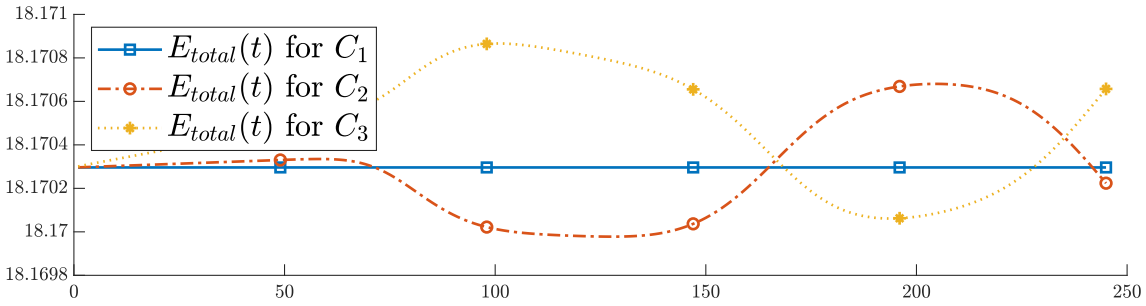

(a) Change in energy on the network in figure 31, due to coupling conditions C_1, C_2, C_3 in (9.25). Here, the vertical axis represents total energy, which is plotted for every time step (horizontal axis). On pipes $e_j,\ j = 1,2,3$, the model $(\mathscr{E}_1)$ has been chosen.

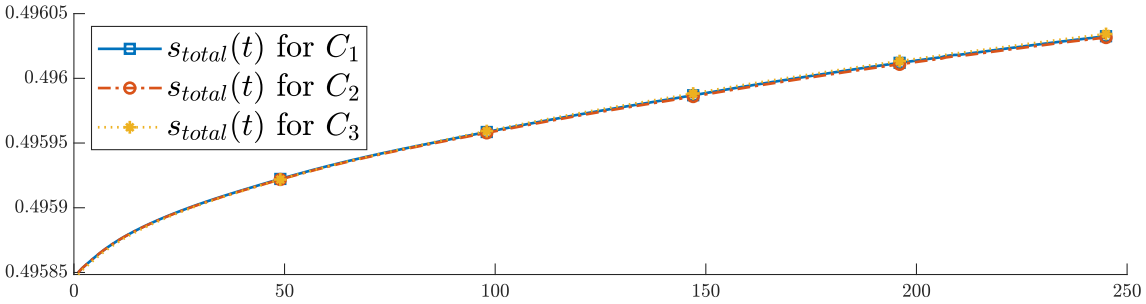

(b) Increase of entropy on the network in figure 31. Here, the vertical axis represents total entropy, which is plotted for every time step (horizontal axis). On pipes $e_j,\ j = 1,2,3$, the model $(\mathscr{E}_1)$ has been chosen.

Figure 32: Change of total energy and entropy in network 31 due to coupling conditions (9.25).

spatial discretization, i.e., $\Delta t = \Delta x/2$ and time horizon $T = 2$. We chose either C_1, C_2 or C_3 in (9.25) at junctions of the network in figure 31. Again, total energy is measured by $E_{total}(t)$ in (9.27). In figure 33, $E_{total}(t)$ is depicted for $C_j,\ j = 1,2,3$, form which an increase in energy can be concluded, if C_2, C_3 are the underlying coupling conditions, while for C_1, energy is non-increasing. These results match with

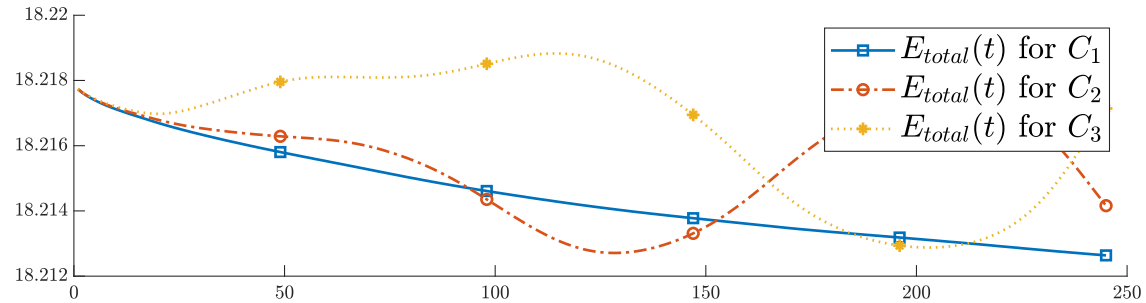

Figure 33: Change in energy on the network in figure 31, due to coupling conditions C_1, C_2, C_3 in (9.25). Here, the vertical axis represents total energy, which is plotted for every time step (horizontal axis). On pipes $e_j,\ j = 1,2,3$, models $(\mathscr{E}_1)$-$(\mathscr{E}_3)$ have been chosen.

those in [36] and [38].

In the next numerical example, we like to demonstrate a possible usage of our model hierarchy. For this purpose, a network is posed with the full inhomogeneous Euler equations $(\mathscr{E}_1)$, i.e., $G \neq 0$ defined by (2.4), on every pipe *first*. At an entry node, we state an input increase up to 50% over a short period of time. However, we will see, that this input increase is damped due to friction and energy exchange in

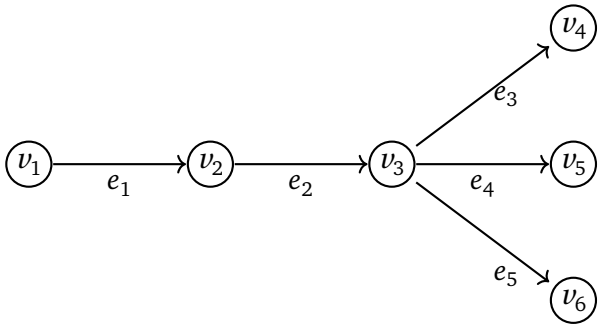

Figure 34: Schematic presentation of a network. Here v_1, v_4, v_5, v_6 are boundary nodes, while v_2 and v_3 are junctions.

the source term (2.4), resulting in rather low dynamics at the exit nodes of the network. Consequently, model $(\mathscr{E}_1)$ might be replaced by models $(\mathscr{E}_2)$ and $(\mathscr{E}_3)$ on certain pipes, which is done in a *second* simulation. Afterwards, the difference between both simulation is evaluated on all pipes, to qualify our model replacement.

Therefore, consider the network in figure 34. All pipes are set to $e_j = [0,1],\ j = 1,...,5$. Obviously, nodes v_2 and v_3 are junctions, while v_1 and $v_j,\ j = 4,5,6$ serve as entry and exit nodes, respectively. On latter nodes, we pose boundary data through

$$\begin{aligned} \rho(v_1,t) &= \begin{cases} 1, & t \in [0,0.04), \\ 3.125(t-0.04)+1, & t \in [0.04,0.2), \\ 1.5, & t \in [0.2,0.3), \\ -5(t-0.3)+1, & t \in [0.3,0.4), \\ 1, & t \in [0.4,2] \end{cases} \\ p(v_1,t) &= \rho(v_1,t)^\gamma, \\ q(v_j,t) &= 0.1, \quad j = 4,5,6 \end{aligned} \tag{9.28}$$

with $t \in [0,T],\ T = 2$ and $\gamma = 1.4$. The profile of $\rho(v_1,t),\ t \in [0,2]$ is also depicted in figure 35. All pipes are equipped with the inhomogeneous model $(\mathscr{E}_1)$, i.e., $G \neq 0$ and defined by (2.4). Furthermore, coefficients in (2.4) are set to $\lambda = 0.1,\ d = 1,\ k_w = R,\ T_w = 1/R$. This is also done in (2.5) for models $(\mathscr{E}_2)$ and $(\mathscr{E}_3)$ later on. All pipes in figure 34 are discretized with 50 inner spatial points, i.e., $\Delta x = 1/51$, Additionally, let $\Delta t = \Delta x$. Referring to subsection 9.2, we denote by U^j the numerical solution at time step $t_j = j\Delta t$ with $T = t_N$, while $\mathbf{U} = (U(t^j))_j = \begin{pmatrix} \rho(t^j) & \cdots & u(t^j) \end{pmatrix}_j$ is the numerical solution vector. In order to get an initial profile, which also matches our boundary condition (9.28), we pose U_0 through

$$\begin{aligned} \rho_0(x) &= 1, & u_0(x) &= 0.1, \\ p_0(x) &= \rho_0(x)^\gamma, & E_0(x) &= p_0(x)/(\gamma-1) + (\rho_0 u_0^2)(x)/2, \\ q_0(x) &= (\rho_0 u_0)(x), \end{aligned}$$

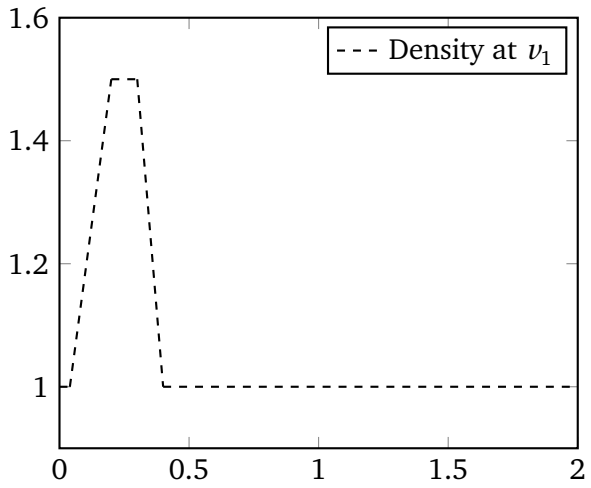

Figure 35: Density profile at entry node v_1 for time $t \in [0,T],\ T = 2$.

and run the network in figure 34, equipped with inhomogeneous model $(\mathscr{E}_3)$ and boundary condition

$$\rho(v_1,t) = \rho(v_1,0), \quad p(v_1,t) = p(v_1,0), \quad q(v_j,t) = q(v_j,0),\ j = 4,5,6,$$

for $t > 0$. This simulation is stopped as soon as the stationary state is reached with tolerance $\Delta t 10^{-4}$, i.e., $\sup \|U^{j+1} - U^j\|_\infty < 10^{-4}\Delta t$. Then, $U_0 := U^{j+1}$ is used as initial condition for our simulation of the network in figure 34, equipped with inhomogeneous model $(\mathscr{E}_1)$. In figures 36a, 36b and 36c numerical solutions for ρ, q, E, p, u are plotted at time points $t = 30\Delta t, 75\Delta t, 100\Delta t$, respectively. From these pictures, one concludes, that the initial input peek (9.28) decays sufficiently until it reaches pipes $e_j,\ j = 4,5,6$. Consequently, models $(\mathscr{E}_2)$ and $(\mathscr{E}_3)$ might be considered on $e_j,\ j = 4,5,6$, instead of $(\mathscr{E}_1)$. In order to qualify our assumption, we examine the conditions of models $(\mathscr{E}_2)$ and $(\mathscr{E}_3)$ referring to table 1, i.e., $s \approx const$ for $(\mathscr{E}_2)$ and additionally $|u|/c \approx 0$ for $(\mathscr{E}_3)$. These conditions are measured on every pipe $e_j,\ j = 1,...,5$ individually and according to

$$\|\Delta_x s(e_k)\|_\infty := \sup_{t_j, x_i \in e_k} \left|(s(x_i,t_j) - s(x_{i-1},t_j))/\Delta x\right|, \tag{9.29a}$$

$$\|\Delta_s s(e_k)\|_\infty := \sup_{t_j, x_i \in e_k} \left|(s(x_i,t_j) - s(x_{i-1},t_j))/s(x_{i-1},t_j)\right|, \tag{9.29b}$$

$$\|(u/c)(e_k)\|_\infty := \sup_{t_j, x_i \in e_k} \left|u(x_i,t_j)/c(x_i,t_j)\right|. \tag{9.29c}$$

Here, (9.29a) represents the maximal spatial change over all discrete temporal points, while (9.29b) stands for the maximal spatial change of entropy s, in relation to the magnitude of s. Our last measure (9.29c), gives the maximal magnitude of $|u|/c$ for all spatial and temporal points.

Then, $(\mathscr{E}_2)$ might be taken into consideration, if $\|\Delta_x s\|_\infty$ and $\|\Delta_s s\|_\infty$ are sufficiently small, for example less then 10^{-2}. An exchange with model $(\mathscr{E}_3)$ is preferable, if additionally $\|u/c\|_\infty < 10^{-2}$ is satisfied.

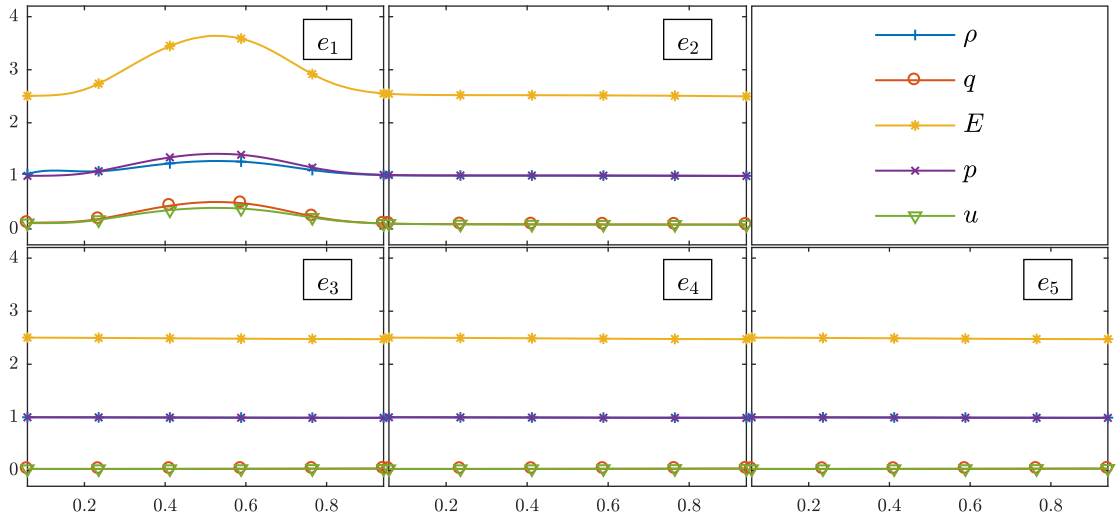

(a) Numerical solution of ρ, q, E, p, u on network in figure 34 at time $t = 30\Delta t$.

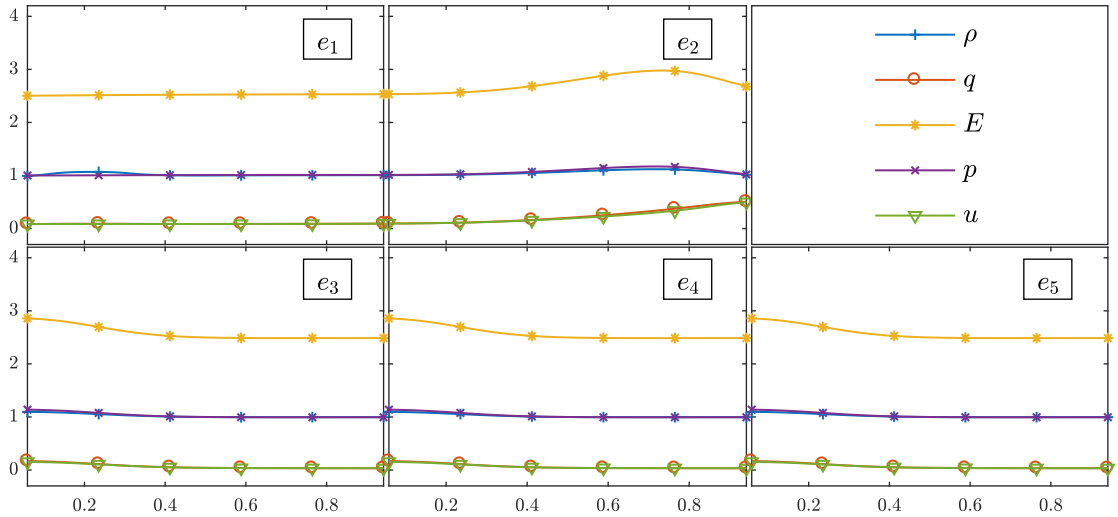

(b) Numerical solution of ρ, q, E, p, u on network in figure 34 at time $t = 75\Delta t$.

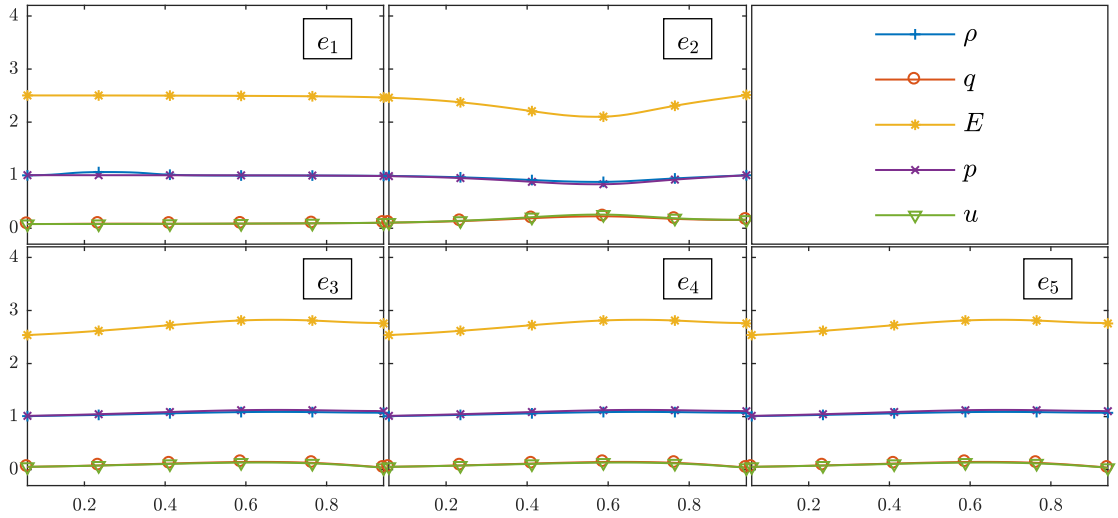

(c) Numerical solution of ρ, q, E, p, u on network in figure 34 at time $t = 100\Delta t$.

Figure 36: Numerical solution of ρ, q, E, p, u at time points $t = 30\Delta t, 75\Delta t, 100\Delta t$ on every pipe e_j.

Now, our previously performed simulation is evaluated in means of (9.29). The resulting data is depicted in table 2, from which we conclude, that an usage of model $(\mathscr{E}_2)$ is indeed justified on pipes

	e_1	e_2	e_3	e_4	e_5
$\|\Delta_t s(e_k)\|_\infty$	2.5538	0.0475	0.0182	0.0182	0.0182
$\|\Delta_s s(e_k)\|_\infty$	0.0363	0.0006	0.0002	0.0002	0.0002
$\|(u/c)(e_k)\|_\infty$	0.3835	0.4213	0.1275	0.1275	0.1275

Table 2: Evaluation of the simulation results with measures (9.29).

$e_j,\ j=3,4,5$, since $\|\Delta_t s(e_j)\|_\infty < 0.02$ and $\|\Delta_s s(e_j)\|_\infty < 0.0002$ for $j=3,4,5$. In contrast, condition $|u|/c < 10^{-2}$ is not fulfilled on any pipe, according to the last raw in table 2.

However, for the purpose of a further demonstration, we select $(\mathscr{E}_2)$ and $(\mathscr{E}_3)$ on pipes e_4 and e_5 respectively, while on pipes $e_j,\ j=1,..,4$ model $(\mathscr{E}_1)$ is kept. Initial, boundary data and network discretization are kept as well. The resulting numerical solution is denoted by $\mathbf{V}=(V(t_j))_j$.

Now, both numerical solutions are compared in $\sup_{t_j,x_i}|\cdot|$ as follows

$$\begin{aligned}\mathtt{err}(e_k) &:= \sup_{t_j,x_i\in e_k} |\mathbf{V}(x_i,t_j)-\mathbf{U}(x_i,t_j)|,\ k=1,...,5,\\ \widetilde{\mathtt{err}}(e_k) &:= \sup_{t_j,x_i\in e_k} |(\mathbf{V}(x_i,t_j)-\mathbf{U}(x_i,t_j))/\mathbf{U}(x_i,t_j)|,\ k=1,...,5,\end{aligned}$$

with $|\cdot|$ applied on every component in $\mathbf{V}-\mathbf{U}$, i.e., ρ,q,E,p,u, separately. We like to mention, that $\mathtt{err}(e_k)$ and $\widetilde{\mathtt{err}}(e_k)$, $k=1,...,5$ are the total and relative total error of $\mathbf{V}$ and $\mathbf{U}$ on every pipe. In tables 3 and 4, those results are presented, respectively.

Error in	$\mathtt{err}(e_1)$	$\mathtt{err}(e_2)$	$\mathtt{err}(e_3)$	$\mathtt{err}(e_4)$	$\mathtt{err}(e_5)$
ρ	0.0011	0.0032	0.0020	0.0023	0.0261
q	0.0022	0.0025	0.0044	0.0037	0.0175
E	0.0039	0.0098	0.0069	0.0078	0.0949
p	0.0017	0.0045	0.0027	0.0031	0.0377
u	0.0022	0.0037	0.0042	0.0036	0.0153

Table 3: Maximal error (err) of ρ,q,E,p,u over all temporal and spatial points (t_j,x_i) and for all pipes separately, i.e., $x_i\in e_k$ for $k=1,...,5$.

Depending on the results in tables 3 and 4, one observes, that the relative error of model $(\mathscr{E}_2)$ on e_4 is smaller than 7%, while the usage of model $(\mathscr{E}_3)$ on pipe e_5 causes a relative error up to 17%. Consequently, $(\mathscr{E}_2)$ might be more preferable than $(\mathscr{E}_3)$ in this scenario, which is consistend to our results in table 2.

However, we also observe an error on pipes $e_k,\ k=1,2,3$, where model $(\mathscr{E}_1)$ was kept. This comes from the fact, that all models have characteristics, which point towards the opposite direction of gas flow and, accordingly, transport any error on pipes e_4,e_5 also onto pipes $e_k,\ k=1,2,3$. But, according to table 4, the error is less than 8%.

Error in	$\widetilde{\mathrm{err}}(e_1)$	$\widetilde{\mathrm{err}}(e_2)$	$\widetilde{\mathrm{err}}(e_3)$	$\widetilde{\mathrm{err}}(e_4)$	$\widetilde{\mathrm{err}}(e_5)$
ρ	0.0011	0.0031	0.0020	0.0023	0.0244
q	0.0281	0.0164	0.0809	0.0686	0.1716
E	0.0014	0.0038	0.0028	0.0031	0.0344
p	0.0015	0.0044	0.0028	0.0031	0.0342
u	0.0280	0.0175	0.0794	0.0666	0.1605

Table 4: Maximal relative error ($\widetilde{\mathrm{err}}$) of ρ, q, E, p, u over all temporal and spatial points (t_j, x_i) and for all pipes separately, i.e., $x_i \in e_k$ for $k = 1, ..., 5$.

Our next example is an illustrative optimization problem, which is designed to test our Gauss-Newton algorithm 2. In order to do so, we pose a network, in which a compressor is located, equipped with a predefined compressor control. Given this setup, a simulation is performed until the compressor influences every outgoing boundary node of the network. There, certain boundary profiles are stored.

Now, these boundary profiles are posed at their underlying nodes *first*, while the compressor control is kept *variable*. With our Gauss-Newton algorithm 2, we want to regain the compressor control of the initial simulation.

Therefore, consider the network in figure 34 with edges $e_j = [0, 1]$, $j = 1, ..., 5$ and include a compressor, described by equation (2.6), at node v_2, see figure 37. Its compressor control is denoted by Π. Again, node v_1 serves as entry, while v_j, $j = 4, 5, 6$ are exit nodes. The edges are equipped with

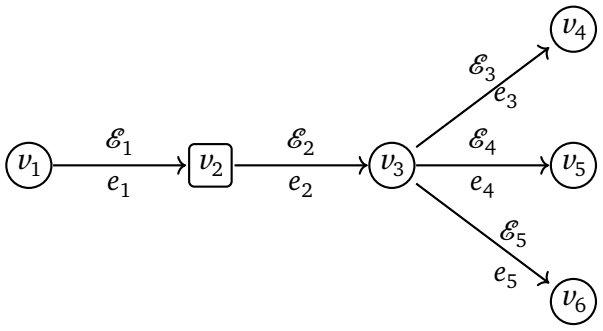

Figure 37: Schematic presentation of a network. Here v_1, v_4, v_5, v_6 are boundary nodes, v_2 is a compressor and v_3 is a junction.

inhomogeneous models $(\mathscr{E}_1)$-$(\mathscr{E}_3)$ according to figure 37. Similar, to our previous numerical illustration, the coefficients in (2.4) and (2.5) are set to $\lambda = 0.1, d = 1, k_w = R, T_w = 1/R$. All edges are discretized with 20 spatial points, i.e., $\Delta x = 1/21$. Additionally, let $\Delta t = \Delta x$. At nodes v_j, $j = 4, 5, 6$, we pose the boundary data

$$\rho(x = v_1, t) = 0.82,\ p(x = v_1, t) = \rho(x = v_1, t)^\gamma,\ q(x = v_j, t) = 0.082,\ j = 4, 5, 6$$

for time $t \in [0,T],\ T = 2.5$. The compressor control $\Pi(t) = H(t),\ t \in [0,T]$ is provided through

$$\Pi(t) = \begin{cases} 0, & x \in [0, 0.25], \\ 0.2(x-0.25), & x \in [0.25, 0.75], \\ 0.1, & x \in [0.75, 1], \\ -0.2(x-1)+0.1, & x \in [1, 1.5], \\ 0, & x \in [1.5, 2.5] \end{cases}$$

which is also depicted in figure 38 Referring to subsection 9.2, U^j denotes the numerical solution at time

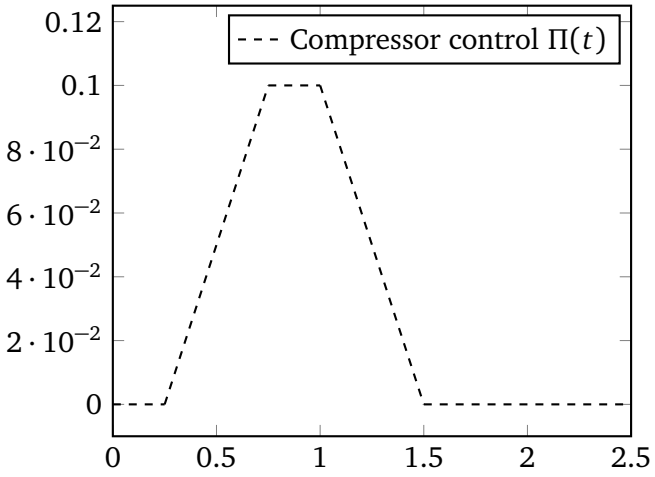

Figure 38: Compressor control $\Pi(t),\ t \in [0, 2.5]$ at node v_2

step $t_j = j\Delta t$ with $T = t_N$. Given the setup above, a simulation is performed and we store all energy profiles of the outgoing nodes $v_j,\ j = 4,5,6$, i.e., $\hat{E} := E(v_j, t),\ j = 4,5,6,\ t \in [0,T]$.

Now, the compressor control is kept variable and $\hat{E}$ is stored at outgoing nodes. By an application of the Gauss-Newton algorithm 2, we like to regain a compressor control $\mathbf{\Pi} = \begin{pmatrix} \Pi(t_1) & \cdots & \Pi(t_N) \end{pmatrix}$, such that $\hat{E}$ is fulfilled. Consequently, the functional

$$\min_{\mathbf{\Pi}} \tilde{J}(\mathbf{\Pi}) := \frac{\Delta t}{2} \sum_{v=4}^{6} \left\langle (E(\mathbf{\Pi}) - \hat{E}), (E(\mathbf{\Pi}) - \hat{E}) \right\rangle (x = v_v) + \frac{\alpha}{2} \langle (I+D)\mathbf{\Pi}, (I+D)\mathbf{\Pi} \rangle. \tag{9.30}$$

needs to be solved for $\mathbf{\Pi}$. In figure 39a, the solutions $\mathbf{\Pi}$ of (9.30) are plotted, depending on different choices for α, namely $\alpha_1 = 1e-3,\ \alpha_2 = 1e-2,\ \alpha_3 = 1e-1,\ \alpha_4 = 5e-1$. In order to make this dependence obvious, set $\mathbf{\Pi}(\alpha) = \Pi$. The resulting boundary profiles $E(\mathbf{\Pi}(\alpha))$ for $\alpha \in \{\alpha_1, \alpha_2, \alpha_3, \alpha_4\}$, as well as the initial boundary profiles $\hat{E}$ are depicted in figure 39b. In table 5, the values of function $\hat{J}(\mathbf{\Pi}(\alpha))$ in (9.30) are given In regard of table 5, $\hat{J}(\mathbf{\Pi}(\alpha))$ takes its minimum for $\alpha_2 = 1e-2$. However, this demonstrates the functionality of our Gauss-Newton algorithm 2. But even more important, we validated our analytic results in sections 5-8, i.e., a coupling of different physical gas models, namely $(\mathscr{E}_1)$-$(\mathscr{E}_3)$, is solvable and stable at junctions.

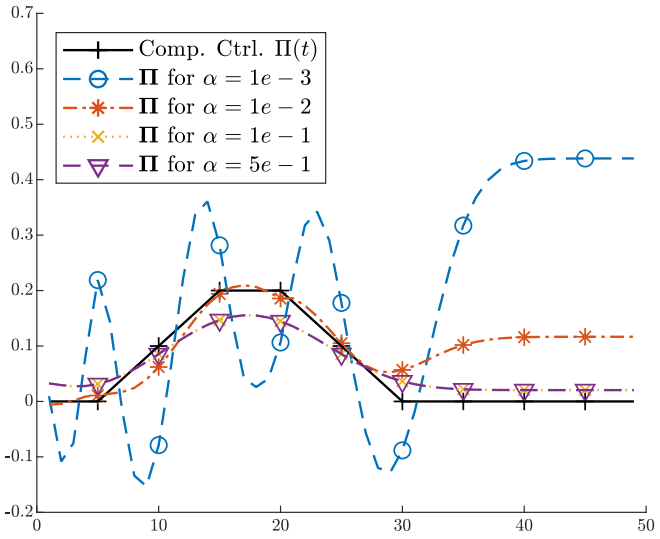

(a) Compressor control for different choices in α as well as the original compressor control.

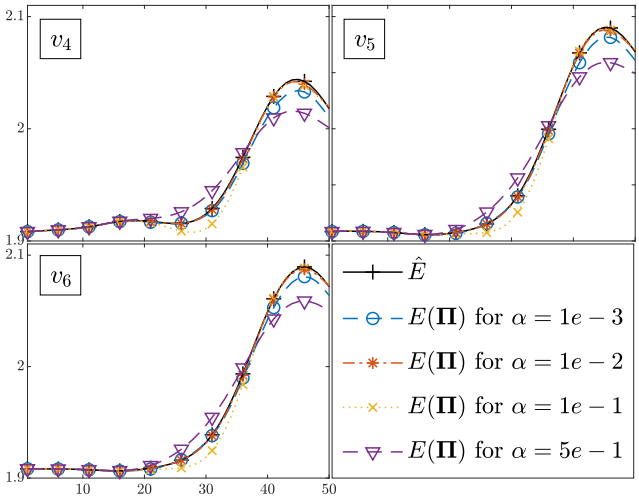

(b) Compressor control for different choices in α as well as the original compressor control.

Figure 39: Grafical results of our Gauss-Newton algorithm 2 applied on (9.30) for $\alpha_j,\ j = 1, ..., 4$.

$\hat{J}(\mathbf{\Pi}(\alpha_1))$	$\hat{J}(\mathbf{\Pi}(\alpha_2))$	$\hat{J}(\mathbf{\Pi}(\alpha_3))$	$\hat{J}(\mathbf{\Pi}(\alpha_4))$
0.0492	0.0094	0.0620	0.1492

Table 5: Values of the function $\hat{J}(\mathbf{\Pi}(\alpha_j))$ for $\alpha_j,\ j = 1, ..., 4$.

10 Conclusion

In this work we presented a novel set of coupling conditions in order to successfully couple the full Euler equations on networks, consisting of a single junction with finitely many ingoing and outgoing pipes. In order to do so, we followed the approach in Lang and Mindt [32].

Under the assumption of homogeneity, our novel set of coupling conditions preserve mass and energy at the junction for the full Euler equations.

However, the problem of an physical correct coupling of the full Euler equations, on networks with a single junction had been open for almost a decade, and can be closed with a positive result now.

Furthermore, the occurring generalized homogeneous Riemann problem at the junction is well-posed

Here, we utilized the same techniques as in Banda, Herty and Klar [3], Colombo and Mauri [18], Colombo and Garavello [11, 12], as well as Lang and Mindt [32], to name just a few references. These techniques consist of a suitable composition of Lax curves with the coupling conditions. Afterwards, solvability of the resulting mapping has been proven by an application of the implicit function theorem.

In a further step, we adapted the coupling conditions for the full Euler equations, such that these gas equations can be coupled with the isentropic and simplified isentropic Euler equations as well.

Under homogeneity, the adapted coupling conditions preserve mass and energy at the junction, if the full Euler equations, the isentropic Euler equations or the simplified isentropic Euler equations are utilized on the network

This modification was motivated by the idea of a model hierarchy on networks to overcome computational effort and is based on the work of Domschke, Kolb and Lang [2, 21, 20] as well as Schmidt, Steinbach and Willert [41]. Our gas network setup was finally extended by two compressor models of Ehrhardt, Steinbach [23] and Menon [34].

The generalized homogeneous Riemann problem of the model hierarchy and the compressor models is well-posed, if coupled with the presented gas equations.

Similar to the full Euler equations, we showed well-posedness of the resulting generalized homogeneous Riemann problems of the model hierarchy and the compressor models under a suitable composition with Lax curves, followed by an application of the implicit function theorem.

The occurring generalized inhomogeneous Cauchy problem of the model hierarchy and the compressor models is well-posed

Here the front tracking algorithm by Bressan [5] as well as the before mentioned well-posedness of all generalized Riemann problems served as building block in our proof. Nonetheless, the theory for well-posedness of homogeneous Cauchy problems on networks was treated before, see for example Colombo and Mauri in [18] as well as Colombo, Guerra, Herty and Schleper [16]. Therefore, the theory needed some minor adaption only. Our theoretical work was closed by the proof of well-posedness for all generalized inhomogeneous Cauchy problems and the existence of an optimal control on networks.

However, these results already existed for general hyperbolic balance laws on networks, see for example the work of Colombo, Guerra, Herty and Schleper in [16], and had been given as overview only.

We closed this work by providing some numerical examples, which illustrated the energy conservation on at a junction, the solvability of our model hierarchy, if coupled on networks, as well as an optimal control problem.

11 Outlook

Finally, we like to discuss some possible extensions to our results and techniques. Through out our work, all gas equations had been equipped with ideal gas only. However, the behavior of gas transport differs with the gas properties. Unfortunately, any assumption beside ideal gas possibly leads to the non existence of the Riemann invariants, which makes a construction of Lax curves impossible.

Nonetheless, there are already multiple approximated Riemann solvers, which consist of the Rankine-Hugoniot condition only and serve as numerical tool, see for example LeVeque [33, Sect. 15] and Toro [45, Sect. 10]. Accordingly, from a numerical point of view, every Lax can be replaced by an approximated Riemann solver, which allows more complex gas assumptions. In this context, well-posedness of the generalized Riemann problem means, that the occurring numerical method admits a solution. Here, one proceeds similar to our proof, i.e., the composition of approximated Lax curves and coupling conditions is differentiated and evaluated in a suitable state, for example the stationary state. With a successfully application of the implicit function theorem, well-posedness is proven.

Besides an extension towards real gases, our research forms a basis for uncertainties in the gas equations or network topology as well. As an example, the adiabatic exponent, pipe roughness or diameter might be unknown through out the network and therefore considered suitably distributed. In such scenarios, simulations are performed by multi-level Monte Carlo algorithms, in which a numerical solution of the network is derived for certain snapshots of the distributed parameters. See for example the work of Mishra, Schwab and Sukys [35]. However, for every single snapshot the resulting problem is deterministic and our results are applicable.

References

[1] Debora Amadori. Initial-boundary value problems for nonlinear systems of conservation laws. *Nonlinear Differential Equations and Applications NoDEA*, 4(1):1–42, 1997.

[2] Pia Bales, Oliver Kolb, and Jens Lang. Hierarchical modelling and model adaptivity for gas flow on networks. *Computational Science–ICCS 2009*, 1:337–346, 2009.

[3] Mapundi K Banda, Michael Herty, and Axel Klar. Gas flow in pipeline networks. *NHM*, 1(1):41–56, 2006.

[4] Ravindra B Bapat. *Graphs and matrices*, volume 27. Springer, 2010.

[5] Alberto Bressan. *Hyperbolic systems of conservation laws: the one-dimensional Cauchy problem*, volume 20. Oxford University Press on Demand, 2000.

[6] Alberto Bressan and Rinaldo M Colombo. The semigroup generated by 2× 2 conservation laws. *Archive for rational mechanics and analysis*, 133(1):1–75, 1995.

[7] John Charles Butcher. *Numerical methods for ordinary differential equations*. John Wiley & Sons, 2016.

[8] Günter Cerbe et al. Grundlagen der gastechnik. *Gasbeschaffung, Gasverteilung, Gasverwendung*, 5, 2008.

[9] Gui-Qiang Chen. Euler equations and related hyperbolic conservation laws. In *Handbook of differential equations: evolutionary equations*, volume 2, pages 1–104. Elsevier, 2005.

[10] Rinaldo M Colombo. Wave front tracking in systems of conservation laws. *Applications of mathematics*, 49(6):501–537, 2004.

[11] Rinaldo M Colombo and Mauro Garavello. A well posed riemann problem for the p-system at a junction. *NHM*, 1(3):495–511, 2006.

[12] Rinaldo M Colombo and Mauro Garavello. On the cauchy problem for the p-system at a junction. *SIAM Journal on Mathematical Analysis*, 39(5):1456–1471, 2008.

[13] Rinaldo M Colombo and Graziano Guerra. Hyperbolic balance laws with a non local source. *Communications in Partial Differential Equations*, 32(12):1917–1939, 2007.

[14] Rinaldo M Colombo and Graziano Guerra. Hyperbolic balance laws with a dissipative non local source. *Communications on Pure & Applied Analysis*, 7:1077, 2008.

[15] Rinaldo M Colombo and Graziano Guerra. Differential equations in metric spaces with applications. *Discrete & Continuous Dynamical Systems - A*, 23:733, 2009.

[16] Rinaldo M Colombo, Graziano Guerra, Michael Herty, and Veronika Schleper. Optimal control in networks of pipes and canals. *SIAM Journal on Control and Optimization*, 48(3):2032–2050, 2009.

[17] Rinaldo M Colombo, Michael Herty, and Veronika Sachers. On 2\times2 conservation laws at a junction. *SIAM Journal on Mathematical Analysis*, 40(2):605–622, 2008.

[18] Rinaldo M Colombo and Cristina Mauri. Euler system for compressible fluids at a junction. *Journal of Hyperbolic Differential Equations*, 5(03):547–568, 2008.

[19] Constantine M Dafermos. Hyperbolic conservation laws in continuum physics, volume 325 of grundlehren der mathematischen wissenschaften [fundamental principles of mathematical sciences], 2010.

[20] Pia Domschke, Oliver Kolb, and Jens Lang. Adjoint-based control of model and discretisation errors for gas flow in networks. *International Journal of Mathematical Modelling and Numerical Optimisation*, 2(2):175–193, 2011.

[21] Pia Domschke, Oliver Kolb, and Jens Lang. Adaptive modelling, simulation and optimization of gas and water supply networks. *PAMM*, 16(1):839–840, 2016.

[22] Carlotta Donadello and Andrea Marson. Stability of front tracking solutions to the initial and boundary value problem for systems of conservation laws. *Nonlinear Differential Equations and Applications NoDEA*, 14(5-6):569–592, 2007.

[23] Klaus Ehrhardt and Marc C Steinbach. Nonlinear optimization in gas networks. In *Modeling, simulation and optimization of complex processes*, pages 139–148. Springer, 2005.

[24] Lawrence Evans. A survey of entropy methods for partial differential equations. *Bulletin of the American Mathematical Society*, 41(4):409–438, 2004.

[25] Eduard Feireisl. *Dynamics of viscous compressible fluids*, volume 26. Oxford University Press, 2004.

[26] James Glimm. Solutions in the large for nonlinear hyperbolic systems of equations. *Communications on pure and applied mathematics*, 18(4):697–715, 1965.

[27] Edwige Godlewski and Pierre-Arnaud Raviart. *Numerical approximation of hyperbolic systems of conservation laws*, volume 118. Springer Science & Business Media, 2013.

[28] Martin Gugat, Michael Herty, Axel Klar, Günther Leugering, and Veronika Schleper. Well-posedness of networked hyperbolic systems of balance laws. In *Constrained optimization and optimal control for partial differential equations*, pages 123–146. Springer, 2012.

[29] Michael Herty and Michel Rascle. Coupling conditions for a class of second-order models for traffic flow. *SIAM Journal on mathematical analysis*, 38(2):595–616, 2006.

[30] Helge Holden and Nils Henrik Risebro. *Front tracking for hyperbolic conservation laws*, volume 152. Springer, 2015.

[31] Tihamér A Kocsis and Adrián Németh. Optimal second order diagonally implicit ssp runge–kutta methods. *arXiv preprint arXiv:1409.8583*, 2014.

[32] Jens Lang and Pascal Mindt. Entropy-preserving coupling conditions for one-dimensional euler systems at junctions. *Networks and Heterogeneous Media*, 13:177, 2018.

[33] Randall J LeVeque. *Finite volume methods for hyperbolic problems*, volume 31. Cambridge university press, 2002.

[34] E Shashi Menon. *Gas pipeline hydraulics*. CRC Press, 2005.

[35] Siddhartha Mishra, Ch Schwab, and Jonas Sukys. Multilevel monte carlo finite volume methods for shallow water equations with uncertain topography in multi-dimensions. *SIAM Journal on Scientific Computing*, 34(6):B761–B784, 2012.

[36] Alexandre Morin and Gunhild A Reigstad. Pipe networks: coupling constants in a junction for the isentropic euler equations. *Energy Procedia*, 64:140–149, 2015.

[37] Gunhild A Reigstad. Numerical network models and entropy principles for isothermal junction flow. *Networks and Heterogeneous Media*, 9(1):65–95, 2014.

[38] Gunhild A Reigstad. Existence and uniqueness of solutions to the generalized riemann problem for isentropic flow. *SIAM Journal on Applied Mathematics*, 75(2):679–702, 2015.

[39] Gunhild A Reigstad, Tore Flåtten, Nils Erland Haugen, and Tor Ytrehus. Coupling constants and the generalized riemann problem for isothermal junction flow. *Journal of Hyperbolic Differential Equations*, 12(01):37–59, 2015.

[40] Daniel Rose, Martin Schmidt, Marc C Steinbach, and Bernhard M Willert. Computational optimization of gas compressor stations: Minlp models versus continuous reformulations. *Mathematical Methods of Operations Research*, 83(3):409–444, 2016.

[41] Martin Schmidt, Marc C Steinbach, and Bernhard M Willert. High detail stationary optimization models for gas networks. *Optimization and Engineering*, 16(1):131–164, 2015.

[42] Chi-Wang Shu. Essentially non-oscillatory and weighted essentially non-oscillatory schemes for hyperbolic conservation laws. In *Advanced numerical approximation of nonlinear hyperbolic equations*, pages 325–432. Springer, 1998.

[43] Joel Smoller. *Shock waves and reaction—diffusion equations*, volume 258. Springer Science & Business Media, 2012.

[44] Marc C Steinbach. On pde solution in transient optimization of gas networks. *Journal of computational and applied mathematics*, 203(2):345–361, 2007.

[45] Eleuterio F Toro. *Riemann solvers and numerical methods for fluid dynamics: a practical introduction*. Springer Science & Business Media, 2013.

[46] Pieter Wesseling. *Principles of computational fluid dynamics*, volume 29. Springer Science & Business Media, 2009.

Wissenschaftlicher Werdegang

Pascal Mindt,

geboren am 21.10.1986 in Bad Soden

2015 – 2018	Wissenschaftlicher Mitarbeiter der Technischen Universität Darmstadt am Fachbereich Mathematik, Arbeitsgruppe Numerik und wissenschaftliches Rechnen
2013 – 2015	Studium der Mathematik mit Nebenfach Informatik an der Technischen Universität Darmstadt. *Abschluss:* Master of Science
2010 – 2013	Studium der Mathematik mit Nebenfach Wirtschaftswissenschaften an der Technischen Universität Darmstadt. *Abschluss:* Bachelor of Science
2007 – 2010	Studium der Wirtschaftswissenschaften an der Goethe Universität Frankfurt am Main. *Abschluss:* Bachelor of Science